



# VLAKNA TEXTIL

**FIBRES AND TEXTILES**



TECHNICAL UNIVERSITY OF LIBEREC  
Faculty of Textile Engineering

STU  
FCHPT



Volume **24.**  
March  
**2017**

ISSN1335-0617

Indexed in:

Chemical  
Abstracts,

World Textile  
Abstracts

EMDASE

Elsevier  
Biobase

Elsevier  
GeoAbstracts



## Fibres and Textiles Vlákná a textil

### *Published by*

- Slovak University of Technology in Bratislava, Faculty of Chemical and Food Technology
- Technical University of Liberec, Faculty of Textile Engineering
- Alexander Dubček University of Trenčín, Faculty of Industrial Technologies
- Slovak Society of Industrial Chemistry, Bratislava
- Research Institute of Man-Made Fibres, JSC, Svit
- VÚTCH – CHEMITEX, Ltd., Žilina
- Chemosvit Fibrochem, JSC, Svit

### *Vydáva*

- Slovenská technická univerzita v Bratislave, Fakulta chemickej a potravinárskej technológie
- Technická univerzita v Liberci, Fakulta textilní
- Trenčianska univerzita Alexandra Dubčeka v Trenčíne, Fakulta priemyselných technológií
- Slovenská spoločnosť priemyselnej chémie, Bratislava
- Výskumný ústav chemických vlákien, a.s. Svit
- VÚTCH – CHEMITEX, spol. s r.o., Žilina
- Chemosvit Fibrochem, a.s., Svit

***Editor in Chief (Šéfredaktor):*** Anna Ujhelyiová

***Executive Editor (Výkonný redaktor):*** Marcela Hricová

**[http://www.ft.tul.cz/mini/Vlakna a textil](http://www.ft.tul.cz/mini/Vlakna_a_textil)**

### *Editorial Board*

### *Redakčná rada*

L. Balogová, M. Hricová, P. Lizák, J. Králiková, P. Michlík, M. Pajtášová, M. Tunák, V. Tunáková, V. Váry

### *Honourable Editorial Board*

### *Čestní členovia redakčnej rady*

R.U. Bauer (DE), M. Budzák (SK), D. Ciechanska (PL), T. Czigani (HU), J. Drašarová (CZ), A.M. Grancarić (HR), M. Jamrich (SK), M. Krištofič (SK), I. Krucinska (PL), A. Marcinič (SK), A.M. Marechal (SL), J. Militký (CZ), R. Redhammer (SK), M. Révus (SK), I. Sroková (SK), J. Šajbidor (SK), J. Šesták (SK), J. Vavro (SK), V. Vlasenko (UA)

### *Editorial Office and distribution of the journal (Redakcia a distribúcia časopisu)*

Ústav prírodných a syntetických polymérov  
Fakulta chemickej a potravinárskej technológie  
Slovenská technická univerzita v Bratislave  
Radlinského 9, 812 37 Bratislava, SK  
Tel: 00 421 2 59 325 575  
e-mail: [marcela.hricova@stuba.sk](mailto:marcela.hricova@stuba.sk)

### *Order and advertisement of the journal (Objednávka a inzercia časopisu)*

Slovenská spoločnosť priemyselnej chémie,  
člen Zväzu vedecko-technických spoločností  
Radlinského 9, 812 37 Bratislava, SK  
Tel: 00 421 2 59 325 575  
e-mail: [marcela.hricova@stuba.sk](mailto:marcela.hricova@stuba.sk)

### *Order of the journal from abroad – excepting Czech Republic Objednávka časopisu zo zahraničia – okrem Českej republiky*

SLOVART G.T.G, s.r.o. EXPORT-IMPORT  
Krupinská 4, P.O.Box 152, 852 99 Bratislava, SK  
Tel: 00421 2 839 471-3, Fax: 00421 2 839 485  
e-mail: [info@slovart-gtg.sk](mailto:info@slovart-gtg.sk)

### *Typeset and printing at*

### *Sadzba a tlač*

FOART, s.r.o., Bratislava

Journal is published 4x per year  
Subscription 60 EUR

Časopis vychádza 4x ročne  
Ročné predplatné 60 EUR

**ISSN 1335-0617**

Evidenčné číslo MKCR SR Bratislava EV 4006/10

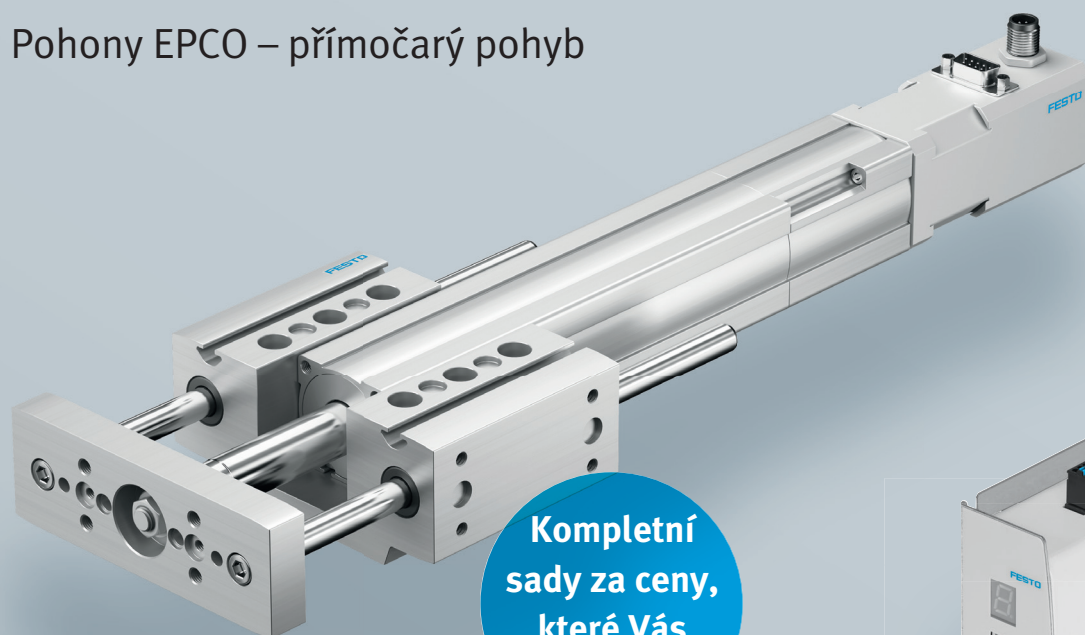


PARTNERS / SPONSORS



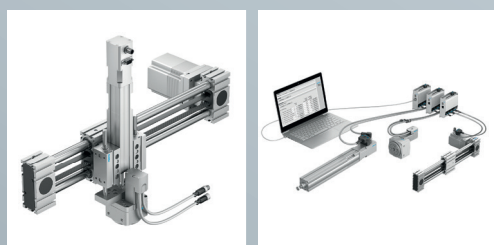
# Nový obor – OMS!

Pohony EPCO – přímočarý pohyb



**FESTO**

Kompletní  
sady za ceny,  
které Vás  
překvapí!



 **IO-Link**  **Modbus**  
 **PROFINET**  **EtherNet/IP**  
 **EtherCAT**

Hledáte jednoduché řešení pro Vaší aplikaci?  
Potřebujete snadno a levně polohovat nebo manipulovat?  
Vyberte si svoji sadu z OMS, nové skupiny elektrických pohonů!

## → WE ARE THE ENGINEERS OF PRODUCTIVITY.

- Polohování ještě nikdy nebylo tak snadné – několik základních údajů o potřebném pohybu postačí k výběru sestavy pohonu s namontovaným motorem, se správným ovladačem i kabely.
- Ušetříte v konstrukci, nákupu i logistice – vše je za velmi nízkou cenu a pod jediným objednávacím číslem.
- Oživení zvládne každý – po vyplnění tabulky na webové stránce ovladače je pohon připraven pracovat.

[www.festo.cz/OMS](http://www.festo.cz/OMS)  
[prodej@festo.com](mailto:prodej@festo.com)  
tel.: 261 099 611



## Rieter CZ s.r.o.

Ústí nad Orlicí

Rieter CZ s.r.o. is part of the Swiss Group, Rieter, that is a leading world producer of textile machinery and complete textile systems. Rieter CZ s.r.o. is characterised by a strong emphasis on innovations that are developed in the company development centre. Other features include precision production of textile machines and components for modern technologies and processes.

**Rieter** – The Comfort of Competence.  
<http://www.rieter.cz>, <http://rieter.jobs.cz>

**RIETER**

ENVIRONMENTAL FRIENDLY TECHNOLOGY

Plasma discharge+working  
gas = ACTIVE PARTICLES

New functional groups  
on the polymeric chain

Hydrophilisation/adhesion  
enhancement

# PLASMA SURFACE TREATMENT

- POWDERS (LDPE, HDPE, UHMWPE, PP)
- excellent dispersion - additives for paints and plastics
- treatment effect stays also on the sintered surface from the treated powder - rotomolding

- PLASTIC PARTS - plain or complex shapes
- activation prior to gluing, printing, etc.
- no chemical/flame pretreatment
- process without altering the bulk material



- atmospheric/vacuum systems
- toll service or machine delivery
- testing and development processes
- production of special equipments for plasma surface treatment
- adjustment of current plasma devices
- R&D in the area of plasma surface treatment



[www.surface-treat.cz](http://www.surface-treat.cz)





**Company Driga Group s.r.o. represents on the Czech and Slovak markets the following manufacturers of a textile machinery and equipments:**

**1/ Bonas Textile Machinery NV** ( Belgium ) is trendsetter in design and manufacture of electronic jacquards for weaving machines.

Principally located in Belgium Bonas Textile Machinery is a brand of VANDEWIELE consisting of several textile machine companies all synonymous within their field of textile machinery expertise: **Van de Wiele**, carpet and velvet looms, **IRO & ROJ**, yarn feeders for weaving, **Memminger-IRO**, advanced knitting technology, **Protechna**, quality assurance for textiles and **Titan**, sewing/finishing machines, to name but a few. Throughout the history of Bonas our philosophy remains unchanged, continual investment in R&D. This resulted in the invention of the electronic jacquard years ago. To our valued customers we have the technology and expertise to consistently offer the very best in speed, reliability, robustness and efficiency within the global marketplace of Jacquard weaving. Manufacturing excellence from our hub in Kortrijk, Belgium enables us to supply the most technologically advanced electronic Jacquards whilst professional dedicated and disciplined sales and service departments, operating throughout the world, ensure that Bonas customers remain continually satisfied with our products of past, present and for the future.,

**2/ CCI TECH INC.** ( Taiwan ) commit ourselves to the development of sampling solutions for the weaving industries. We provide the markets with the most innovative tools for fabric sampling, new designs development as well as small quantity production. This is a brand new dimension to sampling which will give you unexceptional experiences in the most efficient and economical way!

**3/ ICOMATEX** ( Spain ) has continued to broaden its program of machinery, and are today producing a wide range of machinery from continous washing/bleaching, relax dryers, stenter to specialized machinery, for many different industrial segments across the globe.

**4/ Salvadè S.r.l.** ( Italy ) was founded in 1967 by brothers Alberto and Luigi. In the ensuing years it grew as a maintenance company for textile plant of all types and brands ranging from rameuse to printing machines, steaming plant and dryers, and gradually becoming a machine constructor itself. Thanks to the vast experience it acquired in maintenance, and fielding an extremely broad range of machinery for textile dyeing, printing and finishing, Salvadè is now one of the leading companies in the sector, at international level. The company is aware that the production evolves continuously with research and updating, development and innovation; constant monitoring of technological evolution and customer requirements therefore represent a fundamental point of passage towards the objectives that Salvadè has set itself for the near future, such as the expansion of the manufacturing range and the continuous improvement of products. The new solution are in fact seen as a means to improve the customer's production cycles, in terms of space and time.

**5/ Pentek Textile Machinery, Srl** ( Italy ) Design and manufacture of *machinery* for discontinuous washing, scouring, steaming, drying and continuous tumbling in *textile* processing and finishing.

# VeBa

Czech producer  
of first class  
clothing fabrics

life is fashion

## Head Office

VEBA, textilní závody a.s.  
Přadlácká 89, 550 01 Broumov  
Czech republic

## Sale Offices

Přadlácká 89, 550 01 **Broumov**  
Czech republic

U Elektry 830/2b, 190 00 **Prague 9**  
Czech republic

## Call Centre

Tel.: +420 491 502 300  
E-mail: [callcentrum@veba.cz](mailto:callcentrum@veba.cz)  
[www.veba.cz](http://www.veba.cz)



# Fibres and Textiles (1) 2017

## Vlákna a textil (1) 2017

March 2017

Special issue venue the 21<sup>st</sup> International Conference STRUTEX 2016  
*“Structure and Structural Mechanics of Textiles”*  
 held on December 1.- 2. 2016 in Liberec, Czech Republic

### SCIENTIFIC COMITEE

prof. S. M. ISHTIAQUE, Indian Institute of Technology Delhi, India  
 prof. Yordan KYOSEV, Hochschule Niederrhein, Germany  
 prof. Bohuslav NECKÁŘ, Technical University of Liberec, Czech Republic  
 prof. Jakub WIENER, Technical University of Liberec, Czech Republic  
 prof. Luboš HES, Technical University of Liberec, Czech Republic  
 prof. Oldřich JIRSÁK, Technical University of Liberec, Czech Republic

Content	Obsah
3 <i>Yordan Kyosev</i> Geometrical and mechanical modelling of textile structures at fiber and yarn level - software and data structures	3 <i>Yordan Kyosev</i> Geometrický a mechanický přístup k modelování struktury délkových vlákenných útvarů
10 <i>Tomas Pitucha</i> Geometrical model of a knitted fabric made from hyaluronan based fibers	10 <i>Tomáš Pitucha</i> Geometrický model pletené textilie z vláken na bázi hyaluronanu
15 <i>Brigita Kolcavova Sirkova and Iva Mertova</i> Woven fabric structural pore models analysis	15 <i>Brigita Kolčavová Sirková a Iva Mertová</i> Analýza strukturních pórů ve tkanině
25 <i>Selcuk Aslan and Sibel Kaplan</i> Structural and thermal-mechanic properties of filaments produced from shape memory polymers	25 <i>Selcuk Aslan a Sibel Kaplan</i> Struktura a termomechanické vlastnosti vláken z polymerů s tvarovou pamětí
30 <i>Murat Demir and Musa Kilic</i> Investigating possibilities of three-strand yarn production	30 <i>Murat Demir a Musa Kilic</i> Výzkum možností výroby prstencové předeno-skane příze
36 <i>Karolina Cermakova, Michal Ackermann, Lukas Capek and Jana Horakova</i> Tensile properties of synthetic blood vessel replacement	36 <i>Karolina Čermáková, Michal Ackermann, Lukáš Čapek a Jana Horáková</i> Tahové vlastnosti syntetických cévních náhrad
39 <i>Veerakumar Arumugam, Rajesh Mishra, Jana Salacova, Mohanapriya Venkatraman, Dana Kremenakova, Hafsa Jamshaid, Tao Yang, Xiaoman Xiong, Kasthuri Venkatesh and Jiri Militky</i> Functional characteristic evaluation of 3-Dimensional knitted spacer fabrics	39 <i>Veerakumar Arumugam, Rajesh Mishra, Jana Salačová, Mohanapriya Venkatraman, Dana Křemenáková, Hafsa Jamshaid, Tao Yang, Xiaoman Xiong, Kasthuri Venkatesh a Jiří Militký</i> Hodnocení funkčních vlastností 3D distančních pletenin

- |  |   |
|--|---|
| <p>46 <i>Hafsa Jamshaid, Rajesh Mishra, Jiri Militky, Muhammad Tayyab Noman, Mohanapriya Venkataraman, Veerakumar Arumugam, Tao Yang and Xiaoman Xiong</i></p> <p>Performance characterization of basalt hybrid woven fabric reinforced concrete</p>   | <p>46 <i>Hafsa Jamshaid, Rajesh Mishra, Jiří Militký, Muhammad Tayyab Noman, Mohanapriya Venkataraman, Veerakumar Arumugam, Tao Yang a Xiaoman Xiong</i></p> <p>Hodnocení vlastností čedičových hybridních tkanin určených pro výztuže betonu</p>       |
| <p>53 <i>Ales Saman, Lucie Vejsadova, Jana Horakova, Vera Jencova and Petr Mikes</i></p> <p>Electrospun polyesters: comparison of polymeric fibrous structure and its influence on fibroblast proliferation</p>  | <p>53 <i>Aleš Šaman, Lucie Vejsadová, Jana Horáková, Věra Jenčová a Petr Mikeš</i></p> <p>Elektrostatické zvlákňování polyesterů: porovnání polymerních vláknenných struktur a jejich vliv na proliferaci fibroblastů</p>                               |
| <p>57 <i>Lenka Blazkova, Jana Hlavata, Jana Horakova, Tomas Kalous, Patrik Novak, Martin Pelcl, Katerina Strnadova, Ales Saman and Jiri Chvojka</i></p> <p>Comparison of the well known spinning and electrospinning methods for polyvinyl alcohol</p> | <p>57 <i>Lenka Blažková, Jana Hlavatá, Jana Horáková, Tomáš Kalous, Patrik Novák, Martin Pelcl, Kateřina Strnadová, Aleš Šaman a Jiří Chvojka</i></p> <p>Porovnání známých zvlákňovacích metod (elektrospinningových) pro polymer polyvinylalkohol.</p> |
| <p>64 <i>Emilia Frydrysiak, Michał Frydrysiak and Łukasz Tęsiorowski</i></p> <p>A hydrogel phantom for testing biosignals from a textronics T-shirt</p>  | <p>64 <i>Emilia Frydrysiak, Michał Frydrysiak a Łukasz Tęsiorowski</i></p> <p>Stínění hydrogelu na textilií při testování biosignálů</p>  |
| <p>68 <i>Sertaç Güney, Betül Akgünoğlu and Sibel Kaplan</i></p> <p>Parameters affecting sports socks pressure and pressure prediction from tensile characteristics</p>   | <p>68 <i>Sertaç Güney, Betül Akgünoğlu a Sibel Kaplan</i></p> <p>Parametry ovlivňující tlak sportovních ponožek a predikce tlaku na základě tahových charakteristik</p>   |
| <p>73 <i>Michaela Hassmann, Seraphina Stöger, Natalie Mentel and Wolfgang Krach</i></p> <p>Bending behaviour of sports bra fabrics: experimental and finite element simulation of ASTM D1388 Cantilever test</p>                                       | <p>73 <i>Michaela Hassmann, Seraphina Stöger, Natalie Mentel a Wolfgang Krach</i></p> <p>Ohybové vlastnosti textilií určených k výrobě podprsenek: Simulace ASTM D1388 Cantilever testu metodou konečných prvků</p>                                     |
| <p>78 <i>Monika Vysanska</i></p> <p>Image analysis and description of single jersey loop geometry</p>  | <p>78 <i>Monika Vyšanská</i></p> <p>Obrazová analýza a popis geometrie oka jednolící zátahné pleteniny</p>  |

*Príspevky boli prijaté do tlače bez recenzie. Za odbornú a jazykovú úroveň príspevkov zodpovedajú autori a prekladatelia.*

*Contributions were received without review process. The authors are responsible for professional and language level of contributions.*



# GEOMETRICAL AND MECHANICAL MODELLING OF TEXTILE STRUCTURES AT FIBER AND YARN LEVEL - SOFTWARE AND DATA STRUCTURES

Yordan Kyosev

Hochschule Niederrhein - University of Applied Sciences, Faculty of Textile and Clothing Technology,  
Research Institution of Textile and Clothing, Mönchengladbach, Webschulstr. 31, Germany  
[yordan.kyosev@hs-niederrhein.de](mailto:yordan.kyosev@hs-niederrhein.de)

**Abstract:** This paper presents the common strategies for multiscale modelling of textiles, concentrating on the yarn and filament level. The advantages and disadvantages of the both used ways of creation of geometrical models are discussed. Reference to works, related to the generation of the coordinates of the filaments within the yarns and example results for warp knitted and braided structures are given. Overview of the common software solution of textile generators is included. After analysis of the configuration of a braided structure one recursive structure definition for the data storage is proposed. This allows modelling of fabrics with unlimited number of grouping levels of the fibers.

**Key words:** Modelling, geometry, fibers, filaments, data structures, multiscale models

## 1 INTRODUCTION

The mathematical modelling of textile structures allows the computer aided investigation of their behavior without their production. Many textile engineers expect to have tools similar to those of the machine engineers for calculation and evaluation of textiles. Indeed in the last decades the modelling of textiles has been developed significantly, but the complexity of the fibrous structures does not allow the same efficiency and accuracy of the computations as for metal parts. This work presents some methods and problems, related to the multiscale modelling of fibrous structures and represents an overview of some commonly used preprocessors/geometrical generators and simulation programs for textiles.

## 2 STRATEGIES FOR MULTISCALE MODELLING OF TEXTILES

The modelling of the textiles multiple scales - for instance yarn and fiber/filament level requires separate algorithms and methods for each scale. The knitted, woven and braided structures are yarn based and require certain description of the yarn geometry. There are three popular methods for retrieving the yarn geometry:

- By using image processing of 2D or 3D images, for instance by X-ray micro-computer tomography [1, 2]. This method can produce very accurate data about the geometry of the fibrous structure and the orientation of the fibers, but is applicable only over already produced structures. Because of this it is not going to be a point of interest in this paper.
- Simulating the complete production process [3-5]. This method is connected with many computations and a lot of simulation time at current. Nevertheless, considering the rapid development of the computer technic and methods for parallel processing, it is going to become soon more popular.
- Generating the topology of the structure parametrically and refining it by using some mechanical methods. This approach is the common one and allows generation of textile geometry in a very short time. One of the first works regarding woven structures are the ones of Peirce and Kemp [6, 7]. Several geometrical methods are summarized by Behera and Hari in [8]. The modern methods considering the mechanical properties of the yarns are based usually on minimization of the potential energy of the yarns, as described in the book of Ron Postle, Carnaby and Jong [9]. In the software Wisetex [10-12] are implemented the mechanical models for woven and braided structures. The geometry of the loops in knitted structures is investigated by researchers as for instance Leaf [13], Postle and Munden [14, 15], Hart et al [16, 17], Goktepe and Harlock [18], Wu [19]. Software, useful for 3D modelling of knitted structures is the WeftKnit (part of Wisetex) by M. Moesen [20] and the different computer realisations of Kyosev and Renkens [21-23]. Very good photorealistic simulations of knitted fabrics at yarn level are reported by Kaldor et al. [24]. They are extended for complete clothing by Yuksel et al. [25].

Both the techniques which are able to create virtual product without using an existing one - the simulation of the complete production process and generating topology of the structure - require normally the use of the yarns as a main object at the first step. As second step the created yarns are filled with filaments and eventually refined by consideration of the contact between the filaments. The distribution of the fibers or filaments in the yarns can be based on statistical distribution, based on some of the methods used by Neckar and Das [26], Grishanov and Lomov [27], using complete FEM calculation where the fibers are represented as beams as done by Durville in his Multifil package [28, 29] or arbitrary arrangement of the single filaments in circular or parallel layers as implemented in the packages of the TexMind software and described by Kyosev in [30].

### 3 YARN LEVEL TOPOLOGY

The main principle for the creation of the yarn topology is based on the definition of several points of the yarn axis, whose coordinates can be calculated parametrically. One part of the models use not only the points, but defines the curves and lines between these points explicitly. Figure 1a presents a well-known model for woven fabrics produced of yarns with circular cross section, where each yarn axis can be presented by a connected circle arcs and straight lines.

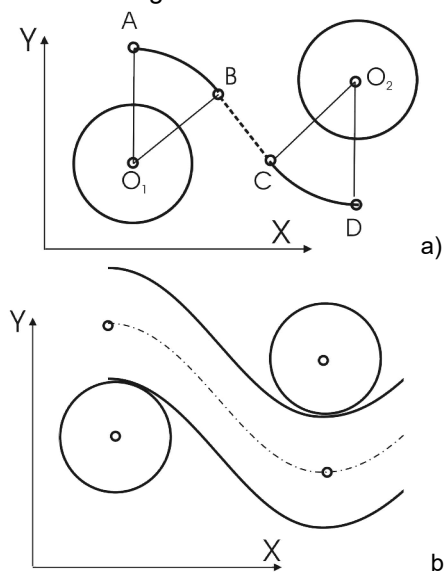


**Figure 1** Idealized geometrical model of the yarn path of a woven structure a) based on circular arcs and lines b) based on spline interpolation between key points [38]

Extended version of such models is implemented very successfully in both commercially and academically used software Wisetex [11, 12] for woven structures. The large number of reported such models for weft knitted structures by Kurbağ [31-37] demonstrate nice geometries rendered within 3DS studio. If these models can be applied in

the general case within textile CAD software depends on the sensibility of the models on the input data, which should be tested in the future. Less accurate, but more flexible for implementation in computer applications are the models, based on the sequence of the key-points only, where the connecting curve is computed at a next step. Drawing for development of such model for woven structure is presented in Figure 1b and for knitted structures in Figure 2.

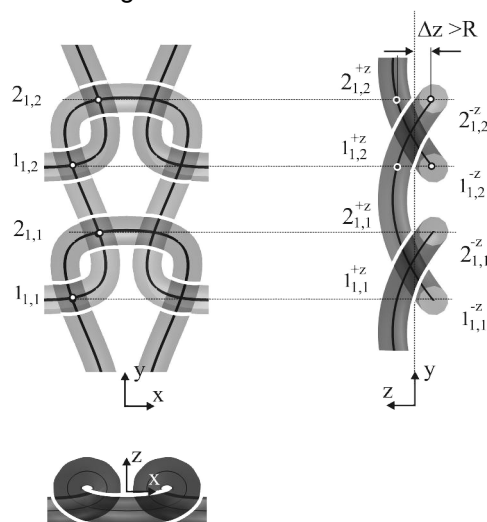


**Figure 2** Idealized geometry of weft knitted loop and common points there for creation of geometrical model of these [23]

The flexibility of these models is in the less relations, which have to be programmed, which allow the extension of such models for larger number of different structural elements to be done in more clear way. For instance for woven structures one algorithm can be used for complete class of pattern or for knitted structures the programming of loops, tucks, missed and transferred stitches can be done with less steps. Actually this simplicity has its price – during the interpolation the curve between the key-points at some positions the yarn volume can intersect the neighbor yarns, as visualized on the Figure 3. This defect happens, because the distance between the yarns is defined only at the places between the key-points and what happens between these key-points is not controlled during the generation of the interpolating curves.

Which of these approaches is more suitable for modelling should be decided case by case from the modeler. For the cases, where more generality is required and with one algorithm several classes of structures have to be covered, the definition of the key-points only has its advantage; for models, created to investigate one type of structures (during Master or PhD thesis or some specific product) the analytical description of the curves can be preferable.

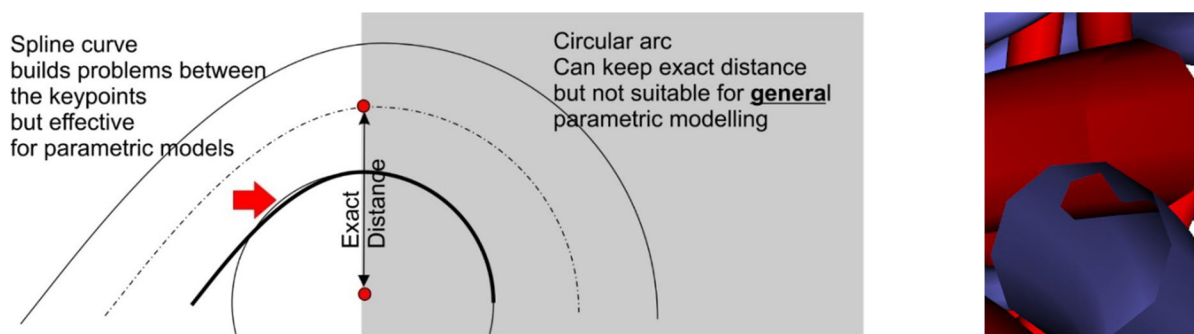


**Figure 3** Defects of the interpolation between key points only

#### 4 FILAMENT LEVEL

The generation of the filaments within the yarns can be done in different ways. Duville [28, 29] creates the filaments with some regular initial arrangement and moves these later to their final position applying artificial forces in order to create the topology of the structure. Checking and adjusting the contact between the filaments generates the filament distribution “automatically”. Kyosev [30] defines the local coordinates of the filaments in one cross section (Figure 4) and then moves this cross section with the set of all coordinates along the yarn axis, considering the orientation of the curve. The yarn cross section is located in the plane of the normal  $\mathbf{n}$  and binormal  $\mathbf{b}$  vectors, but rotated to some angle  $\gamma$  to these, so the main coordinate axes of the local plain are  $\mathbf{p}$  and  $\mathbf{q}$ . Each filament center  $\mathbf{ci}$  can be then defined in local coordinates and placed in the 3D space after simple coordinate transformation.

This approach allows controlled creation of twisted structures or structures with flat (for composites) or circular arrangement (for ropes) of the filaments, but

requires refining step after the generation in order the structure to be compacted

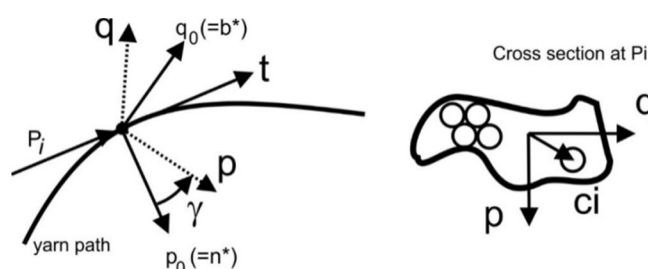


**Figure 4** Yarn axis as a curve and the yarn cross section in local coordinates [30]

Figure 5 demonstrates the starting data for warp knitted structure and the created 3D geometry at yarn level. It is used at the next step for generation of the filament axes, presented in Figure 6. Multifilament model of a tubular braid is presents as well in Figure 6.

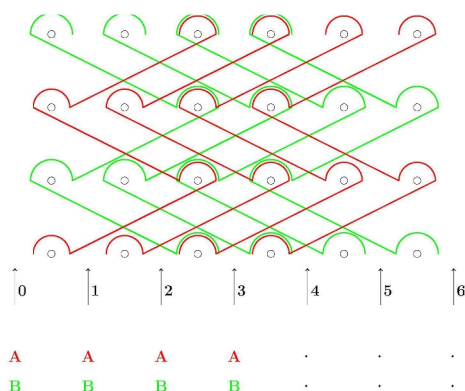


**Figure 5** Starting pattern for warp knitted structure and generated yarn level geometrical 3D model [39]

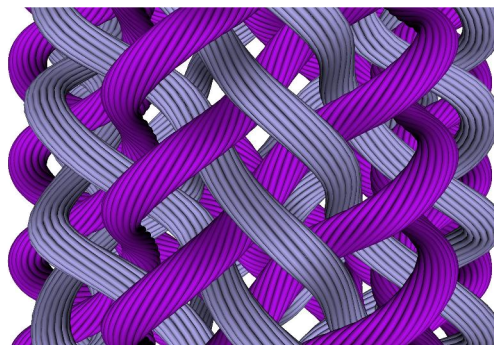
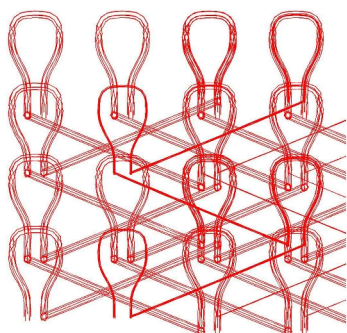


**Figure 6** Multifilament model, generated on the basis of the yarn model from Figure 5 and multifilament model of a tubular braided structure [30, 40]

## 5 SOFTWARE OVERVIEW

The following table visualizes some of the packages known or used by the author for creation of models of textile structures. It presents a moment view of the capabilities of these programs, as all these are continuously being developed and extended. The Multiscale Designer of Altair, acquired of Multiscale Design Systems, LLC, proves, that the commercial FEM Software producers try already to integrate textile generators for calculation of composites in their software.

## 6 LEVELS IN TEXTILE STRUCTURES

Table 1 shows that the filament level is presented at three of the packages currently. The TexMind packages can cover 4 level of grouping of filaments, common are three levels. The actual situation for modelling of textiles at fiber or filament level require several levels, as presented in Figure 7 for the case of a rope – normally several hundred of filaments build one yarn, this build a ply yarn together with another yarns, commonly twisted together.

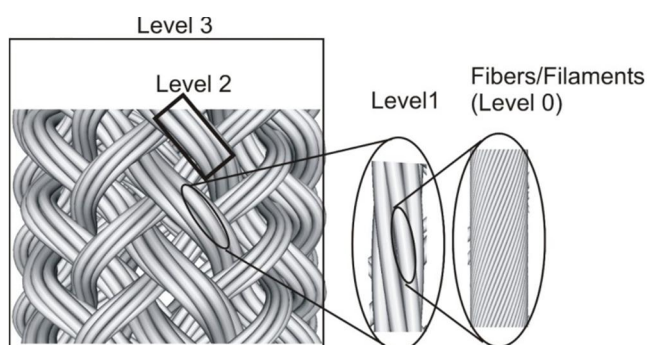


**Figure 7** Example of the basic element (filament) and levels of grouping of the fibrous assemblies in this case for a braided structure

Then often several twisted yarns are again twisted, in order to get required thickness and strength and after the twisting several yarns are braided together. Figure 8 shows this information and makes clear the similarity between the levels. It is well visible,

that only two main types of virtual objects are required for storage of the data for simulation of textile structures – fibers (filaments) and “groups of fibers”.

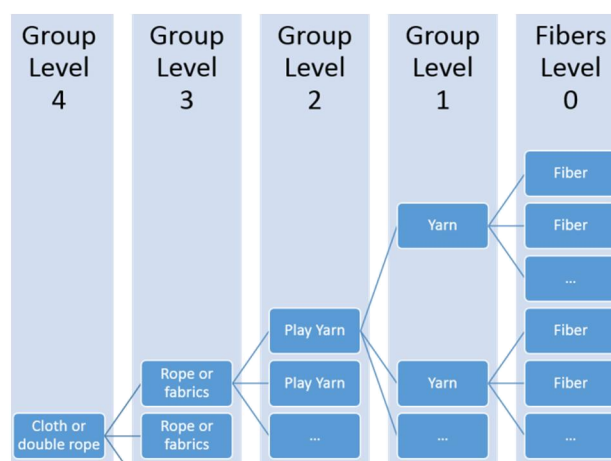


**Figure 8** Fibers (or filaments) are basic object of fibrous structures. All higher levels consists of groups of another groups

Fiber	Group of Fibers
<ul style="list-style-type: none"> <li>• Fineness</li> <li>• Diameter/Cross section</li> <li>• Colour</li> <li>• Mechanical Param.</li> <li>• List of Coordinates</li> </ul>	<ul style="list-style-type: none"> <li>• List of „Group of Fibers“</li> <li>• Group Properties as „Macro-Fiber“ <ul style="list-style-type: none"> <li>• Diameter/Cross section</li> <li>• Colour</li> <li>• Mechanical Param.</li> <li>• List of Coordinates</li> </ul> </li> </ul>

**Figure 9** Two required types of objects (classes) – fibers and “group of fibers” and their principle properties. Each group of fibers can be represented as well as a macro-fiber (yarn, ply yarn) and because of this the definition of fiber-similar properties as resulting color, diameter and mechanical properties can be useful

Each “group of fibers” can be yarn, ply yarn, twisted yarn or braided structure. It is a linear product and it can be characterized from the programming and

modelling point of view as a larger and thicker fiber or “micro-fiber”. In order the properties of this macro-fiber to be visualized at the current level, all its properties – diameter, fineness, color and mechanical properties should be defined or

calculated. In such recursive definition, where the main object is “group of fibers”, consisting another “groups of fibers” there is no limitation of the number of the levels of grouping and all kind of fabrics can be modelled and represented.

**Table 1** Overview of *some* software packages for modelling of textiles, used or known by the author

Generators	Wisetex Suite	TexGen	TexMind Suite	VTMS Virtual Textile Manufacturing Suite	Multifil	Multiscale Designer
Some sources	[11, 12, 41, 42]	[43, 44]	[30, 40]	[45]	[28, 29]	[46]
Developer	KU Leuven	Univ. Nottingham	TexMind UG	The University of Dayton	Laboratoire MSSMat - Centrale Paris	Altair, Multiscale Design Systems
License	Proprietary	GPL	Proprietary	Proprietary	Proprietary	Proprietary
Source	Closed	Open	Closed	Closed	Closed	Closed
<b>Structure Type</b>						
Woven	Single- and Multilayer woven each yarn individually defined	Single layer, orthogonal, angle interlock, layer to layer, yarn group properties	Basic structures, Each yarn individually defined	Single layer, orthogonal, angle interlock, layer to layer, yarn group properties	Basic structures, (manual generator)	5 Basic structures
Weft Knitted	Loop based fine, Tucks need improvement	- Scripting or import from TexMind or Wisetex	Plain Loops in flat and tubular structure	- (import possible)	- (import possible)	-
Warp Knitted	Needle stitched only	- Scripting or import	Loop3D - several classes structures on single and double needle bed machines	- (import possible)	- (import possible)	-
Braided	Unit Cell of biaxial and triaxial braids	- Scripting or import from TexMind or WiseTex	Braider - tubular and flat; Configurator - custom (Geometry)	Unit cell of biaxial and triaxial, Tubular briads	Manual generation (import possible)	-
<b>Yarn Level</b>						
Yarn Level - Mechanics	Beam - Energy minimization	- (scripting possible)	-	Digital Chain	Beam	-
Yarn Contact	Algorithmically included	-	(*)Local Sections	Mesh	Beam-Beam	Surface- Surface
Scripting	-	Python	-	-		-
Imports		WiseTex Weave Pattern	WiseTex,			Abaqus inp File
Exports	Abaqus, Ansys, WiseTex XML (TexGen)	Step, STL, Abaqus, Voxel Grid, (WiseTex)	Abaqus, Ansys, VTMS, WiseTex, TexGen, ImpactFEM, X3D, STL			
Yarn definition	Initially constant cross section	Variable cross section	Constant Cross section	Constant Cross section		Constant Cross section
<b>Filament level</b>						
Filament Visualization	-	-	Yes	yes	Yes	-
Filament Data Stored	Yes	-	Yes	Yes	Yes	
Filament Data Used for computations	Yes	-	Yes	Yes	Yes	-
Initial filament Distribution in the yarn cross section	-	-	Circular layers, flat layers and arbitrary distribution possible	Number of filaments	Program dependent	-
Structural levels	2(3): Fabrics-Yarn- (Fiber data); In LamTex: 3	3: Layered textile - Textiles - Yarn	4: Textile-4: Yarn Groups- Yarns- Fibers	3: Fabrics-Yarn-Fibers	3: Fabrics-Yarns- Fibers	1: Yarn volume mesh



## 7 CONCLUSIONS

This paper gives an overview of the methods for geometrical modelling of textile structures. It points out the advantages and disadvantages of the both popular methods for the description of the yarn geometry – using key-points only or using key-points and explicitly defined curves between these points. Overview of the common used software packages for modelling demonstrates their capabilities at the current time. It shows, that the programs cover two, three and up to four levels of grouping of fibrous objects today. During the analysis of one rope structure is found, that only two classes of objects are required for multiscale modelling of textile structures, if recursive definition is used. These are the “fiber/filament” and “group of fibers”, which can consists list of another “groups of fibers”. Using such objects, structures with unlimited number of levels of grouping can be modeled.

## 8 REFERENCES

- Harjkova G., Barburski M., Lomov S.V., Kononova O., Verpoest I.: Weft knitted loop geometry of glass and steel fiber fabrics measured with X-ray micro-computer tomography, *Textile Research Journal* 84(5), 500-512, 2014, doi: 10.1177/0040517513503730
- Naouar A., Vidal-Salle E., Boisse P.: Meso-FE forming of a non-crimp 3D orthogonal weave E-glass composite reinforcement based on X-ray computed tomography, In: Boussu F., Chen X. (Eds.) *Proceedings of the 7<sup>th</sup> World Conference 3D Fabrics & Their applications*, Roubaix, September 8-9. 2016, pp. 285-293
- Finckh H.: Textile micromodels as a result of idealized simulation of production processes, In: *Finite Element Modeling of Textiles and Textile Composites*, 22<sup>nd</sup> BEM-FEM Conference, Saint-Petersburg, Russia, September 26-28. 2007
- Akkerman R.a.R.B.H.V.: Braiding simulation for rtm preforms, *TexComp* 8, 2006
- Kyosev Y.K.: Machine configurator for braided composite profiles with arbitrary cross section. In: 16<sup>th</sup> European conference on composite materials ECCM 16, June 22-26.2014, Seville-Spain
- Peirce F.T.: 5-The geometry of cloth structure, *Journal of the Textile Institute Transactions* 28(3), T45-T96 (1937), doi: 10.1080/19447023708658809
- Kemp A.: An Extension of Peirce's Cloth Geometry to the Treatment of Non-circular Threads, *Journal of the Textile Institute Transactions* 49(1), T44-T48, 1958, doi: 10.1080/19447025808660119
- Behera B., Hari B.K.: *Woven textile structure, Theory and application*, Woodhead Publishing Ltd, Cambridge, 2010
- Postle R., Carnaby G., Jong S. de: *The mechanics of wool structures*, Ellis Horwood Limited, 1988
- Lomov S., Bernal E., Koissin V., Peeters T.: *Integrated textile preprocessor WiseTex, Version 2.5. Computational models, methods and algorithms*, KU Leuven, Department MTM, Leuven, 2006
- Lomov S., et al.: *WiseTex*. KU Leuven, Leuven, 2011
- Verpoest I., Lomov S.V.: Virtual textile composites software Wisetex: integration with micro-mechanical, permeability and structural analysis, *Composites Science and Technology* 65(15-16), 2563–2574, 2005
- Leaf G.G.A.: The Geometry of a plain Knitted Loop, *Journal of the Textile Institute* 45, 605, 1955
- Postle R., Munden D.: Analysis of the dry-relaxed knitted-loop configuration Part 1: Two-Dimensional Analysis, *Journal of the Textile Institute* 58(8), 329-351, 1967
- Postle R., Munden D.: Analysis of the dry-relaxed knitted-loop configuration Part 2: Three-dimensional analyses, *Journal of the Textile Institute* 58(8), 352-365, 1967
- Hart K., Jong S. de, Postle R.: Analysis of the Single Bar Warp Knitted Structure Using an Energy Minimization Technique: Part I: Theoretical Development, *Textile Research Journal* 55(8), 489-498, 1985, doi: 10.1177/004051758505500807
- Hart K., Jong S. de, Postle R.: Analysis of the Single Bar Warp Knitted Structure Using an Energy Minimization Technique: Part II: Results and Comparison with Woven and Weft Knitted Analysis, *Textile Research Journal* 55(9), 530-539, 1985, doi: 10.1177/004051758505500903
- Goktepe O., Harlock S.: Three-Dimensional Computer Modeling of Warp Knitted Structures, *Textile Research Journal* 72, 266-272, 2002
- Wu W., Hamada H., Maekawa Z.: Computer Simulation of the deformation of weft knitted fabrics for composite materials, *Journal of the Textile Institute* 85(2), 198-214, 1994
- Moesen M.: Modelleren van de vlakke vervorming van gladde inslagbreielsen. <http://liegebeest.studentenweb.org/weftknitEN.html>
- Kyosev Y.: Computational Model of Loops of a Weft Knitted Fabric. In: Dragčević Z. (Ed.), *Book of proceedings: ITC&DC, 3<sup>rd</sup> International Textile Clothing & Design Conference Magic World of Textiles*, October 8-11. 2006, Dubrovnik, Croatia, 2006
- Kyosev Y., Renkens W.: 3D-CAD für die Gestaltung von gewirkten Strukturen. In: 11-Chemnitz Textiltagung, 24-25 October 2007, 110-117, 2007
- Kyosev Y., Renkens W.: Modelling and visualization of knitted fabrics. In: Chen, X. (Ed.) *Modelling and predicting textile behaviour*, Woodhead Publishing; In association with the Textile Institute; CRC Press, Cambridge, Boca Raton, Fla, 225-262, 2010
- Kaldor J., James D.L., Marschner S.: Simulating Knitted Cloth at the Yarn Level, In: *Proceedings of SIGGRAPH 2008*, August 2008, Los Angeles, California
- Yuksel C., Kaldor J.M., James D.L., Marschner S.: Stitch Meshes for Modeling Knitted Clothing with Yarn-level Detail, *ACM Transactions on Graphics (Proceedings of SIGGRAPH 2012)* 31(3), 2012, doi: 10.1145/2185520.2185533
- Neckar B., Das D.: *Theory of Structure and Mechanics of Fibrous Assemblies and Yarns*, Woodhead Publishing India Ser, Woodhead

- Publishing Limited; Ingram Publisher Services [distributor], Sawston, LaVergne, 2012
27. Grishanov S., Lomov S. et.al.: The Simulation of the Geometry of Two-component Yarns. Part I: The Mechanics of Strange Compression: Simulating Yarn Cross-section Shape, *Journal of Textile Institute* 88, Part 1(2), 1997
  28. Durville D.: Finite element simulation of textile materials at mesoscopic scale, In: *Finite element modelling of textiles and textile composites*, September 26-28. 2007, St-Petersburg
  29. Durville D.: Simulation of the mechanical behaviour of woven fabrics at the scale of fibers, *Int J Mater Form* 3(S2), 1241-1251, 2010, doi: 10.1007/s12289-009-0674-7
  30. Kyosev Y.: Generalized geometric modeling of tubular and flat braided structures with arbitrary floating length and multiple filaments, *Textile Research Journal* 86(12), 1270-1279, 2016, doi: 10.1177/0040517515609261
  31. Kurbak A.: Geometrical and mechanical modelings of dry relaxed slack plain-knitted fabrics for the benefit of technical textile applications, Part I. A geometrical model, *Textile Research Journal*, 2016, doi: 10.1177/0040517516641358
  32. Kurbak A., Amreeva G.: Creation of a Geometrical Model for Milano Rib Fabric, *Textile Research Journal* 76(11), 847-852, 2006, doi: 10.1177/0040517507071968
  33. Kurbak A., Ekmen O.: Basic Studies for Modeling Complex Weft Knitted Fabric Structures, Part I: A Geometrical Model for Widthwise Curlings of Plain Knitted Fabrics, *Textile Research Journal* 78(3), 198-208, 2008, doi: 10.1177/0040517507082352
  34. Kurbak A., Soydan A.S.: Basic Studies for Modeling Complex Weft Knitted Fabric Structures, Part III. A Geometrical Model for 1x1 Purl Fabrics, *Textile Research Journal* 78(5), 377-381, 2008, doi: 10.1177/0040517507082465
  35. Kurbak A.: Geometrical models for weft-knitted spacer fabrics, *Textile Research Journal*, 0040517516631320, doi: 10.1177/0040517516631320
  36. Kurbak A.: Geometrical Models for Balanced Rib Knitted Fabrics, Part I: Conventionally Knitted 1x1 Rib Fabrics, *Textile Research Journal* 79(5), 418-435, 2009, doi: 10.1177/0040517508095598
  37. Kurbak A., Kayacan O.: Basic Studies for Modeling Complex Weft Knitted Fabric Structures, Part V: Geometrical Modeling of Tuck Stitches, *Textile Research Journal* 78(7), 577-582, 2008, doi: 10.1177/0040517507087672
  38. Kyosev Y.K.: Simulation of wound packages, woven, braided and knitted structures, In: Veit D. (Ed.) *Simulation in textile technology*, 266-309. Woodhead Publishing Limited, 2012
  39. Renkens W., Kyosev Y.: Geometry modelling of warp knitted fabrics with 3D form, *Textile Research Journal* 81(4), 437-443, 2011, doi: 10.1177/0040517510385171
  40. Kyosev Y.K.: *TexMind Braider*, www.texmind.com, Mönchengladbach, 2012
  41. Moesen M., Lomov S.V.: *WeftKnit*, 2011
  42. Moesen M., Lomov S., Verpoest I.: Modelling of the geometry of weft-knit fabrics, In: *Techtextil (Hg.) 2003 – TechTextil Symposium*, April 7-10. 2003
  43. Sherburn M.: *Geometric and Mechanical Modelling of Textiles*, PhD, University of Nottingham, <http://etheses.nottingham.ac.uk/303/1/thesis-final.pdf> 2007
  44. University of Nottingham: *TexGen*, University of Nottingham, 2011
  45. Zhou G., Sun X., Wang Y.: Multi-chain digital element analysis in textile mechanics, *Composites Science and Technology* 64(2), 239-244, 2004, doi: 10.1016/S0266-3538(03)00258-6
  46. Altair: *Multiscale Design*. <http://www.altair.com/> (2016)

# GEOMETRICAL MODEL OF A KNITTED FABRIC MADE FROM HYALURONAN BASED FIBERS

Tomáš Pitucha

Contipro a.s., R&D department, Dolní Dobrouč, Czech Republic  
Technical University of Liberec, Faculty of Textile Engineering, Liberec, Czech Republic  
[pitucha@contipro.com](mailto:pitucha@contipro.com), +420 467 070 361

**Abstract:** Hyaluronan is a linear polysaccharide that can be manufactured by wet spinning to the form of monofilament fibers. The natural hyaluronan is soluble in water; the solubility can be eliminated by chemical modification (acylation). Nevertheless fibers made from acylated hyaluronan significantly swell when dipped in water. Fabrics made from such fibers are substantially influenced by this swelling: as the fiber thickness increases the textile structure gets closer and tighter and the fabric dimensions change. A geometrical model of a warp knitted fabric has been created and relations between geometrical and structural characteristics of fibers, yarns and fabric have been determined via mathematical formulas. A set of knitted fabrics of different loop density have been manufactured from acylated hyaluronan fibers. Geometry of hyaluronan based fibers, yarns and fabrics in dry and wet state have been analyzed using various optical methods (optical microscopy, SEM, laser scanning). Experimental data have been compared with the results calculated using the geometrical model. The geometrical model enables to explain some causes of the dimensional changes of knitted fabrics due to swelling. Moreover the model seems to be a useful tool for description and prediction of the behavior of knitted fabrics made from fibers of high level of swelling.

**Key words:** Geometrical model, knitted fabric, hyaluronan fibers, swelling

## 1 INTRODUCTION

Hyaluronan is a natural polymer that is widely used in cosmetics and pharmacy. A wet spinning process has been adapted to create monofilaments both from the native hyaluronan and its derivatives [1, 2, 6]. Fibers from hyaluronan modified by fatty acids are insoluble in water but they strongly swell. Fabrics made from these fibers significantly shrink when dipped in water. It is known that the most important factors responsible for shrinkage of knitted fabrics are just swelling of yarn and the relaxation of internal stress imposed during the knitting process. Shrinkage of weft knitted fabrics was studied by Suh [7] who created a geometrical model that explains shrinkage principles of cotton jersey fabric. Structure of warp knitted fabrics has been intensively studied in the last decade and sophisticated 3D models have been developed [3, 5, 8] but influence of fiber swelling is out of their scope. The objective of this study has been to create a simple 2D geometrical model of the tricot-patterned warp knitted fabric that would respect an influence of fiber and yarn swelling and shrinkage.

Each level of the textile structure hierarchy can participate on the total dimensional changes of a fabric so that the total shrinkage/extension results from structural and geometrical changes of fibers, yarns and fabric. Swelling and shrinkage of fibers are connected with the rearrangement

of the polymer chains that interact with water and with the consequent relaxation of the stress imposed during fiber processing. Shrinkage on the yarn structure level relates mainly to the increase of the fiber diameter within the twisted yarn. Neckář [4] created a helical model of the yarn that explains dimensional changes of yarns based on the knowledge of fiber swelling and shrinkage.

### Geometrical model of tricot

Inputs of the proposed model include a dry yarn diameter  $D$ , wet yarn diameter  $D'$ , and yarn shrinkage. Geometry of yarn axis in the model is composed by combination of line segments and circular arcs as shown in Figure 1. The following formulas have been derived for the course distance  $a$  and wale distance  $b$ :

$$a = [L - 2R(\tan \gamma + \pi - \gamma)] \cdot \frac{\cos \gamma}{3} \quad (1)$$

$$b = 2a \cdot \tan \gamma + \frac{R}{\cos \gamma'} \quad (2)$$

where  $L$  is the yarn length in the loop,  $R$  is the radius of loop arcs (both needle and sinker) and  $\gamma$  is the angle between loop legs and the machine (wale) direction.

Based on this general model it is possible to determine 2 special cases, depicted on the Figure 2:



- a) If the fabric is stretched lengthwise the needle loop arcs touch the adjacent loop legs and the radius  $R$  match the value of the yarn diameter  $D$  ( $R=D$ );
- b) if the fabric is maximally relaxed the angle  $\gamma$  between loop legs and the wale direction match the value  $45^\circ$  ( $\pi/4$ ) and the radius  $R$  tend to be as large as possible so that loops touch adjacent loops and the following formula is valid:

$$R = R_{max} = \frac{L - 3D}{8 + \frac{3}{2}\pi} \quad (3)$$

A fabric during knitting on a raschel machine is stretched between the needles and take-down rollers so that the loops are stretched lengthwise and the adjacent wales tend to get closer to each other (see the Figure 3a). It is expected that this state can be approximated by the geometrical model on the Figure 2a.

As soon as the fabric is taken off the machine it can partially relax which results in shrinkage in the wale direction and extension in the course direction. When such fabric from modified hyaluronan is dipped in water (see the Figure 3b) the dimensional changes continue intensively: the fibers significantly swell and the loops become shorter, wider and round. This state of the fabric should correspond to the geometrical model on the Figure 2b.

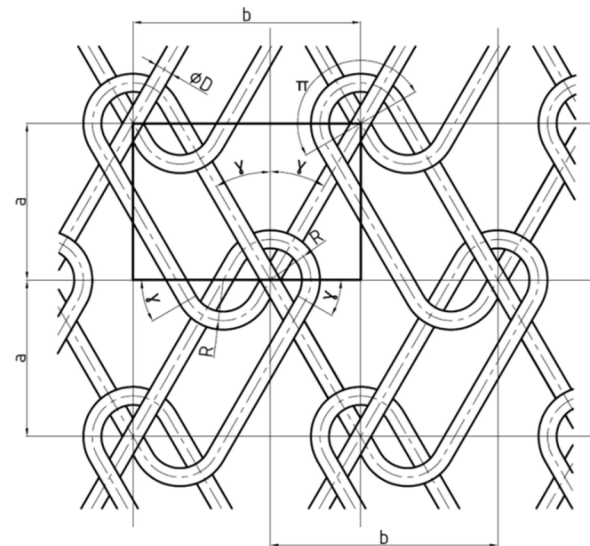


**Figure 1** 2D geometrical model of the tricot-patterned warp knitted fabric

If the fabric is consequently freeze-dried it keeps the loop geometry that is similar to the density of the fabric in the wet swollen state. So if we are able to determine the relation between the stretched state and the swollen state we should be able to set up the knitting process parameters (warp feeding and take-down speed) according to the desired loop density of the final freeze-dried fabric.

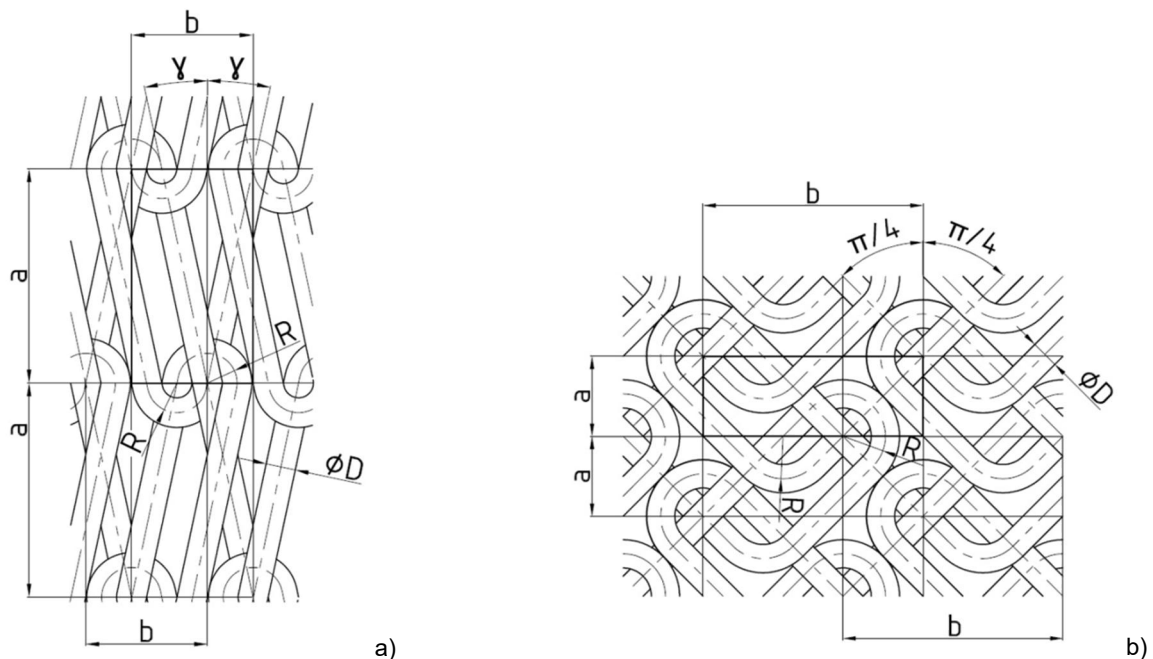


**Figure 2** Special cases of the tricot-patterned warp knitted fabric: a) geometrical model of the fabric stretched lengthwise. b) geometrical model of the relaxed fabric

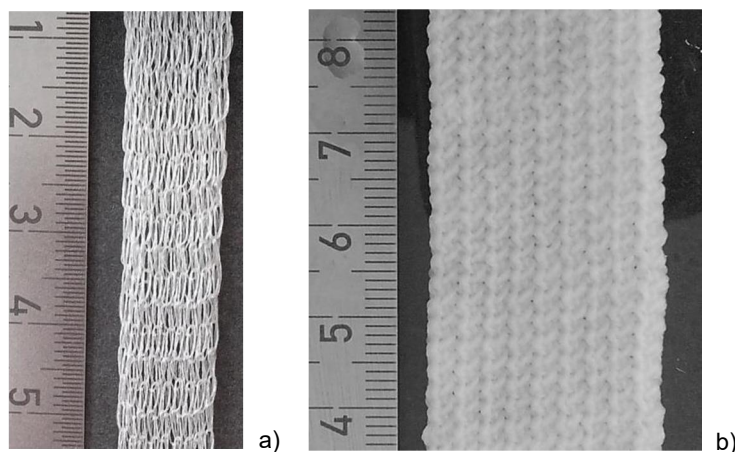


**Figure 3** Photos of the fabric made from the hyaluronan based fibers: a) on the knitting machine - stretched between needles and take-down rollers, b) in the swollen state - after wetting in demineralized water

## 2 EXPERIMENTAL

### 2.1 Materials

Fibers (monofilaments) of 11 tex fineness made from palmitoyl hyaluronan of molecular weight 320 kDa and degree of substitution 55% were employed (product of Contipro a.s.). Yarns composed from 3 monofilaments (300 twists/meter) were used for the knitting trials. The geometrical characteristics of the fibers and yarns are listed in the table 1.

**Table 1** Geometrical characteristics of the fibers and yarns

	Average value	Standard deviation	Coefficient of variation [%]
Fiber fineness [tex]	10.8	0.5	4
Dry fiber diameter [ $\mu\text{m}$ ]	109	9	8.5
Wet fiber diameter [ $\mu\text{m}$ ]	530	72	14
Fiber shrinkage [%]	12.4	2.2	18
Dry yarn diameter [ $\mu\text{m}$ ]	207	7	3.3
Wet yarn diameter [ $\mu\text{m}$ ]	733	64	8.8
Yarn shrinkage [%]	17.0	1.6	9.2

### 2.2 Methods

The fabric samples were made on the double needle bed warp knitting machine Comez DNB-80, gauge 12. All the samples had the same tricot pattern composed from two layers knitted simultaneously on the front and back needle bar and locked together by underlaps. Various loop densities of individual samples were reached by changing feeding and take-down speeds. Fabrics were washed in ethanol at 40°C for 2 x 20 min and dried at room temperature. Then the samples were immersed in demineralized water for 20 min, frozen at -20°C for 5 hours and freeze-dried for 16 hours (Lyophilizator Christ Alpha).

Diameter of dry fibers and yarns were determined using 4-direction laser scanning during rewinding of the fibers/yarns (Accuscan 6012). Diameters

of the wet (swollen) fibers and yarns were measured using optical microscopy (Nikon Eclipse Ci-L). Course and wale distances in the knitted fabric were determined as a reciprocal value of the corresponding loop densities; the loop densities were determined for the fabric at the machine (stretched between needles and taken-down rollers), for the relaxed fabric (without external stress) and for the wet fabric in the swollen state.

## 3 RESULTS AND DISCUSSION

### 3.1 Dimensional changes of the knitted fabric

Both the experimental and the theoretical values of the course distances are shown on the Figure 4. For each sample the course distance is maximal when the fabric is on the machine (the stretched state), after relaxation the distance decreases and after swelling is minimal. The curves calculated using the geometrical model shows the trend of the course distance in dependence on the yarn length in the loop. Experimental values of the fabric on the machine are near the corresponding model values of the stretched fabric and the experimental values of the wet fabric are near the corresponding model values of the swollen fabric.

The divergence between the theoretical and experimental values results mainly from the simplified loop shape geometry used in the model. The real fabric fixed on the machine during knitting is not so stretched in order that the loop legs would be perfectly straighten and the yarn arc would curve tightly over the yarn segments of the next loop. In case of the swollen state the important factors is the yarn shrinkage and especially increase of the yarn diameter. These changes result in considerable three-dimensional character of the knitted structure and the consumption of the yarn increases because the yarn has to crimp over and under the other yarn segments.

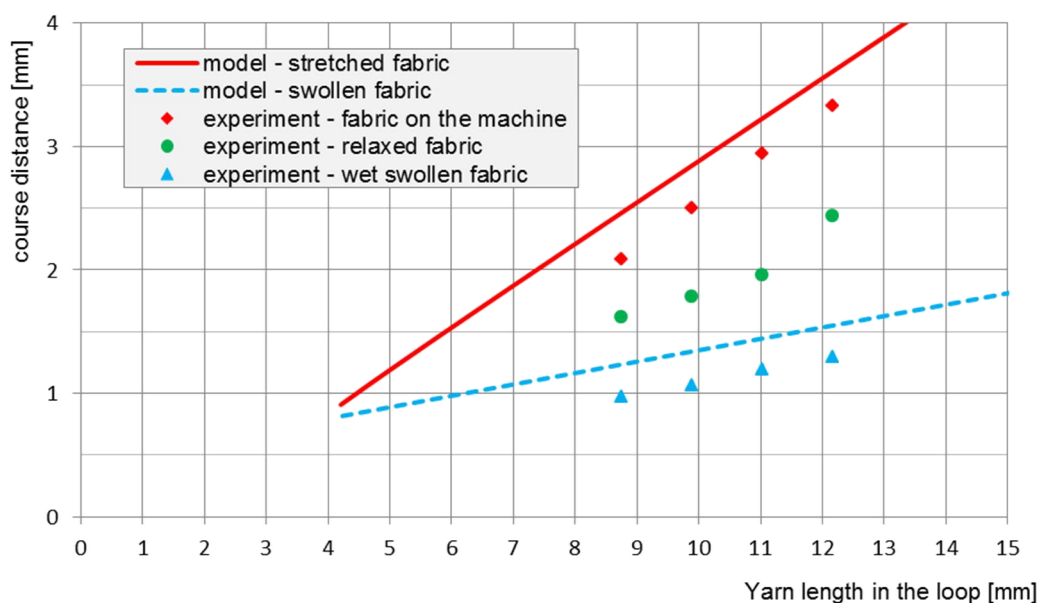


**Figure 4** Dependence of the course distance on the yarn length in the loop - comparison of the model and experimental data

When we calculate dimensional changes of the fabric samples between the swollen state and the stretched state (Table 2) we find out that the fabric shrinkage in the wale direction is not constant but increases with the yarn length in the loop. This result is logical because the larger loops have longer legs that can get round and transform themselves into parts of loop arc segments of higher diameter which results in decrease of the course distance.

**Table 2** Fabric shrinkage in the machine direction - dimensional changes between the stretched and swollen states, comparison of the theoretical and experimental results

Sample	Yarn length in the loop [mm]	Shrinkage in the wale direction [%]	
		model	experimental
A	8.74	50	53
B	9.88	53	57
C	11.02	55	60
D	12.16	57	61

### 3.2 Participation of individual structural levels

The experimental results prove that all three levels of the textile structure (fiber, yarn and fabric) participate markedly on the total shrinkage of the knitted fabric (see the Tables 1 and 2). Anyway the most important share pertains to the dimensional changes caused by the rearrangement of the knitted structure that lies in the change of the loop shape and size. Calculation of the dimensional changes using the geometrical model can be helpful to predict shrinkage of other variants of fabrics, e.g. made from fibers of different fineness or swelling rate.

## 4 CONCLUSIONS

A simple geometrical model of a warp knitted fabric has been developed and employed to explain shrinkage of fabrics made from hyaluronan based fibers. The fabric shrinkage is caused not only by the fiber and yarn shrinkage but mainly by changing of the loop geometry, esp. by increase of loop leg angle and the loop arc radius which is significantly supported by huge swelling of the used fibers. Both the model and experimental results show a similar dependence of the course distances on the yarn length in the loop. The model can be utilized for designing of fabrics that are made from fibers of high level of swelling.

## 5 REFERENCES

1. Betak J., Buffa R., Nemcova M., Pitucha T., et. al.: Endless fibres on the basis of hyaluronan selectively oxidized in the position 6 of the n-acetyl-d-glucosamine group, preparation and use thereof, threads, staples, yarns, fabrics made thereof and method for modifying the same, Patent. PCT/CZ2013/000157, WO2014082610 A1
2. Burgert L., Hrdina R., Masek D., Velebny V.: Hyaluronan fibres, method of preparation thereof and use thereof, Patent. PCT/CZ2011/000126. WO 2012089179 A1
3. Honglian C., Mingqiao G., Gaoming J.: Three-Dimensional Simulation of Warp-knitted Fabric, *Fibres and Textiles in Eastern Europe* 3(74), 66-69, 2009
4. Neckář B.: *Příze* (1<sup>st</sup> ed.), SNTL Praha, 1990
5. Renkens W., Kyosev Y.: Geometry modelling of warp knitted fabrics with 3D form, *Textile Research Journal* 81(4), 437-443, 2011
6. Scudlová J., Betak J., Wolfova L., Buffa R., et. al.: Fibres based on hydrophobized derivatives

of hyaluronan, method of their preparation and use, textiles on base thereof and use thereof, Patent. PCT/CZ2013/000158, WO2014082611 A1

7. Suh M.W.: A study of the Shrinkage of Plain Knitted Cotton Fabric, Based on the Structural Changes of the Loop Geometry Due to Yarn Swelling and Deswelling, Textile Research Journal 37(5), 417-431, 1967
8. Xu H.-Y., Chen N.-L., Jiang J.-H., Jin L.-X., Wang Z.-X.: 3D Simulation of Warp Knitted Structures with a New Algorithm Based on NURBS, Fibres and Textiles in Eastern Europe 1(109), 57-60, 2015

# WOVEN FABRIC STRUCTURAL PORE MODELS ANALYSIS

Brigita Kolčavová Sirková and Iva Mertová

Technical University of Liberec, Faculty of Textile Engineering, Department of Textile Technologies  
Studentská 2, 461 17 Liberec, Czech Republic  
[brigita.kolcavova@tul.cz](mailto:brigita.kolcavova@tul.cz), [iva.mertova@tul.cz](mailto:iva.mertova@tul.cz)

**Abstract:** This paper is focused on description of woven structural pore models and their basic geometrical, forces and deformation ratios in woven structure. Necessary regularities about the balance of variable forces, the transformation of binding element (cell), the achievable densities, stability weaving can be deduced from the description of relationships between the stress and the geometric changes in the binding cell. Study of geometric, strength and deformation ratios in woven fabric are based on definition of the basic binding element in a plain weave. The element of binding point in plain weave is part of the four basic structural pores of woven fabric. Definition of individual pores is based on the mutual interlacing of two neighbouring threads in the warp and in the weft direction. Dobby as well as jacquard pattern is possible to create by the various combinations of these structural pores in repeat.

**Key words:** Structure, pore, models, interlacing, warp, weft, force, deformation

## 1 INTRODUCTION

Woven fabric structure and its mechanical and end-use properties are given by planar and spatial geometry. Based on the geometry, it is possible to analyse the external and internal relations in woven fabric resulting by mutual relations entering thread systems. Planar geometry defines the basic structure of woven fabric, and is determined by the input parameters of the yarn as well as parameters of woven fabrics [1]. Among the priority parameters of the planar geometry we classify material fineness, thread density and weave. Spatial geometry is defined by the internal arrangement of threads in woven fabric relative to axis of the fabric, by force and deformation ratios in the binding element of woven fabrics, the transverse deformation of the threads, etc. Structural change of woven fabric given by mutual interlacing is based on four basic pores - structural pore models: pore type 1 (P1) - full interlacing, pore type 2 (P2) - partial interlacing, pore type 3 (P3) - doubling interlacing and pore type 4 (P4) - full float. Definition of individual pores is based on the mutual interlacing of two neighbouring threads in both the warp and in the weft direction [2]. On the basis of these pores it is possible to create all design solutions for dobby as well as jacquard woven fabrics.

## 2 GEOMETRICAL DISPOSITION, FORCES AND DEFORMATIONS IN THE BINDING ELEMENT OF WOVEN FABRIC

The whole process of weaving is the process of creating of binding points. Their dimensions and the tension gradually changes from the cloth fell in the forming zone as far as some place of the steady state inside of fabric. The structure of the formed

fabric is determined by a) the quantity of weft, which is inserted into the binding point, b) tension which is formed in weft during insertion, c) the tension of warp [3].

Study of geometric, strength and deformation ratio in the fabric is based on description of the basic binding element in a plain weave. Plain interlacing is formed only mutual crossing of warp and weft threads, thereby is limiting structure of woven fabric. All other weaves are looser weaves with specific float part. Float part is non-interlacing length of threads, where the position of float is given by the effect of woven fabric (warp and weft effect). Study of basic element of the plain weave can be used for clarification and explanation of action during weaving and forming of woven fabric. During weaving, the warp threads are under tension  $Q$  (we can analyse the tensile strength  $S_Q$  in centreline of warp threads) and weft threads under tension  $U$  (we can analyse the tensile strength  $S_U$  in centreline of weft threads) and waviness ratio of warp and weft systems is given by the ratio of these two forces [3].

Basic element of binding point in woven fabric will be evaluated in the steady state, which is assumed symmetrical steady element, see Figure. 1, apart from the forming zone (on the fell of woven fabric), where the binding point is asymmetrical in the warp direction. For simplicity, the evaluated element of binding point, due to the shape of the input yarn, based on the circular cross section. Geometric ratios ( $GE$ ) in woven fabric are determined by the areas of one interlacing point; its dimension is given by distances  $A \times B$ . Warp and weft are in binding point defined by waviness having a height of binding wave  $H_{1,2}$  by the shape of the binding wave as well as the resulting rake angle of binding waves, see Figure 1.

Individual parameters of geometric ratios are possible to write as vector of geometric parameters  $GE$ , see equations (1).

Force ratios ( $FO$ ) are described by force equations for a given geometrical ratios of binding point, see Figure 1. Ratios in threads interlacing of woven fabric are determined by tension  $Q$  in the plane of warp threads, and the tensile force  $S_2$  in the centreline of the weft thread. From the tension of warp thread interlacing  $Q$  and interlacing angle  $\varphi$ , which is known from the vector of structures can be calculated tensile force in the centreline of the warp threads  $S_1$  and the normal force  $N_1$  warp to weft. From the reaction of weft (where is valid  $N_2 = -N_1$ ) can be expressed tensile force in the weft  $S_2$ .

From the force  $S_2$  and the known angle  $\psi$  can be expressed tensile force in the direction

of the temples  $U$ . At the same can be expressed from tensile force  $S_2$  elongation of the weft  $\varepsilon_2$  in the binding element. Based  $\varepsilon_2$  and extension of the length of the thread  $L_2$  in binding wave may be expressed crimp of threads, which means expressing consumption of weft converted to untensioned state [3]. Force ratios are given by vector or forces parameters in structure of woven fabric, see equations (2).

Deformation - Force ratios ( $DF$ ) based on the fundamental relation between the tensile force on the border of the binding element and the arising extension of the thread, see Figure 1. Deformation - Force ratios is given by vector of deformation parameters in structure of woven fabric, see equations (3).

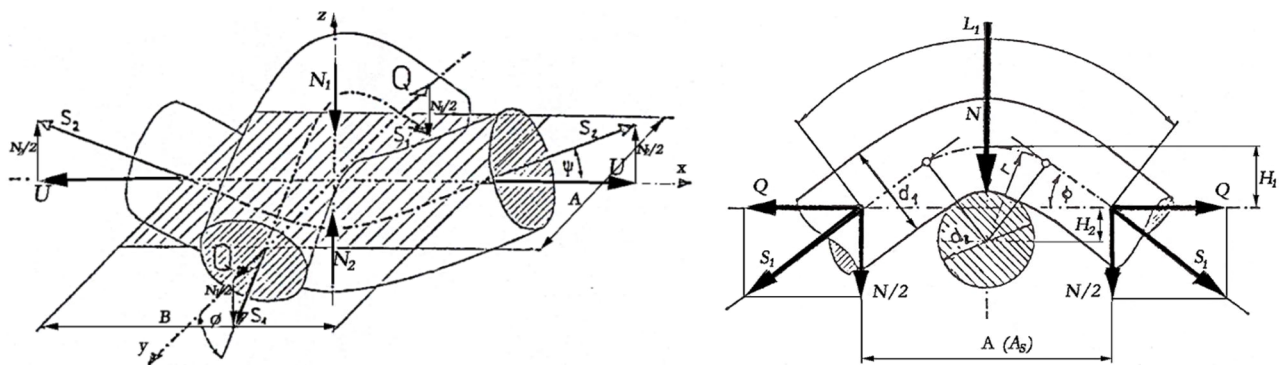


**Figure 1** Geometrical and forces ratios in binding element of woven fabric

$$\begin{aligned}
 GE = & \begin{bmatrix} d_s = \frac{d_1 + d_2}{2} \\ A = \frac{1}{D_1} \\ B = \frac{1}{D_2} \\ H_1 = e_1 \cdot d_s \\ H_2 = e_2 \cdot d_s \\ e_2 = 1 - e_1 \\ \varphi = \arctg\left(\frac{dy}{dx}\right) \\ \psi = \arctg\left(\frac{dy}{dx}\right) \end{bmatrix} \begin{pmatrix} d_s = \text{mean diameter of thread; } d_1 = \text{diameter of end} \\ d_2 = \text{diameter of pick} \\ A = \text{distance of ends; } D_1 = \text{density of ends} \\ B = \text{distance of picks; } D_2 = \text{density of picks} \\ H_1 = \text{height of binding wave of warp; } e_1 = \text{warp waviness} \\ H_2 = \text{height of binding wave of weft; } e_2 = \text{weft waviness} \\ \varphi = \text{angle of ends interlacing is given by shape of binding wave} \\ \psi = \text{angle of picks interlacing is given by shape of binding wave} \end{pmatrix} \quad (1)
 \end{aligned}$$



$$FO = \left[ \begin{array}{l} Q \\ S_1 = \frac{Q}{\cos \varphi} \\ S_2 = \frac{U}{\cos \psi} \\ N_1 = 2.Q.tg \varphi \\ N_1 = -N_2 \\ U = \frac{N_2}{2.tg \psi} \end{array} \right] \left( \begin{array}{l} Q = \text{force ( tensile stress) in warp threads} \\ S_1 = \text{final force in end on interface of binding elements} \\ S_2 = \text{final force in pick on interface of binding elements} \\ N_1 = \text{the normal force of warp thread} \\ N_2 = \text{the normal force of weft thread} \\ U = \text{force ( tensile stress) in weft direction} \end{array} \right) \quad (2)$$

$$DF = \left[ \begin{array}{l} L_1 = \int_0^{T_1} \sqrt{1 + \left( \frac{dy}{dx} \right)^2} dx \\ L_1 = A + \Delta l_1 + \Delta l_1 \\ l_1 = A + \Delta l_1 \\ L_2 = \int_0^{T_2} \sqrt{1 + \left( \frac{dy}{dx} \right)^2} dx \\ L_2 = B + \Delta l_2 + \Delta l_2 \\ l_2 = B + \Delta l_2 \\ \Delta l_1 = L_1 - l_1 (\text{respectively}) \\ \Delta l_1 = \frac{S_1}{E_1.F_1} . l_1 \\ \Delta l_2 = L_2 - l_2 (\text{respectively}) \\ \Delta l_2 = \frac{S_2}{E_2.F_2} . l_2 \\ \varepsilon_1 = \frac{\Delta l_1}{l_1} \\ \varepsilon_2 = \frac{\Delta l_2}{l_2} \\ S_1 = E_1.F_1.\varepsilon_1 \\ S_2 = E_2.F_2.\varepsilon_2 \end{array} \right] \left( \begin{array}{l} L_1 = \text{lenght of warp thread in binding wave with elongation of end } \Delta l_1 \\ l_1 = \text{inserted length of pick during weft insertion with over supply of weft } \Delta l_1 \\ L_2 = \text{lenght of weft thread in binding wave with elongation of end } \Delta l_2 \\ l_2 = \text{inserted length of pick during weft insertion with over supply of weft } \Delta l_2 \\ \Delta l_1 = \text{elongation of end,} \\ E_1.F_1 = \text{rigidity of warp thread in tension where} \\ E_1 = \text{Young' s modulus of thread,} \\ F_1 = \text{cross - section thread} \\ \Delta l_2 = \text{elongation of pick,} \\ E_2.F_2 = \text{rigidity of weft thread in tension where} \\ E_2 = \text{Young' s modulus of thread,} \\ F_2 = \text{cross - section of thread} \\ \varepsilon_1 = \text{elongation of end after interlacing of threads} \\ \varepsilon_2 = \text{elongation of pick after interlacing of threads} \\ S_1 = \text{final force in end on interface of binding elements} \\ S_2 = \text{final force in pick on interface of binding elements} \end{array} \right) \quad (3)$$

### 3 DEFINITION AND ANALYSIS OF STRUCTURAL PORE MODELS OF WOVEN FABRIC INTERLACING

The method of mutual interlacing of the two sets of threads in woven fabric gives the weave. The correct choice of weave in woven fabric is important not only for the construction of the fabric, but it adds additional necessary mechanical and end-use properties (strength, elongation, permeability, roughness, feel, flexibility, etc.). Weave in woven fabric are usually illustrates by patterns, which show the fabric design and way of interlacing. Patterns are usually drawn on squared paper as a sequence of dark and light pixels (show the position of the warp threads relative to the median plane of the fabric) [4]. Structural change in woven fabric formed by weave is based on definition of four basic pores - structural models in the weave repeat. In terms of structural pores are distinguished: Pore type 1 - full interlacing, Pore Type 2 - partial interlacing, Pore type 3 - doubling and Pore Type 4 - full float.

In the description of the planar geometry of woven fabric weave, besides writing of weave in pattern paper, it is possible to use a weave pattern depiction based on the matrix of structural pore models. The size of the matrix is based on the size of the pattern repeat. The number of warp threads in a pattern repeat no determines the number of rows and the number of weft threads nu number of columns. Definition of individual pores is based on mutual interlacing of two neighbouring threads in the warp direction and in the weft direction.

On the basis of these pores it is possible to create all structural binding solutions as dobby so jacquard fabrics. Repeat of dobby weave, jacquard repeat of the pattern is based on the distribution of the individual pores in the area of pattern. The relative frequency of each RP1-4 pores in the area of the pattern (weave repeat) influences the behaviour of woven fabric during weaving as well as the resulting end-use and mechanical properties.

Definition of woven fabric structure of the binding element of structural pores in terms of geometric, strength and deformation ratios is identical with the abovementioned general relationships defined for the binding element in a steady state, see equation fabric structures (1-3). Expressing the relative frequency of each structural pore in the pattern repeat is given by equations (4).

$$RP1 = \frac{\sum P1}{n_o \cdot n_u} \quad RP2 = \frac{\sum P2}{n_o \cdot n_u} \quad (4)$$

$$RP3 = \frac{\sum P3}{n_o \cdot n_u} \quad RP4 = \frac{\sum P4}{n_o \cdot n_u}$$

Full interlacing structural pore model is illustrated in Figures 2-3. It is only one pore which is given by crossing point only. The final length of binding weave is higher the input length of inserts threads. The final forces in threads we obtain for each thread in repeat. Full interlacing pore has maximal compactness of fabric. Plain weave is created only with this pore.

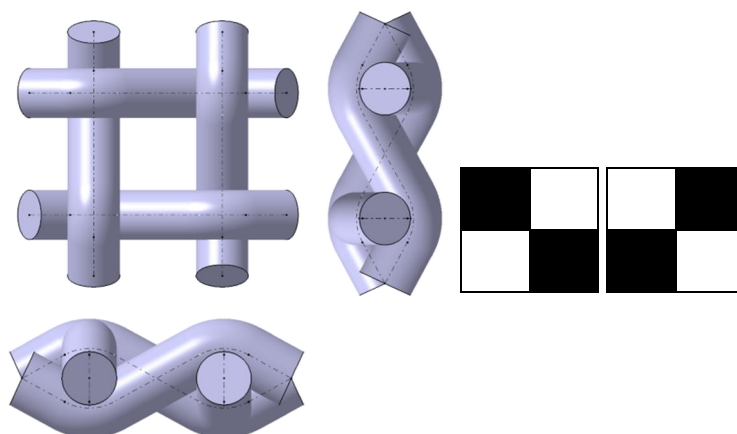


**Figure 2** Woven fabric structural pore model “type 1 (P1)” – full interlacing pore. Spatial structure of pore model “type 1” (left side), positive and negative areal depiction of pore model “type 1” (right side)



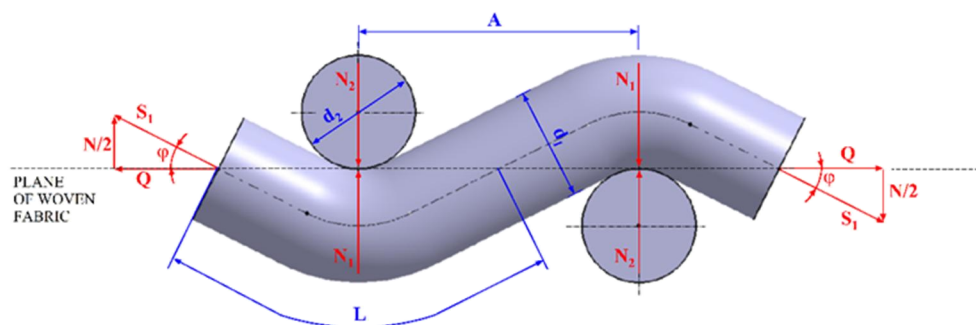


**Figure 3** Geometrical and forces depiction of woven fabric structural pore model P1, (definition is identical for longitudinal and transversal cross section of woven fabric)

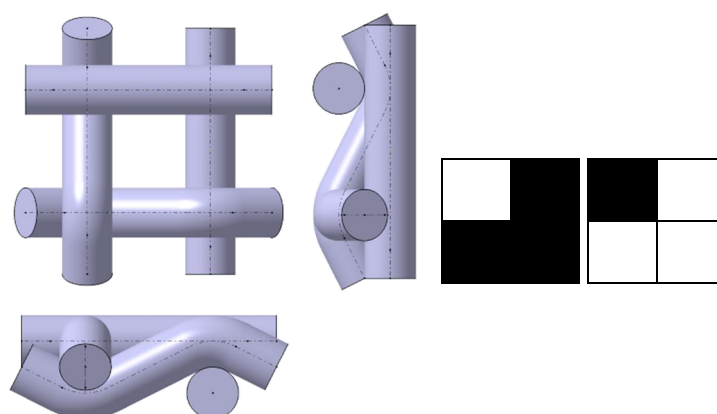


**Figure 4** Woven fabric structural pore model "type 2 (P2)" – partial interlacing pore. Spatial structure of pore model "type 2" (left side), positive and negative areal depiction of pore model "type 2" (right side)

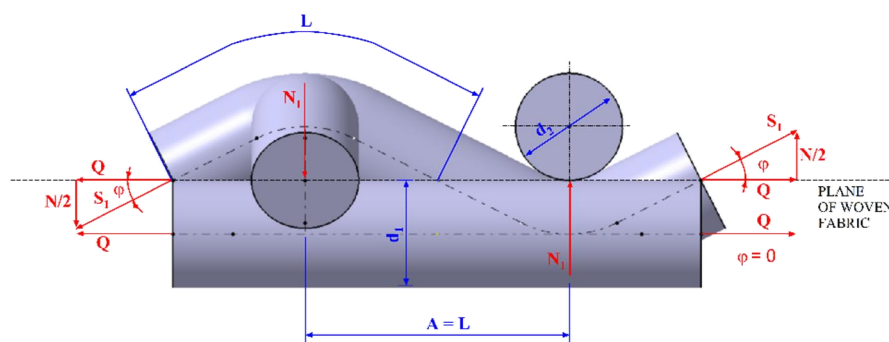


**Figure 5** Geometrical and forces depiction of woven fabric structural pore model P2, (definition is identical for longitudinal and transversal cross section of woven fabric)

Partial interlacing structural pore model is described in Figures 4-5. One thread in same cross section is created by interlacing of threads and one in the same direction is full float. Woven fabric structure compactness is increasing in comparison with pores 3, 4. Forces and deformations vector is possible to write identical for both cross section of woven fabric (only with definition for weft, warp). This pore in woven fabric structure is possible to use only with combination with the others pores. Double effect structural pore model is described in

Figures 6-7. Woven fabric structure has the compactness in one direction only. The other direction is given by interlacing of threads. The forces reaction is possible to see in the Figure 7. First figure illustrates one direction of cross section of woven fabric a second figure illustrates the other direction of cross section of woven fabric. Final force in threads is created only in second case. This pore in woven fabric structure is possible to use only with combination with the others pores.

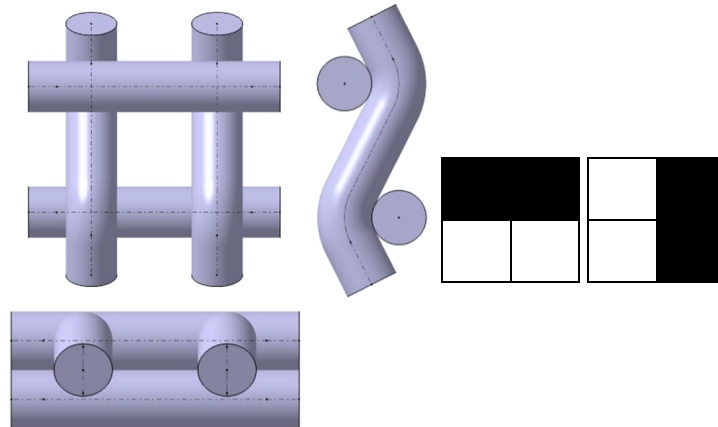


**Figure 6** Woven fabric structural pore model “type 3” – double effect pore. Spatial structure of pore model “type 3” (left side), positive and negative areal depiction of pore model “type 3” (right side)

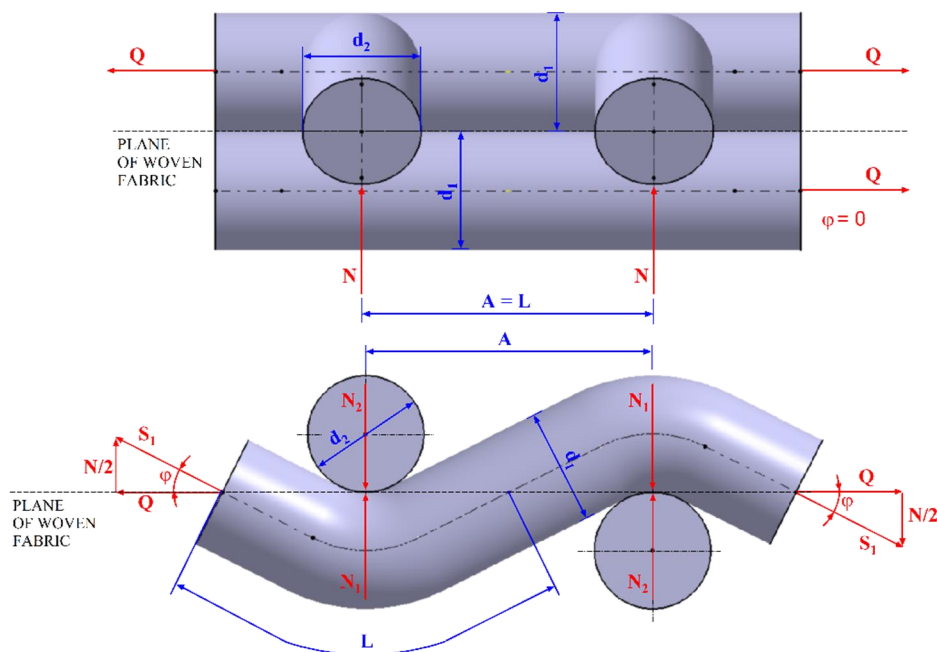


**Figure 7** Geometrical and forces depiction of woven fabric structural pore model P2

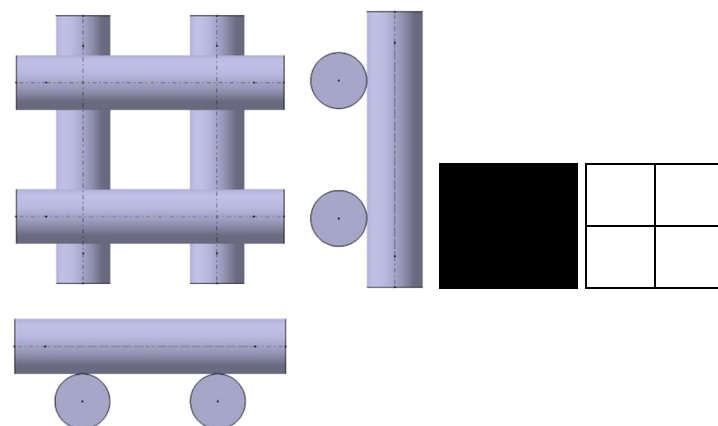


**Figure 8** Woven fabric structural pore model “type 2 (P2)” – partial interlacing pore. Spatial structure of pore model “type 2” (left side), positive and negative areal depiction of pore model “type 2” (right side)

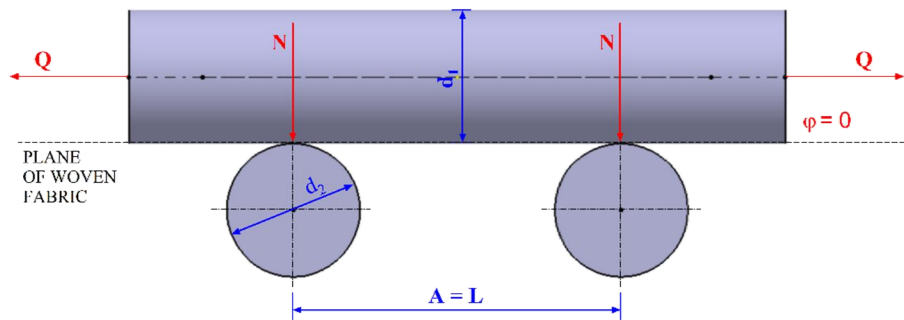


**Figure 9** Geometrical and forces depiction of woven fabric structural pore model P1, (definition is identical for longitudinal and transversal cross section of woven fabric)

Full float structural pore model is described in Figures 8-9. It is only one pore where we do not have interlacing of threads. Woven fabric structure has not compactness. On the basis of forces vectors view point the compactness is given by angel of interlacing and input tension of warp threads  $Q$ . On the basis these parameters create the final force in thread. This pore in woven fabric structure is possible to use only with combination with the others pores. When the weave repeat is increasing then is increasing the number of pore 4.

#### 4 EVALUATION OF THE IMPACT OF STRUCTURAL PORE MODELS ON WARP AND WEFT CRIMP

By mutual interlacing of warp and weft threads arises waviness of threads. Subsequently, threads have a greater length of yarn than the threads dimension of the final fabric in the appropriate direction. This difference in length of yarn is expressing the threads crimp. The thread crimp is expressed in a percentage from the dimension of the fabric. The length of yarn in cross section is given of position of yarn in interlacing. Pore 1, full interlacing pore, has maximal length of yarn in repeat which is possible to create in weave. Pore 4, full float pore, it is opposite pore with minimal length of yarn in repeat.

Basic parameters of woven fabric structure and weaving process with influence on crimp threads in the fabric are: input parameters of yarn (yarn fineness), mutual interlacing of threads, weave –

distribution of structural pores in repeat, the relative frequency of each RP1-4 pores in the area of the pattern, sett threads in fabric, thread waviness in the fabric, tension of warp, etc.

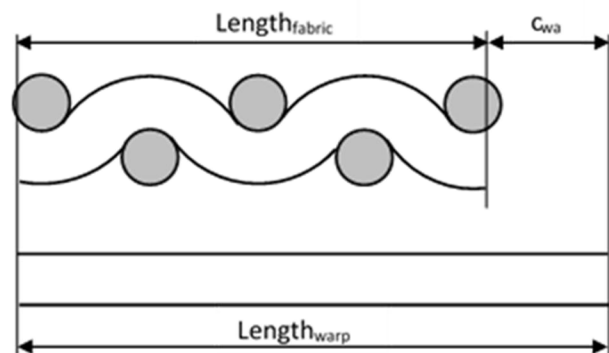


**Figure 10** Depiction of threads interlacing - expression of thread crimp

Warp crimp  $s_{wa}$  and weft crimp  $s_{we}$  is given by equation (5):

$$c_{wa} = \frac{Length_{warp} - Length_{fabric}}{Length_{fabric}} \cdot 10^2 \quad (5)$$

$$c_{we} = \frac{Length_{weft} - Width_{fabric}}{Width_{fabric}} \cdot 10^2$$

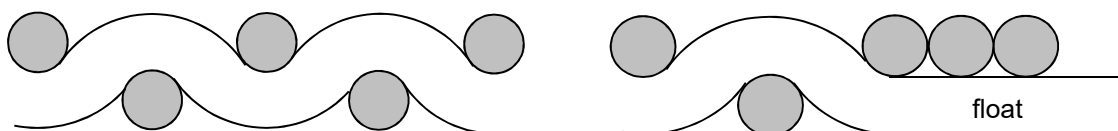


**Figure 11** Influence of weave on warp and weft crimp. Depiction of plain weave (max crimp of weave) (left side), depiction of looser float weave (float = min crimp) (right side)

Parameters of experimental polyester samples for evolution of structural pore models influence on warp and weft crimp are given in Table 1. Spatial

structure of individual samples weaves and areal depiction of weaves with pores definition in area are demonstrated by Figures 12-14.

**Table 1** Basic parameters of experimental woven fabric samples

Fabric number	Woven fabric weave	Yarn count [tex]		Thread sett [1/cm]	
		warp	weft	warp	weft
1	Plain weave	25	25	19	19
2	Twill 1/5 Z	25	25	19	19
3	Sateen 1/5	25	25	19	19
4	Plain	25	25	22.4	22.4
5	Twill 1/5 Z	25	25	22.4	22.4
6	Sateen 1/5	25	25	22.4	22.4
7	Plain weave	25	25	26	26
8	Twill 1/5 Z	25	25	26	26
9	Sateen 1/5	25	25	26	26

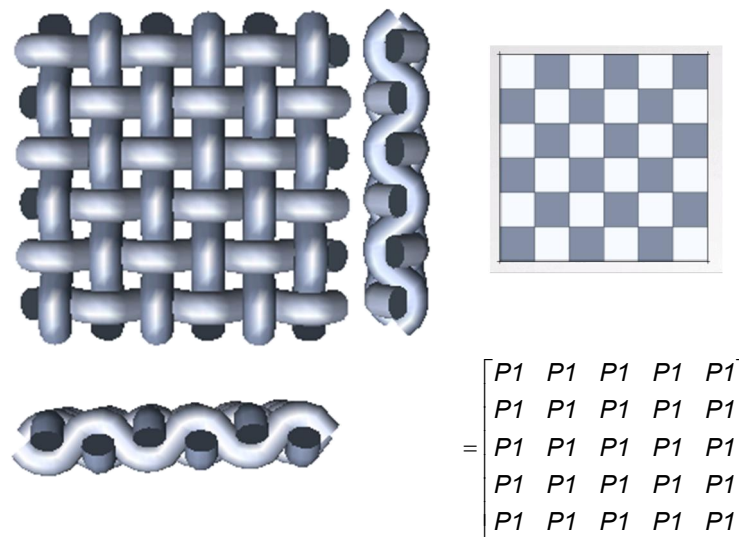


**Figure 12** Analysis of structural pore models in plain weave. Spatial structure of plain weave (left side), areal depiction of plain weave with pores definition in area (right side)

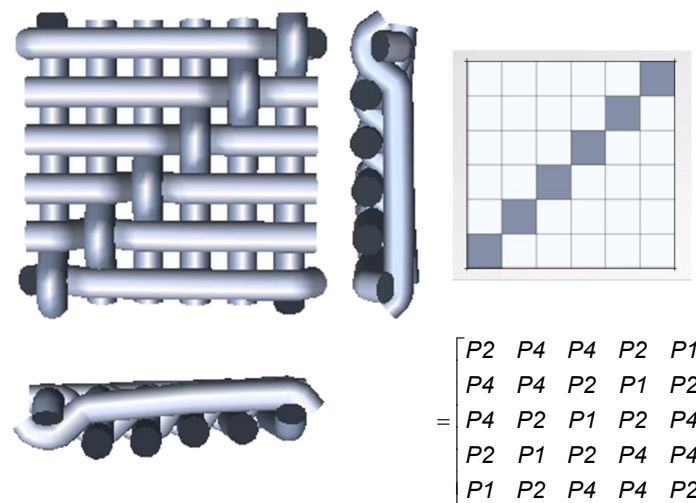


**Figure 13** Analysis of structural pore models in twill weave. Spatial structure of plain weave (left side), areal structure of plain weave with pores definition in area (right side)

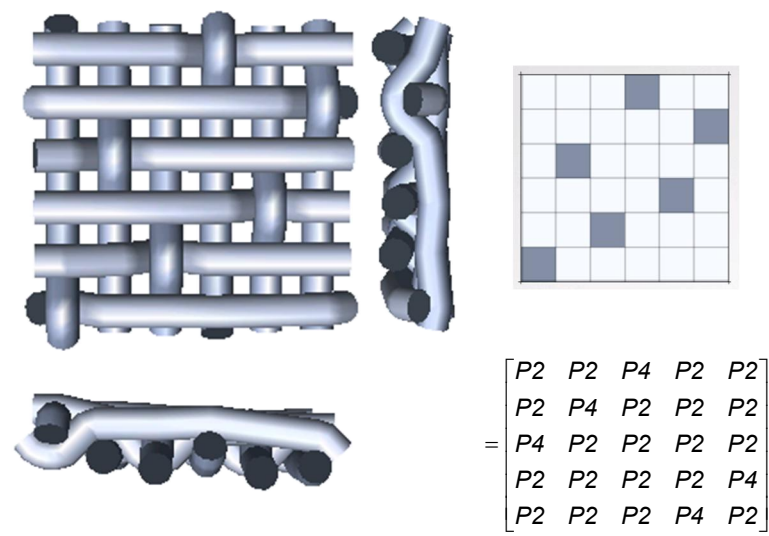


**Figure 14** Analysis of structural pore models in satin weave. Spatial structure of plain weave (left side), areal structure of plain weave with pores definition in area (right side), weave was created in CAD system EAT at FT TUL

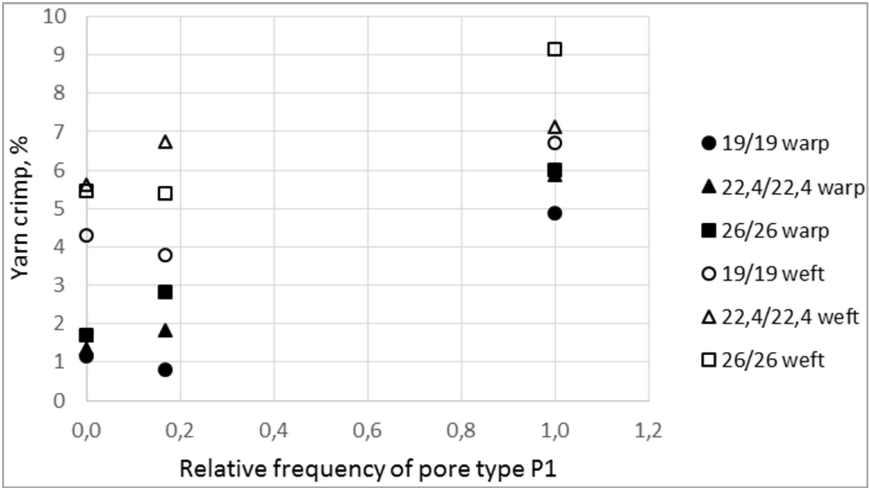


**Figure 15** Dependence between yarn crimp and relative frequency of pore type P1

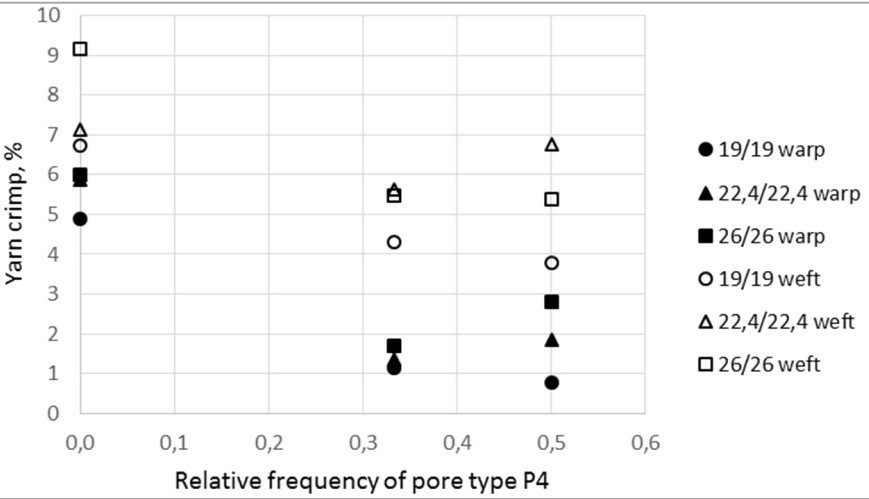


**Figure 16** Dependence between yarn crimp and relative frequency of pore type P4

**Table 2** Relative frequencies of pores and yarn crimp

Fabric number	Woven fabric weave	Relative frequency of pores (pore P3=0)			Yarn crimp [%]	
		P1	P2	P4	warp	weft
1	Plain 1/1	1.00	0.00	0.00	4.89	6.72
2	Twill 1/5	0.17	0.33	0.50	0.79	3.79
3	Sateen 1/5	0.00	0.67	0.33	1.16	4.30
4	Plain 1/1	1.00	0.00	0.00	5.87	7.13
5	Twill 1/5	0.17	0.33	0.50	1.84	6.75
6	Sateen 1/5	0.00	0.67	0.33	1.35	5.61
7	Plain 1/1	1.00	0.00	0.00	6.00	9.15
8	Twill 1/5	0.17	0.33	0.50	2.81	5.39
9	Sateen 1/5	0.00	0.67	0.33	1.71	5.46

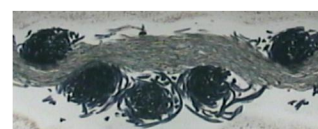
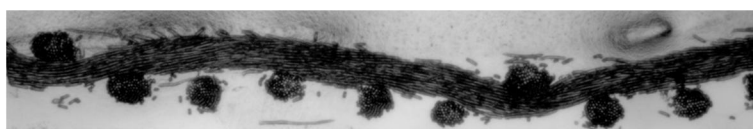
**Figure 17** Illustration of spatial structure of float weave for analysing of shape of float part

Table 2 shows the relative frequencies of pores and warp and weft crimp. The number of pores in a pattern repeat of the individual interlacing is shown in Figures 9 to 11. Relative frequency was calculated according to equation (3). Crimp of threads is shown in Table 2. The resulting values of thread crimp are obtained by evaluation of tensile operating curves of yarn before weaving and yarns removed from the fabric. The experiment is described in detail in [5]. The Table 2 presents only mean values of threads crimp.

In the graph of Figure 15 shows the growing dependence of warp and weft crimp on the relative frequency of the pore type P1. This trend was anticipated. Pore type 1 is a full interlacing pore where the waviness of warp and weft threads is greatest. Conversely, pore type 4 contains only from float sections this is full float pore, see Figure 8. We can therefore assume that number of pore type 4 is increasing then the final threads crimp is decreasing. Also is decreasing the compactness of woven fabrics. The relationship between the threads crimp and the relative frequency of the pores of type 4 can be seen in Figure 16.

## 5 CONCLUSIONS

Mutual interlacing of woven structure is given by weave. It is possible to select only four structural pore models for creation of each type of woven fabric design. As is possible to see from above mentioned description of structural, forces and deformation vectors the mutual interlacing and yarn elongation in binding point is given by structural pore type 1. When the number of structural pore model 1

in repeat is increasing then is increasing elongation of the yarn in binding point, final yarn crimp is increasing too. The compactness of woven fabrics is increasing too. If we want to keep the compactness of woven fabric, at reducing the pore 1, it is necessary to increase the thread density. This is a case of float weave. In the repeat of float weave the number of pore 1 is decreasing. The length of yarn in cross section of woven fabric is a sum of individual lengths of yarn parts in individual pores. Theoretically the length of yarn in cross section is increasing on the basis of the shape of binding wave. Theoretical pore models use for calculation and modelling the linear part for substitution of float part. From the Figure 17 is possible to see the construction of woven fabric can influence the final shape as well as the yarn length in binding wave in float part.

## 6 REFERENCES

1. Nosek S.: The theory of weaving process, part I., Dům techniky ČSVTS, 1988
2. Kolcavová Sirková B., Mertová I.: Prediction of woven fabric properties using software protkatex, Autex Research Journal 13(1), 11-16, 2013
3. Nosek S.: The structure and geometry of the woven fabrics, Liberec 1996
4. Backer S.: The relationship between the structural geometry of textile fabric and its physical properties, Part IV: Interstice geometry and air permeability, Textile Research Journal 17(10), 703-714, 1951
5. Mertová I., Neckář B., Ishtiaque S.M.: New method to measure yarn crimp in woven fabric, Textile Research Journal 86(10), 1084-1096, 2016



# STRUCTURAL AND THERMAL-MECHANIC PROPERTIES OF FILAMENTS PRODUCED FROM SHAPE MEMORY POLYMERS

Selcuk Aslan and Sibel Kaplan

Suleyman Demirel University, Textile Engineering Dept., Isparta, Turkey  
[selcukaslan0444@gmail.com](mailto:selcukaslan0444@gmail.com)

**Abstract:** In this study, shape memory polyurethane (SMPU) fiber was spun by wet spinning process and chemical/mechanical characterization was carried out. SMPU solutions were prepared with two different concentrations (20 and 25%) and three different coagulation bath concentrations (0, 1 and 3%). Influences of solvent and coagulation bath concentrations on mechanical, thermal and shape memory performances of fibers were investigated. For this aim, differential scanning calorimetry (DSC), dynamic mechanical analysis (DMA) and mechanical tests were conducted. DSC and DMA analysis results show that shape memory polyurethane filaments have a glass transition temperature about 35-40°C and solvent concentrations in coagulation bath did not have a remarkable effect on glass transition temperature of filaments. SMPU fibers showed good tensile performance with an average tenacity of 1.74 cN/tex and elongation at break of 1343%. Thermo mechanical test results showed that all shape memory filaments have good shape memory effect with recovery and fixity ratios up to 91% and 71% respectively.

**Key words:** shape memory polyurethane, wet spinning, characterization, glass transition temperature, shape memory behavior

## 1 INTRODUCTION

Shape memory polymer (SMP) have gained much popularity because of their special capability to return their original (permanent) shapes from a temporary shape under appropriate external stimulus such as heat, light, pH, moisture etc. [1-4]. When compared to other shape memory materials, SMPs have been widely studied and used in academic researches and industrial applications owing to its lightweight, good processing ability, high shape recoverability and large range of shape recovery temperature [5, 6]. Nowadays, most studies of SMPs focus on thermal induced SMPs because of their wide possible applications in different fields such as textile, engineering and biomedical devices [7-9].

Shape memory polyurethanes (SMPU) are the most notable kind of SMPs and they have the advantage of broad switch temperature (glass transition or melting transition) by changing soft segment and hard segment type and contents [3, 10]. SMPUs are phase separated due to the thermodynamic incompatibility between hard and soft segments. Thus, they exhibit remarkable shape memory effect. Various applications of shape memory polymers with different forms such as fiber, yarn, film have been used in textile field. In recent years, many researchers have focused on development of functional fibers and smart textile products with shape memory effects [1, 2, 4, 6-8, 11-13].

In this study, shape memory fibers were spun from SMPUs by wet spinning and their mechanical,

thermal and shape memory behaviors were investigated.

## 2 EXPERIMENTAL

### 2.1 Materials

Pellet-type MM-3520 SMPU (SMP Technologies Inc. Japan) was used for production of shape memory fibers (SMF). Shape memory polymer solution was prepared with N, N-dimethylformamide (DMF) [1] as solvent and shape memory fibers were spun by wet spinning.

#### Preparation of SMPU fibers

Shape memory fibers were spun by wet spinning method with DMF as solvent of polymer solutions. After some pre-trials, solid concentrations of the SMPU solution in DMF were adjusted to 20% and 25% to meet the viscosity requirements for wet spinning process. For investigating the effects of solvent concentration of coagulation bath on mechanical and shape memory effect of SMPU fiber, 0%, 1% and 3% concentrations were applied. SMPU solution is extruded through single spinneret capillary hole horizontally through a coagulation bath with arranged concentrations to diffuse out the solvent with a spinning speed of 3.2 m/min. Mono-filament which is formed in coagulation bath are taken up to a second bath including water for removal of residual DMF. Then, the SMPU filament was wound with 90 rpm on a cylindrical bobbin. Totally, six type of SMPU fibers with different parameters were produced (Table 1).

## 2.2 Methods

Thermal properties of the prepared SMPU filaments were determined using a differential scanning calorimeter (DSC) device with nitrogen as purge gas. First, SMPU sample was cooled to -30°C at the cooling rate 10°C/min, then the polymer was heated from -30°C to 240°C at 10°C/min heating rate. Pellet type SMPU polymer was also investigated by DSC. The heat flow change with increasing temperature was recorded. The dynamic mechanical properties of the shape memory filaments were determined by using dynamic mechanical analysis (DMA) device at a frequency of 2 Hz. The gauge length for each filament between the clamps was 15 mm and temperature was scanned from -120°C to 200°C with 2°C/min heating rate.

Tensile test of the SMPU fibers was carried out with a Lloyd Tensile Testing Machine (LR5K) according to ASTM D2236. All tests were conducted under standard atmospheric conditions (20°C and RH 65%).

**Table 1** Production details and mechanical characteristics of SMPU filaments

Yarn code	Polymer concentration in solution [%]	Coagulation bath concentration [%]	Linear density [tex]
SMPU200	20	0	55
SMPU201	20	1	45
SMPU203	20	3	68
SMPU250	25	0	74
SMPU251	25	1	71
SMPU253	25	3	81

The thermo-mechanical cyclic tensile test was conducted to investigate the shape memory behavior of shape memory filaments. Test was performed on Lloyd tensile tester (AMETEK Test&Calibration Instruments, UK) within a temperature controlled chamber. The fiber gauge length was 25.4 mm. Steps of a typical thermo-mechanical cycle test procedure for shape memory filaments are as follows:

- I) The fiber was initially stretched to 100% elongation ratio at 40°C with a speed of 100 mm/min, which is above the glass transition temperature (switch temperature) of filaments.
- II) The sample is cooled down to 22°C and temperature was maintained for 15 minutes to fix temporary elongation.
- III) The upper clamp was returned to original position and the filament shrank from 100% strain ( $\epsilon_m$ ) to strain after unloading at 22°C ( $\epsilon_u$ ) because of instant elastic recovery.
- IV) Sample was heated to 40°C again to allow shape memory recovery enabling the filament elongation returning to residual strain ( $\epsilon_p$ ) [10].

After the cycle was completed, another cycle began and a total of three cycles were carried out in order to investigate the shape memory effect of filaments.

## 3 RESULTS AND DISCUSSION

### 3.1 Thermal property analysis of shape memory filaments

The glass transition temperature of the shape memory polyurethane was determined by using differential scanning calorimetry (DSC) and results are shown in Table 2. Generally, glass transition temperature is determined from the second heating cycle to provide  $T_g$  value independent of the thermal history during processing. In the second heating scan, glass transition of soft segment of shape memory polyurethane filaments can be found between the range 36.43-37.37°C. This glass transition is used as the switch temperature to fix the shape of the filament (below and above the thermal transition temperature).

### 3.2 Dynamic mechanical analysis of shape memory filaments

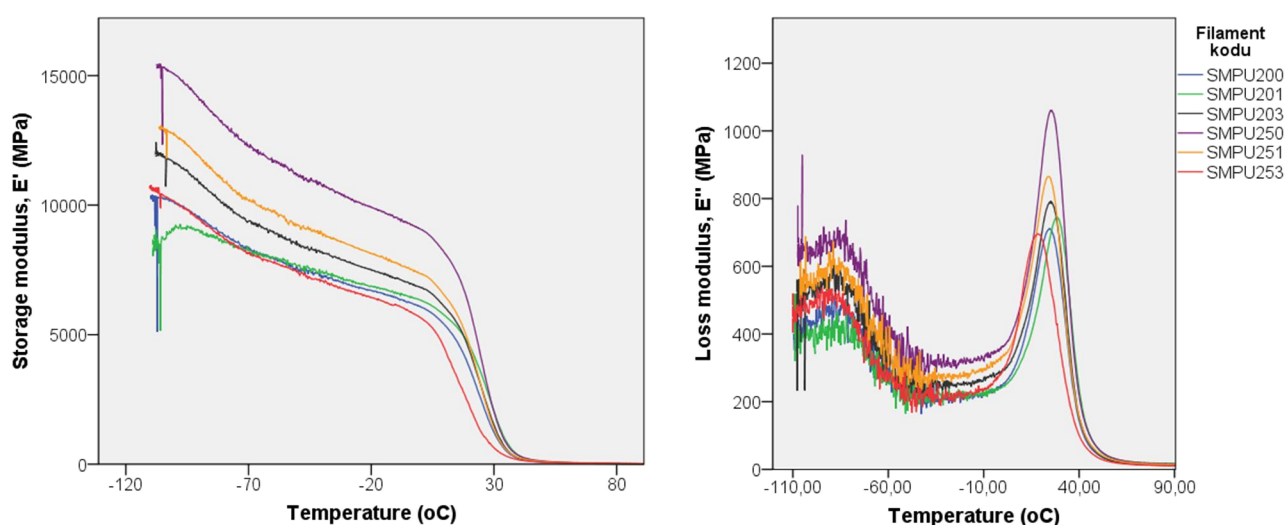
The storage modulus, loss modulus and phase angle results of shape memory filaments are shown in Figure 1 and Figure 2 respectively. Elasticity of shape memory filaments is directly related to density of crosslinks contained in the structure and elasticity properties are reduced with increasing crosslink density. According to storage modulus curves, increasing difference storage modulus between plateau regions obtained on before and after  $T_g$  value means a reduction in the amount of crosslinking. In this case, storage modulus of SMPU251 and SMPU250 which are spun with 25% polymer concentration in solution and 1% and 0% concentration of coagulation bath, respectively, has a sharp decrease at 27°C and highest storage modulus were obtained for these filaments. As shown in Figure 1, SMPU251 and SMPU250 have the lowest crosslink density, accordingly, these filaments have been found to have the highest elasticity value.

Loss modulus is related to the hysteretic energy dissipation and it shows mobility of polymer chains. High and wide loss modulus relate with mechanical properties of material such as impact resistance. It means that, material have better mechanical properties with increasing width of loss modulus curve [14]. According to loss modulus curve of shape memory filaments, SMPU250 and SMPU251 which are spun with 25% polymer concentration in solution, 0% and 1% concentration in coagulation bath, respectively, have better loss modulus and consequently mechanical properties. Moreover, SMPU201 which is spun 20% polymer concentration in solution and 1% concentration in coagulation bath has lowest loss modulus.



**Table 2** DSC analyses results for shape memory samples

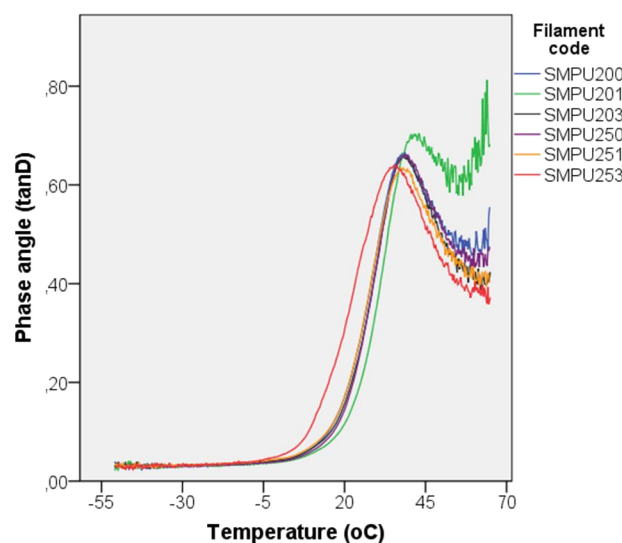
Sample code	1. Heating glass transition temp $T_g$ [°C]	1. Heating heat capacity $\Delta C_p$ [J/g]	Cooling glass transition temp. $T_g$ [°C]	Cooling heat capacity $\Delta C_p$ [J/g]	2. Heating glass transition temp. $T_g$ [°C]	2. Heating heat capacity $\Delta C_p$ [J/g]
SMPU200	29.26	0.645	35.26	0.395	37.37	0.440
SMPU201	22.10	0.305	33.45	0.433	37.03	0.493
SMPU203	20.97	0.313	34.09	0.396	36.43	0.434
SMPU250	20.80	0.251	35.26	0.287	36.58	0.415
SMPU251	22.24	0.253	34.70	0.415	36.95	0.390
SMPU253	21.79	0.268	32.33	0.444	36.81	0.375
SMPU polymer	26.17	0.297	33.96	0.315	37.69	0.338

**Figure 1** Storage and loss modulus of shape memory filaments

This result is in harmony with the tensile test results of filaments. Besides, the loss modulus peak locating at 38-40°C is due to glass transition of soft segment phase. The loss modulus has a sharp decrease at highest temperature than  $T_g$ . This means that, filaments can be easily deformed at temperatures above  $T_g$  and shape can be fixed at temperature below  $T_g$ .

Figure 2 shows that the  $(\tan \delta)$  peak of the shape memory filaments range between 35.7-40.5°C, which is associated with the glass transition temperature of shape memory filaments. It is generally accepted that the transition temperature measured by DMA is slightly higher than that obtained from DSC as the working principles of DSC and DMA are different [12]. Confirming literature there is a difference of 2-3°C between glass transition temperatures measured by DSC and DMA. The peak height of  $(\tan \delta)$  provides information about the mobility of molecule chains of the materials and  $(\tan \delta)$  peak width give information about homogeneity of crosslinking. The mobility of molecular chains in the material structure rises with increasing peak height of  $(\tan \delta)$ . The width of  $\tan(\delta)$  gives idea about heterogeneity of material crosslinking. When phase angle curves

$(\tan \delta)$  of shape memory filaments obtained by DMA analyses are analyzed (Figure 2), SMPU201 filament which is spun with 20% polymer concentration in solution and 1% concentration of coagulation bath has the highest peak value.

**Figure 2** Phase angle curve of shape memory filaments

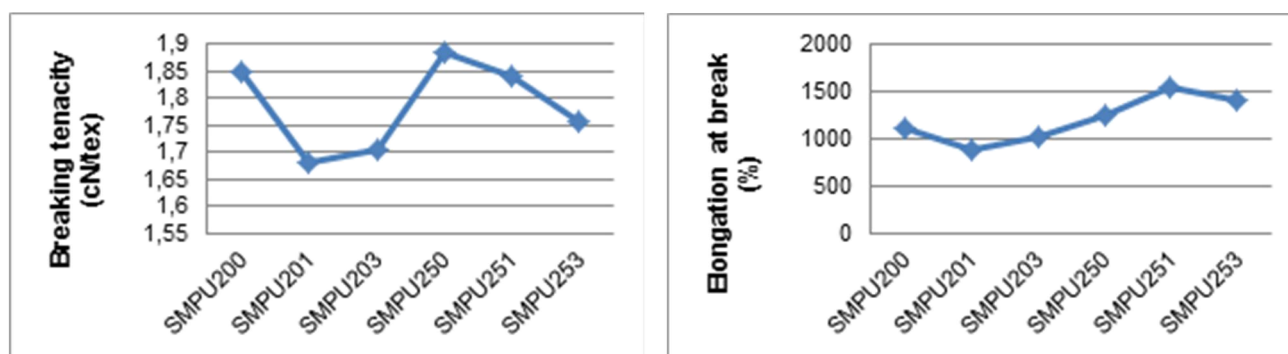


**Figure 3** Tensile properties of SMPU fibers

Consequently, its chain mobility is more than the other filaments. Moreover, SMPU251 filament which is spun with 25% polymer concentration in solution and 1% concentration of coagulation bath has the lowest chain mobility. Besides, SMPU251 and SMPU253 filaments which are spun with 25% polymer concentration in solution, 1% and 3% concentration of coagulation bath, respectively, has a more heterogeneous structure than the others.

### 3.3 Mechanical properties of shape memory filaments

According to test results, there are not significant differences between breaking tenacity performances of shape memory fibers. However, as shown in Figure 3, SMPU200 and SMPU250 fibers which are produced with 0% solvent concentration in coagulation bath showed the highest breaking tenacity among other shape memory fibers. Strain test results showed that, high polymer concentration increased significantly elongation performance of filaments. SMPU251 and SMPU253 which are spun with 25% polymer concentration in solution, 1% and 3% concentration of coagulation bath, respectively, had the highest strain performance while SMPU203 and SMPU251 fibers had lower values. According to the statistical analysis results of strain, polymer content in solution had a positive effect on the elongation values of fibers. As a general result, it can be said that all fibers showed acceptable tensile and elongation performances.

### 3.4 Shape memory effect of fibers

The results of thermo-mechanical cyclic tensile test are summarized in Table 3. The shape memory filaments have a fixity ratio about 72.5% and recovery ratio of up to 91.5% in the first cycle. The filaments show up to 95% recovery ratio and 71% fixity ratio in the other two cycles. This results show that, prepared filaments have good shape memory effect. Because of molecule orientation and crystallization, there were differences between the first cycle and others. The shape memory effect and stress-strain behavior of filaments were very

similar except for the first cycle. Beside this, shape memory filaments were not completely fixed to temporary shapes due to instant elastic recovery after releasing external stress.

**Table 3** Thermomechanical properties of shape memory filaments under drawing temperature

Cycle code	Shape recovery ratio [%]	Shape fixity ratio [%]
1	91.5	72.5
2	95.2	71.3
3	95.9	71.6
4	97.3	71.3

The results of thermomechanical cyclic tensile test of shape memory filaments are shown in Figure 4. According to thermomechanical test results, all shape memory filaments showed similar shape memory performances. However, SMPU251 fiber which is spun with 25% polymer concentration in solution and 1% concentration of coagulation bath has slightly higher recovery and fixity ratio values, demonstrating a better shape memory effect than other filaments.

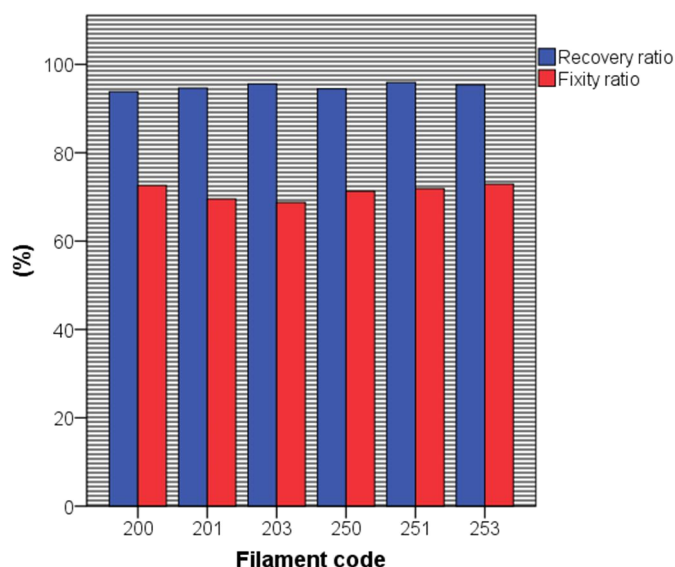


**Figure 4** Shape recovery and shape fixity of shape memory filaments

#### 4 CONCLUSIONS

Summing up, it can be concluded that, glass transition of soft segment of shape memory polyurethane filaments spun by wet spinning method were found between the range 36-40°C by DSC and DMA analyses. Shape memory polyurethane filaments showed good tensile performances, especially the fibers spun with high polymer solution concentration and without solvent in coagulation bath. Similarly, shape memory filaments have remarkable shape memory performances. They have a fixity ratio about 72.5% and recovery ratio of up to 91.5% in the first cycle. The filaments show up to 95% recovery ratio and 71% fixity ratio in the other cycles. Shape memory polymers have great potential for developing functional and smart textile products such as breathable, waterproof, modified structures.

**ACKNOWLEDGEMENTS:** *This study was funded by a project of Suleyman Demirel University Scientific Research Projects Coordination Unit (4393-D2-15). We want to thank for their support.*

#### 5 REFERENCES

1. Meng Q.: Studies of Functional Shape Memory Fibers, Institute of Textiles & Clothing, The Hong Kong Polytechnic University, 2010
2. Zhuo H., Hu J., Chen S.: Study of Water Vapor Permeability of Shape Memory Polyurethane Nanofibrous Nonwoven, Textile Research Journal 81(9), 883-891, 2011
3. Ahmad M., Xu B., Purnawali H., Fu Y., Huang W., Mirafatab M., Luo J.: High Performance Shape Memory Polyurethane Synthesized with High Molecular Weight Polyol as the Soft Segment, Applied Sciences 2(2), 535-548, 2012
4. Han H.R., Chung S.E., Park C.H.: Shape memory and breathable waterproof properties of polyurethane nanowebs, Textile Research Journal 83(1), 76-82, 2013
5. Zhu Y., Hu J., Yeung L.Y., Liu Y., Ji F., Yeung K.: Development of shape memory polyurethane fiber with complete shape recoverability, Smart Materials and Structures 15, 1385-1394, 2006
6. Meng Q., Hu J., Zhu Y., Lu J., Liu Y.: Polycaprolactone-Based Shape Memory Segmented Polyurethane Fiber, Journal of Applied Polymer Science 106(4), 2515-2523, 2007
7. Yan L., Aggie C., JinLian H., Jing L.: Shape memory behavior of SMPU knitted fabric, Journal of Zhejiang University Science A 8(5), 830-834, 2007
8. Liu Y., Lu J., Hu J., Chung A.: Study on the bagging behavior of knitted fabrics by shape memory polyurethane fiber, The Journal of The Textile Institute 104(11), 1230-1236, 2013
9. Jing L., Hu J.: Study on the Properties of Core Spun Yarn and Fabrics of Shape Memory Polyurethane, FIBRES & TEXTILES in Eastern Europe 18(4), 39-42, 2010
10. Meng Q., Hu J., Zhu Y., Lu J., Liu B.: Biological Evaluations of a Smart Shape Memory Fabric, Textile Research Journal 79(16), 1522-1533, 2009
11. Mondal S., Hu J.L.: Temperature Stimulating Shape Memory Polyurethane for Smart Clothing, Indian Journal of Fibre&Textile Research 31(1), 66-71, 2006
12. Yan Y.L.: Structure and Thermal-Mechanical Properties of Shape Memory Polyurethanes and Textiles, Institute of Textiles & Clothing, The Hong Kong Polytechnic University, 2009
13. Zhu Y., Hu J., Yeung L.Y., Lu J., Meng Q., et al.: Effect of steaming on shape memory polyurethane fibers with various hard segment contents, Smart Materials and Structures 16(4), 969-981, 2007
14. Gultekin G.: Production of Fatty Acid Based Polyurethane Films for Application of Wound Dressing Materials, The Istanbul Technical University, 2006

# INVESTIGATING POSSIBILITIES OF THREE-STRAND YARN PRODUCTION

Murat Demir and Musa Kilic

Dokuz Eylül University, Department of Textile Engineering, Tinaztepe Campus, 35397, İzmir, TURKEY  
[murat.demir@deu.edu.tr](mailto:murat.demir@deu.edu.tr), [musa.kilic@deu.edu.tr](mailto:musa.kilic@deu.edu.tr), Phone: +902323017730 Fax: +902323017750

**Abstract:** Conventional ring spinning system is used for the largest proportion of total yarn production today and has kept same principle since 19<sup>th</sup> century. Analyzing new spinning systems shows that some modifications on conventional systems aid to produce yarn in better quality. Siro-spun spinning can be counted amongst one of the modern systems that enable to produce yarn in better quality and more economical way with help of some modifications. In this study, it was aimed to produce three-strand yarn in single process inspiring from siro-spun spinning. For this purpose, some modifications developed on siro-spun system and three-strand yarns were produced. Physical and mechanical properties of yarns that produced from different materials were measured and compared with three-ply yarns. Results showed that three-strand yarns are superior in terms of hairiness and elongation, but inferior in terms of unevenness. Moreover, there is no statistically significant difference between strengths of three-strand and three-ply yarns.

**Key words:** Yarn technology, twist spinning, siro-spun spinning

## 1 INTRODUCTION

Twist spinning has been known many years and has an increasing popularity within the recent years. Twist spinning is also known as two-strand spinning. Currently, two systems are used for two strand spinning: Duospun (designed by Ems Sa and Huber and Suhner) and Sirospun (designed by Zinser Textilmaschinen GmbH).

During the production process of twist spinning, two fibre strands are given into the drafting area of conventional ring spinning machine and leave drafting area together. At the same time, single yarn is produced by twisting individual fibre strand on themselves with aid of spindle, ring and traveler and then two individual single yarns are twisted for production of two-ply yarn.

In siro-spun spinning, elimination of plying and twisting machines provide economic superiority against conventional plied yarns and related with economic advantages and less production process siro-spun has become a big competitor against conventional two-fold yarns [1]. However, because of the variety of twists, siro-spun yarns cannot take all market from two-ply yarns [2]. Production of siro-spun yarns is provided by some modifications on conventional ring spinning machine. Two rovings are fed individually through slightly modified but generally conventional ring drafting area. After drafting area, the fibre strands leave front cylinder separately and they become single yarn with the help of common spindle and spinning triangle. These two yarns bound together to form of composite yarn [3].

Inside the literature, there are many studies that compare two-strand yarns and two-ply yarns in terms of physical, mechanical and structural properties. Siro-spun yarns have more strength and abrasion resistance and less hairiness when compared to single fold yarns [4]. Comparing compact and siro-spun yarns showed that, siro-spun yarns are superior in terms of hairiness, degrees of imperfections and strength [5]. At same twist level, siro-spun yarns have less hairiness and degrees of imperfections while more elongation compared with two fold yarns [6].

Strand space and spinning triangle are important production parameters that affects properties of siro-spun yarns. During the production of siro-spun three spinning triangles are occurred and structure of those triangles are directly related with strand space [7]. There is a positive influence between strand space and cohesion forces between fibres that affect yarn strength [8].

Inside the literature, it can be seen that many researchers attempt to modify conventional and modern systems in order to obtain superior yarn properties. Yilmaz and Usal [9], applied air nozzle and yarn guide on compact spinning machine and it is called compact-jet. With this new spinning system, it is possible to produce yarn with less hairiness. Moreover, it is also possible to produce yarns in better quality by combining siro and compact spinning systems [10]. Moreover, some researchers investigate the possibilities of production of multi-spun yarns. These studies mostly focused on yarn structure or mathematically analysed spinning conditions [11, 12].



In the scope of this study, possibilities for the production of three-strand yarn will be investigated. For this purpose, some modifications on conventional ring spinning machine is planned. It is predicted that these modifications will provide great impacts on physical, mechanical and structural properties of three-strand yarns.

## 2 EXPERIMENTAL

In the study, three-strand and three-ply yarns were produced from cotton, PES, Tencel and 50% cotton-50% nylon 6.6 based on given structural properties in Table 1. Investigating literature and analyzing some practical experiences are showed that better guiding strands during production have positive influence on yarn properties. Therefore, it is thought that some modifications should be made on siro-spun spinning machine to produce better quality yarns (Figure 1). In this study, only an extra funnel for the third roving was placed on the machine for better guiding. Future studies might be focused on improving strand delivery by using additional

attachments such as three-grooved delivery cylinder.

In the study, physical, structural and mechanical properties such as unevenness, imperfections, hairiness, strength and elongation were measured by using Uster Tester and Uster Tensorapid.

## 3 RESULTS AND DISCUSSION

Properties of three-strand and three-ply yarns that produced from different materials were statistically analyzed. For this purpose, ANOVA analysis at  $\alpha = 0.05$  were performed and graphs for confidence intervals at 95% were illustrated.

### 3.1 Hairiness

Result of eliminating plying and twisting machine, hairiness values ( $H$ ) of three-strand yarns were found lower than three-ply yarns (Figure 2). As it seen from Table 2, differences between three-strand and three-ply yarns in terms of hairiness is statistically significant for all raw material types.

**Table 1** Structural properties of three-strand and three-ply yarns

Yarn	Number of single yarn	Number of produced yarn	Twist of single yarn	Twist of produced yarn
Three-strand yarn	Ne 60	Ne 60/3	650 T/m (Z)	650 T/m (Z)
Three-ply yarn	Ne 60	Ne 60/3	1300 T/m (Z) → before plying 650 T/m (Z) → after plying	650 T/m (S)

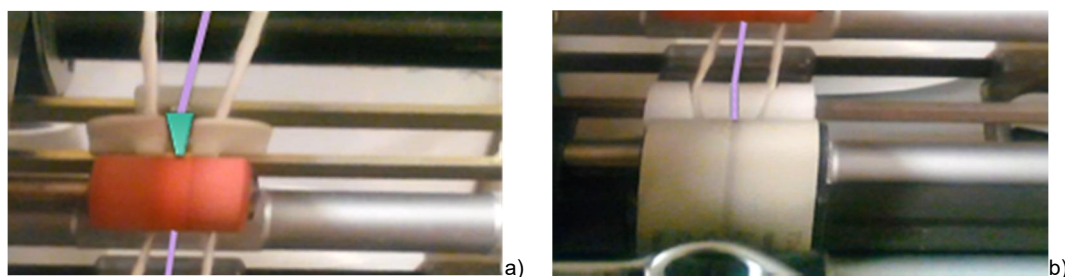


**Figure 1** Modifications on drafting zone a) embedding third roving funnel, b) third groove on delivery cylinder

**Table 2** ANOVA table for  $H$  values

	Type III Sum of Squares	df	Mean Square	F	Sig.
100% Cotton	1.815	1	1.815	335.445	0.000
100% Tencel	9.506	1	9.506	381.700	0.000
100% Polyester	0.471	1	0.471	378.225	0.000
50%-50% Cotton-Nylon 6.6	0.581	1	0.581	6.148	0.038

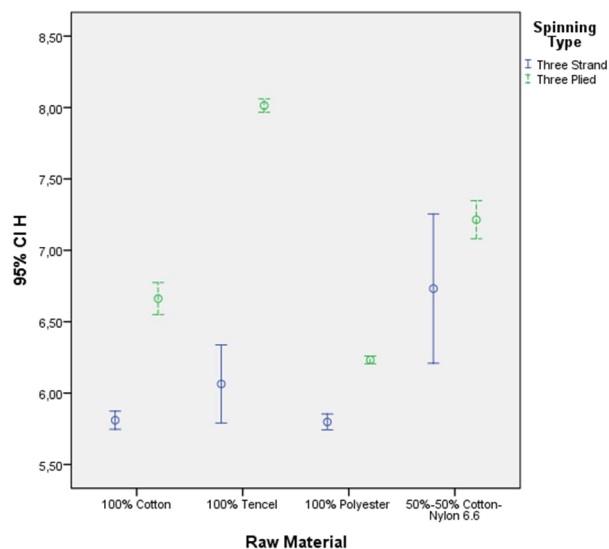


**Figure 2** Hairiness ( $H$ ) values of three-strand and three-ply yarns

### 3.2 Mechanical Properties

Comparing mechanical properties of three-ply yarns and three-strand yarns show that part from cotton yarns, there is no statistically significant difference between strength values of three-strand and three-ply yarns. Moreover, elongation

properties of three-strand yarns are higher than three-ply yarns. As it seen from Table 3 and Table 4, differences between three-strand and three-ply yarns in terms of breaking force and breaking elongation are not statistically significant in general.

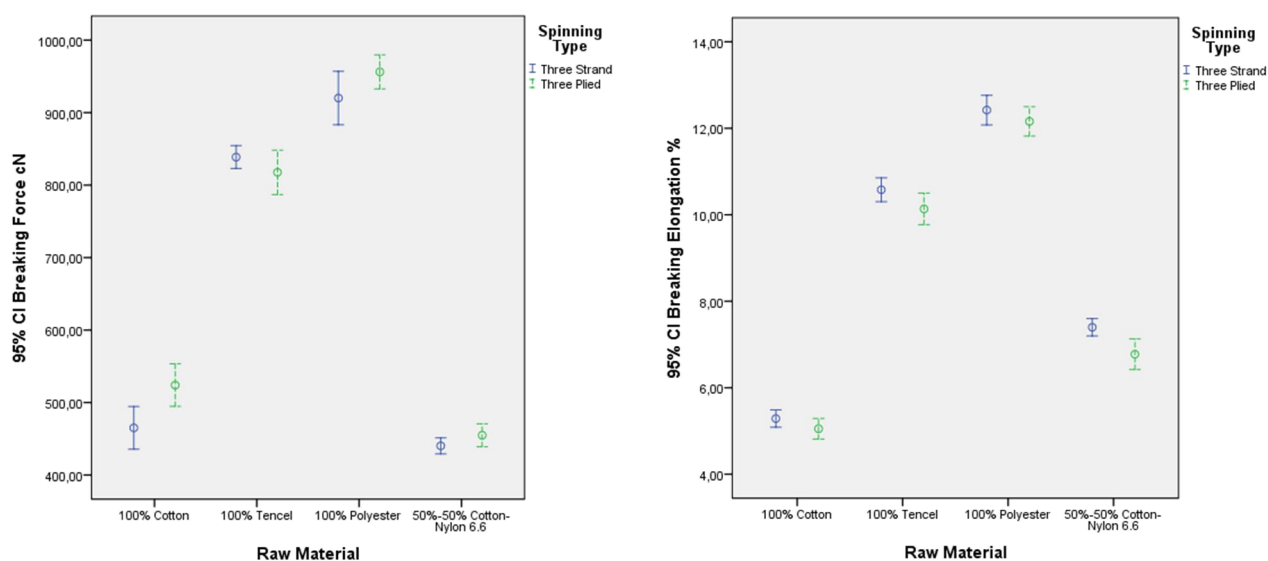


**Figure 3** Breaking force [cN] and breaking elongation [%] values of three-strand and three-ply yarns

**Table 3** ANOVA table for breaking force [cN] values

	Type III Sum of Squares	df	Mean Square	F	Sig.
100% Cotton	8702.500	1	8702.500	15.499	0.004
100% Tencel	1102.500	1	1102.500	2.867	0.129
100% Polyester	3261.636	1	3261.636	5.257	0.051
50%-50% Cotton-Nylon 6.6	532.900	1	532.900	4.370	0.070



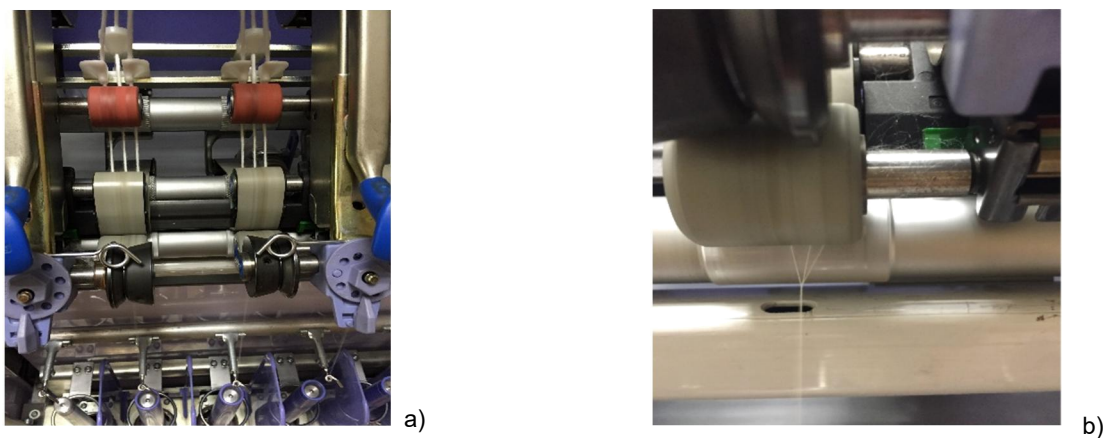
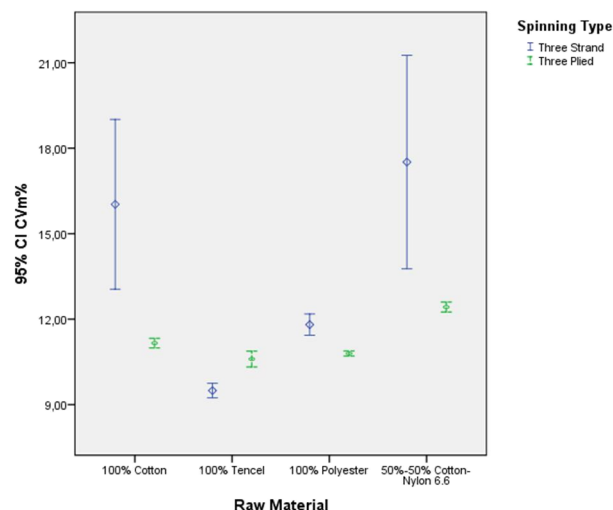
**Table 4** ANOVA table for breaking elongation [%] values

	Type III Sum of Squares	df	Mean Square	F	Sig.
100% Cotton	0.139	1	0.139	4.401	0.069
100% Tencel	0.488	1	0.488	7.164	0.028
100% Polyester	0.172	1	0.172	2.284	0.169
50%-50% Cotton-Nylon 6.6	0.973	1	0.973	18.018	0.003

### 3.3 Unevenness

Results showed that unevenness values of three-strand yarns are higher than three-ply yarns in general. It is assumed that this situation might be the result of lack of control on strand delivery. In the present work, strand delivery is only tried to be controlled by using third sliver funnel. As it seen from Figure 4a, strand spaces can be changed when the strands are fed into the drafting zone. As a result

of this situation, irregularity between strand spaces is seen on spinning triangle (Figure 4b). This situation which has direct influence on yarn properties is assumed to be fixed with the better controlled strand delivery. Moreover, it is also seen from Table 5, there is significantly statistical difference in unevenness values for all raw materials.

**Figure 4** Modifications on drafting zone a) strand delivery, b) three-strand yarn spinning triangle**Figure 5** Unevenness (CVm%) values of three-strand and three-ply yarns**Table 5** ANOVA table for Unevenness (CVm%) values

	Type III Sum of Squares	df	Mean Square	F	Sig.
100% Cotton	59.341	1	59.341	20.538	0.002
100% Tencel	3.069	1	3.069	65.918	0.000
100% Polyester	2.570	1	2.570	53.413	0.000
50%-50% Cotton-Nylon 6.6	64.770	1	64.770	14.200	0.005

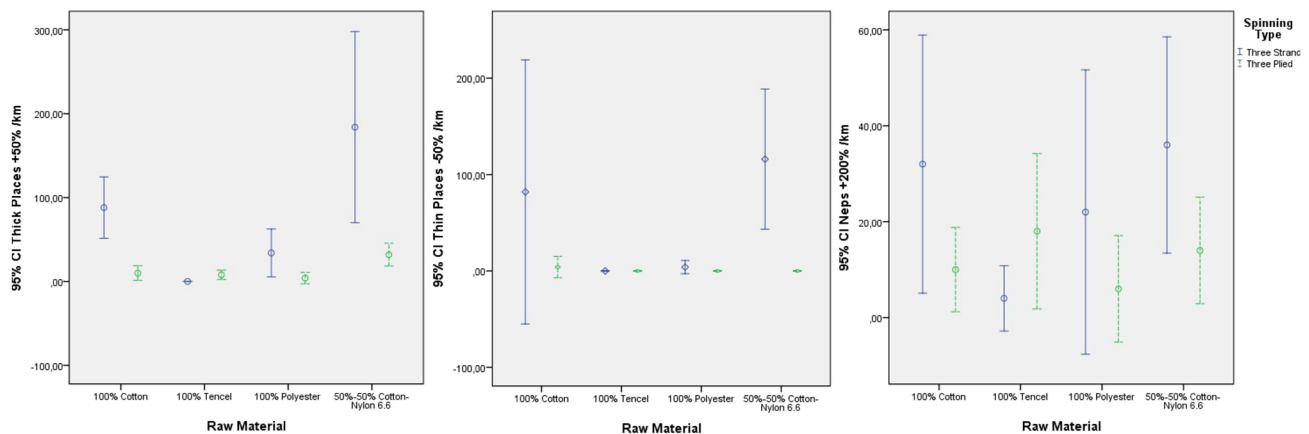


**Figure 6** Imperfections values of three-strand and three-ply yarns

**Table 6** ANOVA table for thick places (+50% /km) values

	Type III Sum of Squares	df	Mean Square	F	Sig.
100% Cotton	15210.000	1	15210.000	33.065	0.000
100% Tencel	160.000	1	160.000	16.000	0.004
100% Polyester	2250.000	1	2250.000	8.036	0.022
50%-50% Cotton-Nylon 6.6	57760.000	1	57760.000	13.511	0.006

**Table 7** ANOVA table for thin places (+50% /km) values

	Type III Sum of Squares	df	Mean Square	F	Sig.
100% Cotton	15210.000	1	15210.000	2.483	0.154
100% Tencel	0.000	1	0.000	.	.
100% Polyester	40.000	1	40.000	2.667	0.141
50%-50% Cotton-Nylon 6.6	33640.000	1	33640.000	19.615	0.002

**Table 8** ANOVA table for neps (+200% /km) values

	Type III Sum of Squares	df	Mean Square	F	Sig.
100% Cotton	1210.000	1	1210.000	4.654	0.063
100% Tencel	490.000	1	490.000	4.900	0.058
100% Polyester	640.000	1	640.000	1.969	0.198
50%-50% Cotton-Nylon 6.6	1210.000	1	1210.000	5.902	0.041

### 3.4 Imperfections

Due to lack of strand guiding, thick place values of three strand yarns are higher than three-plies yarn, as it similar with unevenness values. Comparing thin places (+50% /km) and neps (+200% /km) values of three-strand and three-ply yarns show that there are no statistically significant differences in general. Due to the fact that neps values are mostly related with spinning preparations, results are obtained independent of spinning type.

## 4 CONCLUSIONS

In this study, it was aimed to investigate the production possibilities of three-strand yarns with the same principle of siro-spun spinning. For production of three-strand yarns, third funnel was attached on laboratory type siro-spun spinning machine and 100% Cotton, 100% Tencel, 100%

polyester and 50%-50% Cotton-Nylon 6.6 yarns were produced. Properties of three-strand yarns were compared with three plyed yarns.

Hairiness values of yarns are mostly related with production processes. Eliminating twisting and doubling machines from production flow, three-strands yarns have better hairiness value than three-plyed yarns for all material types. It is also seen from the results that there is no statistically significant difference between mechanical properties of three-strand and three plyed yarns.

Investigating literature and experimental results showed that strand delivery and strand spacing have significant impact on unevenness. When the strands leave drafting zone, spaces between strands have direct influence on geometry of spinning triangle. It is expected that controlling strands from strand feeding to condensing zone of yarn will provide to

produce yarns in better quality. Siro-spun spinning has been placed in market and has become a strong rival against two-ply yarns. It is believed that, three-strand yarn spinning with the same production principle of siro-spun spinning will be placed in market as a big competitor of three-ply yarns with the economic benefit of eliminating plying and twisting process.

**ACKNOWLEDGEMENTS:** *This study is carried out in cooperation with KİPAŞ Mensucat A.Ş., Kahramanmaraş, TURKEY.*

## 5 REFERENCES

1. Mansour S. & Tawfik M.: Production of Siro-spun Yarns from Short-staple Fibers, Indian Journal of Textile Research 11(2), 70-72, 1986
2. Stalder H.: Rieter Manuel of Spining, Issue 6: Modern Spining Systems, Winterthur: Rieter Machine Works, 2014
3. Kılıç M., Balcı Kılıç G., Okur A.: Eğirme Sisteminin İplik Özelliklerine Etkileri, Tekstil ve Mühendis 18(81), 22-34, 2011
4. Salhotra K.: Some Quality Aspects of Ply-Spun Yarn, Indian Journal of Fibre and Textile Research 12(4), 197-200, 1987
5. Örtlek H., Kılıç G., Bilgin S.: Comparative Study on the Properties of Yarns Produced by Modified Ring Spining Method, Industria Textila 3(62), 129-133, 2011
6. Sun M., Cheng K.: Structure and Properties of Cotton Sirospun Yarns, Textile Research Journal 70(3), 261-265, 2000
7. Lawrence Carl.A.: Fundamentals of Spun Yarn Technology, CRC Press New York Document, 2003
8. Gokarneshan N., Anbumani N., Subramaniam V.: Influence of Strand Spacing on the Interfibre Cohesion in Siro Yarns, The Journal of the Textile Institute 3(98), 289-292, 2006
9. Yılmaz D., Usal M.R.: Comparison of Compact-Jet, Compact and Conventional Ring Spun Yarns, Textile Research Journal 81(5), 459-470, 2010
10. Han C., Wei M., Xue W., Cheng L.: Numerical Simulation and Analysis of Airflow in the Condensing Zone of Compact-siro Spining, Textile Research Journal 85(14), 1506-1511, 2015
11. Matsumoto Y., Kimura H., Yamamoto T., Matsuoko T., Fukushima K.: Characteristics of Novel Triplet Spun Yarns Made from Fibers of Differing Fineness, Textile Research Journal 79(10), 947-952, 2009
12. Xu W., Xia Z., Wang X., Chen J., Cui W., Ye W., Ding C., Wang X.: Embeddable and Locatable Spining, Textile Research Journal 81(3), 223-229, 2011

# TENSILE PROPERTIES OF SYNTHETIC BLOOD VESSEL REPLACEMENT

Karolina Čermáková, Michal Ackermann, Lukáš Čapek and Jana Horáková

Technical University of Liberec, Studentska 2, 461 17 Liberec, Czech Republic  
[lukas.capek@tul.cz](mailto:lukas.capek@tul.cz), phone +420485352949

**Abstract:** Determination of tensile properties of synthetic blood vessel is an essential knowledge for researchers so that the biomechanical behavior of natural physiological vessel can be easily substituted. In this contribution, tensile tests of electrospun double layered vascular grafts made from polyesters were done. In order to analyze the developed vessel replacement in virtual simulations, a phenomenological material model was fitted to measured data.

**Key words:** Synthetic graft, uniaxial test, finite element method

## 1 INTRODUCTION

Heart attack is worldwide one of the most risky health accident which frequently leads to death of the patient [1]. The consequence of the heart attack is usually a surgery of the heart during which so called bypasses are placed. Nowadays, the autograft veins are used in clinical practice [2]. This solution brings several complications, among all the long term surgery that might be risky for the patients. The state of the art in this domain is the synthetic vascular graft development.

Much effort was put into biocompatibility tests and material research in development of synthetic blood vessel replacements [3, 4]. Only few studies are dealing with mechanical behavior and none of them with finite element modelling. The aim of this study is to present the uniaxial experiments of selected synthetic tubular grafts followed by finite element modelling.

## 2 EXPERIMENTAL

Experimental samples are electrospun double layered vascular grafts made from polyesters. Inner layer of the graft is made from copolymer of polylactide and polycaprolactone (70/30, PURASORB) and the outer layer is made from polycaprolactone (Mn 80.000, Sigma Aldrich). The thickness of the final graft is 200 µm (100 µm inner layer + 100 µm outer layer) as depicted in Figure 1. The samples were sorted into two groups, one of which was not sterilized. The second one was sterilized by ethylene oxide (37°C).

### 2.1 Uniaxial structural tests

The uniaxial tests were done on universal one column traction machine. The loading speed was 5 mm/min for all samples. The samples were loaded up to the rupture of the specimen. The initial length of samples was 50 mm. In the following step,

the stress-strain curves were built on the basis of the measured data

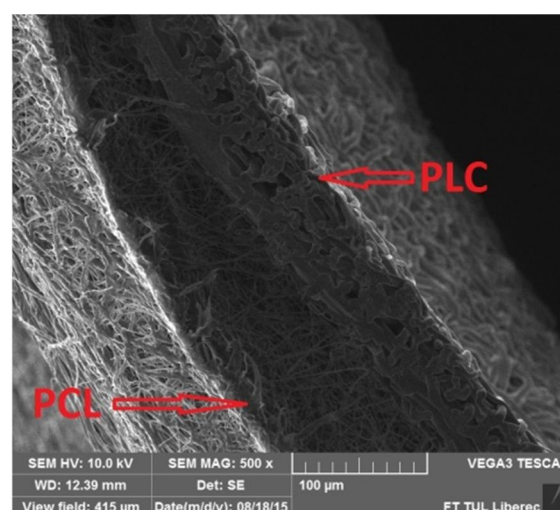


**Figure 1** Scanning electron microscopy picture of cross section of double-layered vascular graft made from electrospun copolymer PLC in the inner layer and from electrospun polycaprolactone in the outer layer

### 2.2 Finite element simulation

The engineering stress strain curves were calculated by true strain and true stress by following equations

$$\sigma_{true} = \sigma \cdot (1 + \varepsilon) \quad (1)$$

$$\varepsilon_{true} = \ln(1 + \varepsilon) \quad (2)$$

The true data were imported into the software MSC.MARC where experimental data fitting was done, Figure 2.

The material model used for simulation is two-parametric Ogden model. The calculated material parameters are in Table 1.

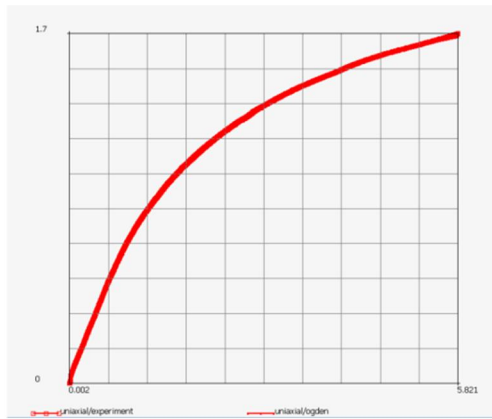


**Figure 2** Experimental data fitting

**Table 1** Material parameters of the Ogden model

$\mu_1$ [MPa]	$\alpha_1$ [-]	$\mu_2$ [MPa]	$\alpha_2$ [-]
4.05	0.84	10.45	- 0.26

$$W = \sum_{n=1}^N \frac{\mu_n}{\alpha_n} \left[ J^{\frac{-\alpha_n}{3}} (\lambda_1^{\alpha_n} + \lambda_2^{\alpha_n} + \lambda_3^{\alpha_n}) - 3 \right] \quad (3)$$

The finite element model of the sample consists of eight node shell elements (1600). The nodes of the left free edge are constrained via control node in all direction of movement. The nodes of the right free edge are constrained via control node and axial displacement of 8 mm is prescribed.

### 3 RESULTS

#### 3.1 Experiment

The measured data from uniaxial tensile tests of sterilized and non-sterilized samples are seen on Figure 3.

The true strain and stress distribution along the axis of the model can be seen on Figure 4.

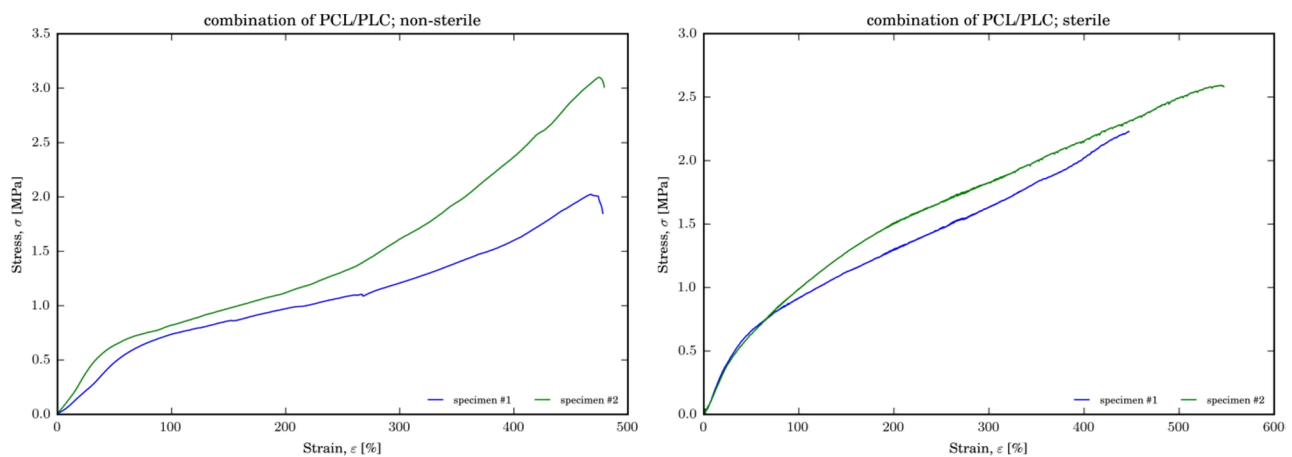


**Figure 3** Force strain curve for non-sterilized samples (left) and sterilized samples (right)

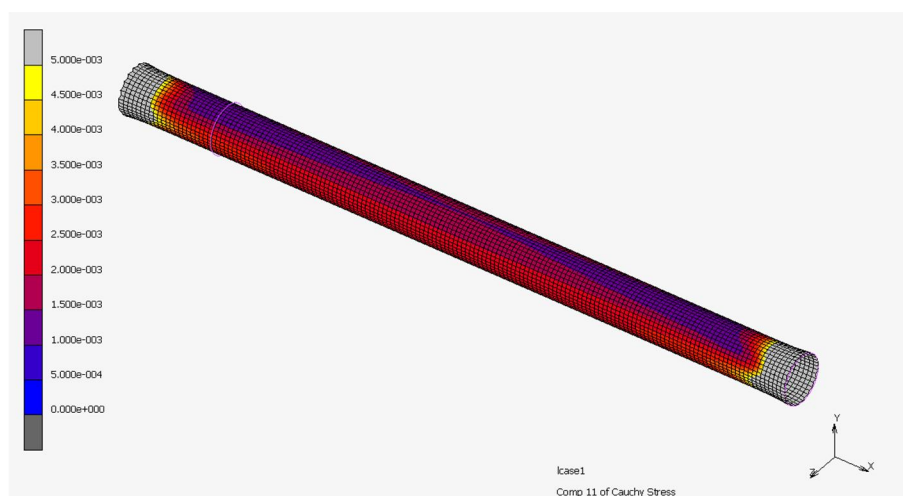


**Figure 4** Cauchy stress distribution in sample axis [MPa]

#### 4 CONCLUSIONS

Development of synthetic veins used for bypass surgery is of a great interest in the field of cardiovascular surgery. To our knowledge, none of them was applied yet. The research in this field cannot be done without understanding mechanical behavior of these artificial vascular replacements. The goal is to approximate its mechanical properties to the biologic ones.

The loading the samples up to the failure showed that extreme strains can be observed. There is no physiological meaning for loading veins up to 500% that is why the FEM analysis was provided only up to 160% strain. Phenomenological Ogden material model was used for finite element simulation.

In spite of favorable agreement between experimental data curves and results gained by finite element method, it should be noted that the future of FEM modelling of electrospun vein replacement must be in multiscale modelling. Using this method, the real morphology of the structure can be captured.

**ACKNOWLEDGEMENTS:** *The authors are thankful to the grant of the Ministry of Health of the Czech Republic: NV15-29241A (Nanofibrous Biodegradable Small-Diameter Vascular Bypass Graft).*

#### 5 REFERENCES

1. [http://ec.europa.eu/eurostat/statistics-explained/index.php/Cardiovascular\\_diseases\\_statistics](http://ec.europa.eu/eurostat/statistics-explained/index.php/Cardiovascular_diseases_statistics)
2. Prim D.A., Zhou B., Hartstone-Rose A., Uline M.J., Shazly T., Eberth J.F.: A mechanical argument for the differential performance of coronary artery grafts, *J Mech Behav Biomed Mater* 54, 93-105, 2016
3. Tan Z., Wang H., Gao X., Liu T., Tan Y.: Composite vascular grafts with high cell infiltration by co-electrospinning, *Mater Sci Eng C Mater Biol Appl* 67, 369-77, 2016
4. Xie Y., Guan Y., Kim S.H., King M.W.: The mechanical performance of weft-knitted/electrospun bilayer small diameter vascular prostheses, *J Mech Behav Biomed Mater* 61, 410-418, 2016



# FUNCTIONAL CHARACTERISTIC EVALUATION OF 3-DIMENSIONAL KNITTED SPACER FABRICS

**Veerakumar Arumugam, Rajesh Mishra, Jana Salacova, Mohanapriya Venkatraman, Dana Kremenakova, Hafsa Jamshaid, Tao Yang, Xiaoman Xiong, Kasthuri Venkatesh and Jiri Militky**

*Dept. of Materials Engineering, Technical University of Liberec, 461 17 Liberec, Czech Republic*  
[veerakumar27@gmail.com](mailto:veerakumar27@gmail.com), [arumugam.veerakumar@gmail.com](mailto:arumugam.veerakumar@gmail.com)

**Abstract:** Nowadays, the utilization of 3-Dimensional (3D) porous textile materials by the civil and mechanical engineers for improved acoustical environment and shear behavior during composite forming has widened the research scope. Since spacer textile fabrics have superior functional characteristics such as acoustical, thermal and shear characteristics compared to conventional woven/knitted structures or nonwovens due to their wonderful 3D sandwich pattern and porous nature. Hence this research paper presents an experimental evaluation on the sound absorption behavior and in-plane properties of 3D knitted spacer fabrics. The Sound absorption coefficient (SAC) was measured using two microphone impedance tube. Moreover, tortuosity of the spacer fabrics was carefully calculated analytically and compared with experimental results. This study deeply discusses the influence of material parameters and characteristics on acoustical properties of 3D spacer knitted fabrics. The results show that the fabric surface property, porosity, flow resistivity and tortuosity have significant effects on the sound absorbability. Also, a fixture was designed to analyze the intra-ply shear properties of these fabrics. The nonlinear behavior of shear force versus shear angle and the deformation mechanism were analyzed. The curves for shear force versus shear angle and position of buckling for intra-ply shear test are recorded. Load-displacement curves of intra-ply shear tests are also analyzed. In addition to this, a program was developed in MATLAB using Hough transform to analyze the shear angle in the real-time image taken during displacement of specimen at various positions. These findings are important requirement for the further improvements in designing of picture frame fixture and to study the in-plane shear properties of 3D fabrics.

**Key words:** Sound absorption, 3D spacer knitted fabrics, shear, tortuosity, porosity, acoustic property

## 1 INTRODUCTION

Due to new emerging textile material of this decade, only very few researchers are evaluated and analyzed the advance characteristics of spacer fabrics. Here those literatures are presented with advantages and limitations of spacer fabrics. Spacers knitted fabrics are known to possess excellent comfort properties. They not only allow for stretching and ease of movement, but they also have relatively good hand related characteristics and facilitate the easy transmission of water vapor from the body. These attributes make knitted fabrics the commonly preferred choice for sportswear, casual wear and underwear. Due to technological development and increases in demand of 3D knitted fabrics, many researchers carry out work on various technical applications. 3D knitted spacer fabrics are like a sandwich, consisting of two complementary fabrics with a third layer tucked in between [8]. These fabrics are produced with different thicknesses and can be used in thermal insulation applications because of their higher thickness compared to woven and knitted fabrics. These are lightweight and breathable structures. They have good physiological and thermal comfort.

They transport moisture easily; their air permeability and water vapor permeability values are high. Their compression characteristic is also better than conventional textile structures. Compression resilience is an important attribute of spacer fabrics, which is related to sensation of mechanical comfort. Modern consumers consider compression as one of the most important attributes in the comfort sensation such as hand of clothing material. Fabric thickness and compressibility have a linear relationship with thermal conductivity. Compression characteristic of knitted fabrics has been studied by various researchers [1]. Postle indicated that bulk density or compression property of knitted structures is related to the effective diameter of the yarn inside of the fabric and also to the fabric thickness [2].

Xu-Hong and Ming-Giao analyzed the stress-strain behavior of warp knitted spacer fabrics when compressed [3]. Mecit Armakan and Roye investigated the compression characteristic of warp knitted spacer fabrics on the basis of spacer yarns in their structure. They noted that, the material, pattern and threading of the spacer yarns have significant effect on compression characteristic of the fabrics. It was also observed that the location angle and the amount of the spacer yarns influence

the compression behavior of fabrics [4]. Yip and Ng found that warp knit spacer fabrics have a lower thermal conductivity rating than the weft knit fabrics, which means the excess heat from the body would not be quickly transferred if a warp knit spacer fabric is being utilized as compared to a weft knit fabric [5].

Shear properties influence draping, flexibility and also the handle of fabric. Shear properties are important not only for standard fabrics but for textile reinforced composites preforming as well. Automated manufacturing of textile composite shell-like products typically requires draping of dry or pre-impregnated textile sheets. Large local deformations occur in the textile sheet in order to adapt to the curved shape [6]. These deformations affect the local fiber directions, volume fractions, and thickness. Several factors together with the consolidation level and the occurrence of flaws (e.g. wrinkling and tearing) determine the product quality. Simulation tools that link product quality to material, mold and process parameters are being developed to support design and process optimization [7]. Three dimensional (3D) textile structural composites provide excellent strength through thickness, outstanding damage tolerance and good impact and fatigue resistance. As one type of the 3D textile structural reinforcements for composites, the 3D spacer fabric has been widely used in engineering field owing to its easy and efficient processing in warp and weft knitting. In addition, the most attractive advantage of spacer fabric is the three dimensional shape forming capacity to manufacture composites. The 3D spacer fabric preforms have excellent mechanical properties and good formability. With the development of the preforming technology, complex shape and different size of the structural parts can be produced. In the structure integrated manufacture of composites, the 3D spacer fabric is preformed according to the shape of the final composite that can be complex [8]. The in-plane behavior and the inter-laminar behavior are the most important deformations in 3D fabrics, and also shear

behavior predominates the deformation mode of the material [9]. It is necessary to study the inter/intra-ply shear behavior of 3D fabric because of their wide application in production especially in the case of forming process. Dial et al. introduced fabric with spacer structure to improve sound absorption performances. Their studies analyzed and reported that acoustic performance of plain weft knitted spacer is good in middle and high frequency range. Liu and Hu analyzed and compared the effects of different fabric layers and arrangement sequences of both warp and weft knitted spacer fabrics on the noise absorption coefficient. They suggested that sound absorption behavior of spacer fabrics are effective with multilayer arrangements backed up with air cavity. There is only few research studies conducted on acoustic performance of spacer fabrics. The lack of comprehensive studies on the functional characteristics especially on thermo-physiological, mechanical and properties of weft knitted 3D spacer fabrics are sound basis for this research. So, this paper deeply discusses the advance characteristics of knitted spacer fabrics such as thermal, in-plane shear and sound absorption behavior.

## 2 EXPERIMENTAL

### 2.1 Materials

The six spacer fabric samples were classified into two groups for convenient analysis of results, the first group has been developed using Polyester/Polypropylene (PES/PP) blend with three different proportions and second group with Polyester/Polypropylene/Lycra (PES/PP/Lycra) blend having another 3 different compositions.

As a spacer yarn, three different types of 88 dtex PES monofilament yarn and PES multifilament yarns (167 dtex and 14.5 tex) were used. 14.5 tex PP and 44 dtex multifilament yarns with Lycra were also used for the face and back side of the spacer fabrics.

**Table 1** Fabric particulars

Fabric sample No.	Fabric layers	Technical face	Spacer yarn	Technical back	Fiber composition [%]
Group 1 - Without Lycra					
S1	Type of yarns and linear density	PP - 14.5 tex	PES mf - 88 dtex	PP - 14.5 tex	58% PP, 42% PES mf
S2		PP - 14.5 tex	PES - 14.5 tex	PP - 14.5 tex	45% PP, 55% PES
S3		PP - 14.5 tex	PES - 167 dtex	PP - 14.5 tex	41%PP, 59% PES
Group 2 - With Lycra					
S4	Type of yarns and linear density	PP - 14.5 tex Lycra - 44dtex	PES mf - 88 dtex	PP - 14.5 tex	55% PP, 39% PES mf, 6% Lycra
S5		PP - 14.5 tex Lycra - 44dtex	PES - 14.5 tex	PP - 14.5 tex	42% PP, 52% PES, 6% Lycra
S6		PP - 14.5 tex Lycra - 44dtex	PES - 167 dtex	PP - 14.5 tex	39% PP, 55% PES, 6% Lycra

mf - monofilament

## 2.2 Methods

The Structural properties including the yarn linear density and fabric weights per unit area were determined according to ASTM D1059 standard using electronic weighing scales. The thickness of the fabrics was measured according to ASTM D1777-96 standard with the SDL digital thickness gauge at a pressure of 100 Pa. Air flow resistance of spacer fabric was calculated from air permeability value obtained from Textest FX-3300 air permeability tester. The Stitch density was calculated from wales per centimeter (WPC) and course per centimeter (CPC) with the help of optical microscope. Porosity,  $H$ , was calculated with bulk density of spacer fabrics and weighted average absolute density of fibres in the spacer fabric, expressed in  $\text{kg/m}^3$ . These results are shown in Table 2.

### 2.2.1 In-plane shear

The picture frame is an effective way for characterizing intra-ply (in-plane) shear property of fabrics. The 3D spacer fabrics for shear tests were prepared according to the size of the picture frame and the characteristics of samples. Shear tests were conducted on a TIRA - universal tensile testing machine with a crosshead speed of 10 mm/min. The test was conducted for 5 samples of each type under the same conditions [5].

Direct measurement of axial load and shear angle is possible through this following relationship:

$$F_s = \frac{F_x}{2 \cos \varphi} \quad (1)$$

Shear force ( $F_s$ ) is determined by the axial force ( $F_x$ ) frame rig length ( $L$ ) and the frame angle ( $\varphi$ ). Meanwhile frame angle can be determined directly from cross head displacement ( $d$ ). Shear angle ( $\gamma$ ) can be obtained from frame angle by using the following equations 2 and 3:

$$\varphi = \cos^{-1} \left[ \frac{L\sqrt{2} + d}{2L} \right] \quad (2)$$

$$\gamma = \frac{\pi}{2} - 2\varphi \quad (3)$$

In this research, the impedance tube method was used to determine the normal incident sound absorption coefficient, SAC ( $\alpha$ ). A minimum of three specimens for each sample were tested according to ASTM E 1050-07. Standard test method for impedance and absorption of acoustic materials using a tube with two microphones and a digital frequency analysis system was used.

### 2.2.2 Thermal properties

Air permeability tests were performed according to standard ISO 9237 using a Textest FX-3300 air permeability tester. Thermal conductivity measurements were performed using C-Therm Thermal Conductivity Analyzer Tci. The standard test method EN 61326-2-4:2006 was used for this testing using TCI. This test was performed under room temperature. The results are reported in figures.

### 2.2.3 Measurement of sound absorption coefficient

In this research, the impedance tube method was used to determine the normal incident sound absorption coefficient, SAC ( $\alpha$ ). A minimum of three specimens for each sample were tested according to ASTM E 1050-07. Standard test method for impedance and absorption of acoustic materials using a tube with two microphones and a digital frequency analysis system was used (Figure 1).

### 2.2.4 Calculation of NRC (noise reduction coefficient)

The "Noise Reduction Coefficient" (NRC) is a measure of how much sound is absorbed by a particular material, and is derived from the measured Sound Absorption Coefficients. The NRC was determined using the following formula (Eqn. 4) [10].

$$NRC = \frac{\alpha_{250\text{Hz}} + \alpha_{500\text{Hz}} + \alpha_{1000\text{Hz}} + \alpha_{2000\text{Hz}}}{4} \quad (4)$$

**Table 2** Spacer Fabric characteristics

Samples	Areal Density [ $\text{g.m}^{-2}$ ]				Thickness [mm]				Density [ $\text{kg.m}^{-3}$ ]	Stitch Density [Stitches/ $\text{cm}^2$ ]			
	Mean	ME	LL	UL	Mean	ME	LL	UL		Mean	ME	LL	UL
S1	493.00	0.16	492.84	493.16	4.40	0.88	3.52	5.28	112.00	200.00	0.10	199.90	200.10
S2	443.00	0.12	442.88	443.12	2.62	1.10	1.52	3.72	169.10	150.00	0.04	149.96	150.04
S3	477.00	0.20	476.80	477.20	2.74	0.61	2.13	3.35	174.10	150.00	0.12	149.88	150.12
S4	632.00	0.10	631.90	632.10	4.40	0.55	3.85	4.95	144.80	350.00	0.06	349.94	350.06
S5	657.00	0.12	656.88	657.12	3.50	0.86	2.64	4.36	187.70	280.00	0.10	279.90	280.10
S6	695.00	0.22	694.78	695.22	3.40	0.45	2.95	3.85	205.40	280.00	0.10	279.90	280.10

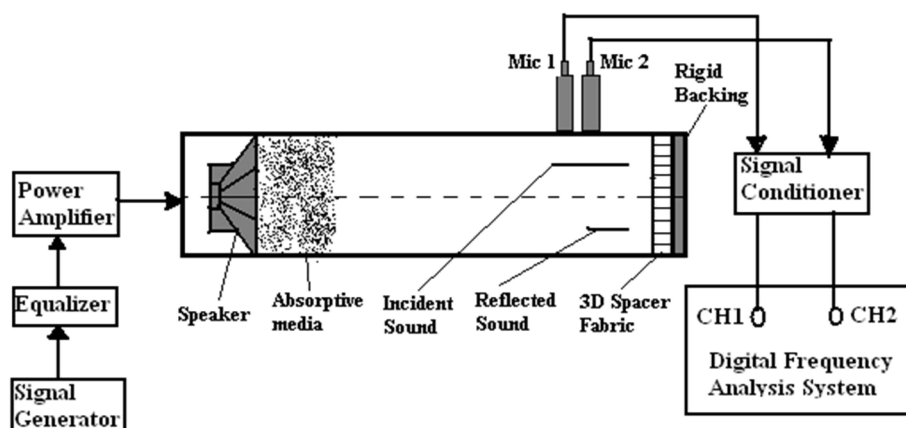


Figure 1 Impedance tube method (ASTM E 1050-08 and Bruel & Kjaer, 2009)

### 3 RESULTS AND DISCUSSION

#### 3.1 In-plane shear properties-comparative discussion

The shear angles are calculated by considering sample length as a substitute for  $L$  in Equation 2 and it is further used for calculation of shear force. Figure 2 shows the comparison of shear angles between image analysis and experimental measurements for all six specimens. The differences between image analysis and calculated shear angle using sample length at the chosen points are relatively small. Less than 8% CV was obtained in all measurements. It does not show any significant difference until pre-buckling occurs (up to 20 mm displacement) but significant difference is observed after 20 mm displacement. It is also believed that during image processing in MATLAB, detection of X and Y coordinates on the image is not accurate due to wrinkling in the central zone of samples. Also, it is noted that dimension of the frame and rig length can cause big difference in shear angle. Further study is required on the effect of different frame rig length and ratio of frame length to specimen size on in-plane shear behavior of 3D spacer fabrics.

#### 3.2 Effect of density and air permeability on thermal properties

This study found that spacer fabrics with lower density and higher air permeability exhibit relatively lower thermal conductivity for both the group of samples as shown in Figure 3. Also denser fabric has better thermal conductivity. It is also found that the spacer fabrics composed of monofilament spacer yarn (S1 & S4) have higher capacity to resist conduction of heat as compared to fabrics with multifilament spacer yarn (S2, S3 & S5, S6).

It is mainly because monofilament spacer yarns make the fabric more bulky with lower density which offers more space to entrap air between the face and back layer. A remarkable difference between the heat transfer rates of group 1 and 2 fabrics are also justified here. It is also observed that fabrics made up of 6% of Lycra yarn in the face layers (S4, S5 & S6) have lower thermal conductivity value than group 1 samples without Lycra (S1, S2 & S3). The air trapped within the fabric structure starts to circulate and that's why the heat transfer rate of group 2 is lower than that of group 1. Due to higher stitch density and Lycra based filament yarns on the surface layers, these spacer fabrics have lower air permeability value and consequently a lower thermal conductivity. The thickness is also a significant factor which influences the thermal resistance of spacer fabrics, higher thickness leads to higher thermal resistance.

Fabrics with a lower value of thermal effusivity give us a "warm" feeling as shown in Figure 3. 3D spacer fabrics have a much lower value of thermal absorption, so they give us warmer feeling than other commercial 2D fabrics, which are not ideal for summer clothes [8]. Thermal effusivity is a very important parameter from the point of view of thermal insulation; it is directly proportional to the fabric density and inversely proportional to air permeability. Due to increase in density between the samples S1 to S3 and S4 to S6, one can observe the increase in thermal effusivity value (Figure 3), and in contrast effusivity decreases as air permeability increases. So spacer fabrics with lower thermal conductivity and effusivity are perfect option for some special climate sportswear.

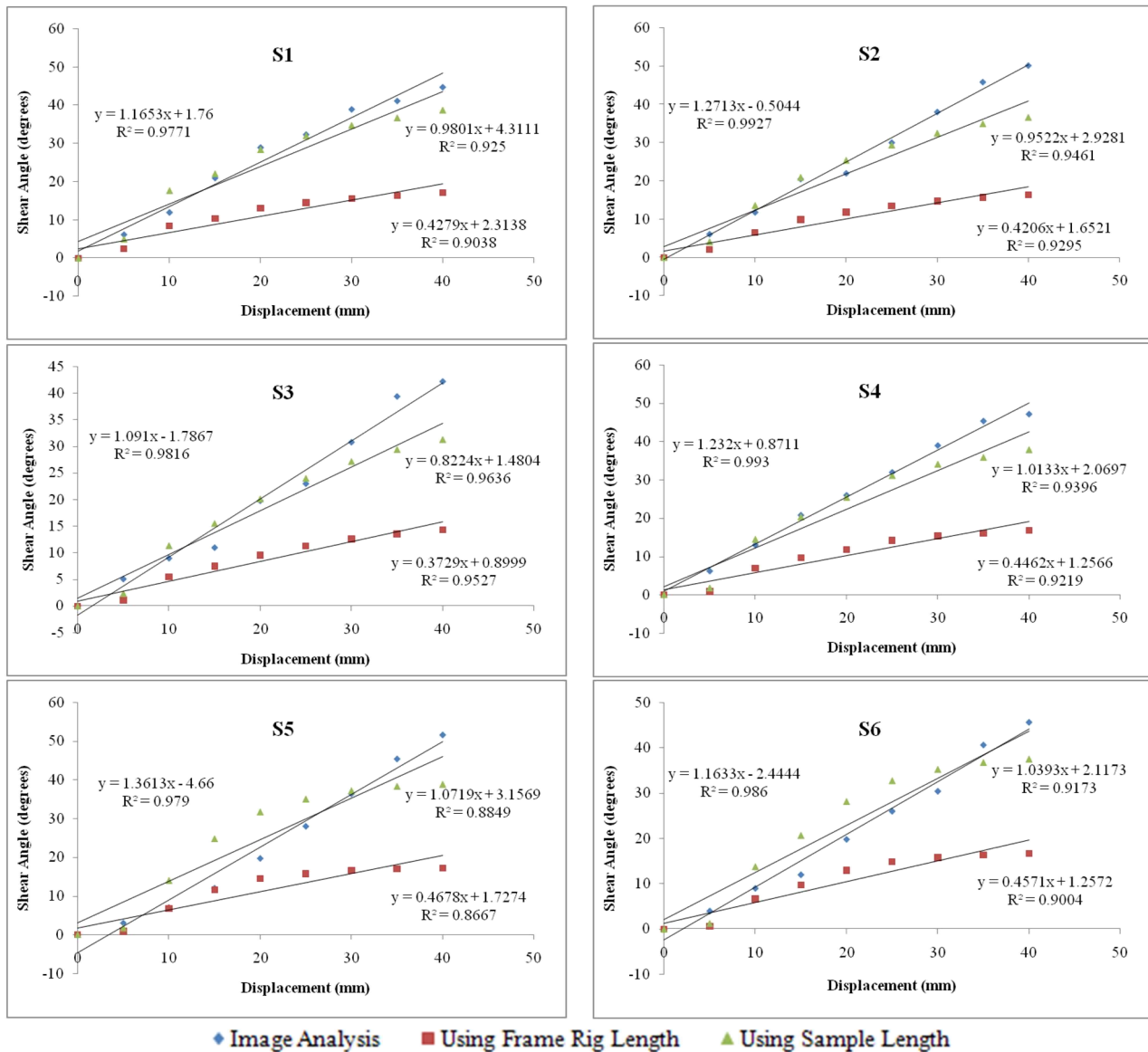


**Figure 2** Comparison of shear behavior of samples using different methods

### 3.3 Influence of material characteristics on sound absorption coefficient

For the range of considered porosity, the influence on the sound absorption is complicated. When porosity increases from 85 to 90% for group 1 samples, the changes on sound absorption is insignificant for low frequency range (50 Hz to 2000 Hz). But for frequency range above 2000 Hz, the absorption coefficient decreases drastically when the porosity increases to 90%. This is mainly because of too much space between the two layers in spacer fabrics which entraps excess of air, hence, the sound energy dissipation is substantially weakened, especially when the porosity is higher than 90%. In case of group 2 samples with porosity (83 to 87%), there is significant sound absorption both in low and high frequency ranges. In case of spacer fabric samples with monofilament (S1), the sound absorption is comparatively lower

than samples with multifilaments (S2 and S3) because of higher porosity. In contrast, the trend is reversed for group 2 samples, S4 shows higher sound absorption than S5 and S6, though the porosity is higher (87%) for S4. This is mainly because of surface roughness and stitch density of the spacer fabrics which causes sound waves to reflect more on the surface itself. Variations of porosity in the range of 2 or 3% have minor influence on the acoustic behavior of spacer fabrics (Figure 4).

As can be seen, sound absorption coefficient increases with decrease in the tortuosity values for both the group of samples (S1 to S6) for middle and high frequency ranges. At higher values of the tortuosity, the behavior shifts towards lower values of sound absorption. The thickness of the porous material layer has a great influence on the position of the peak value in the frequency

spectrum. The sound absorbency of spacer fabrics increases with the reduction in its porosity for group 1 samples (S1 to S3) but the trend is reversed in case of group 2 samples (S4 to S6). This may be

because of tortuous path in the middle layer and closeness of surface yarns in case of 3-dimensional knitted spacer fabrics.

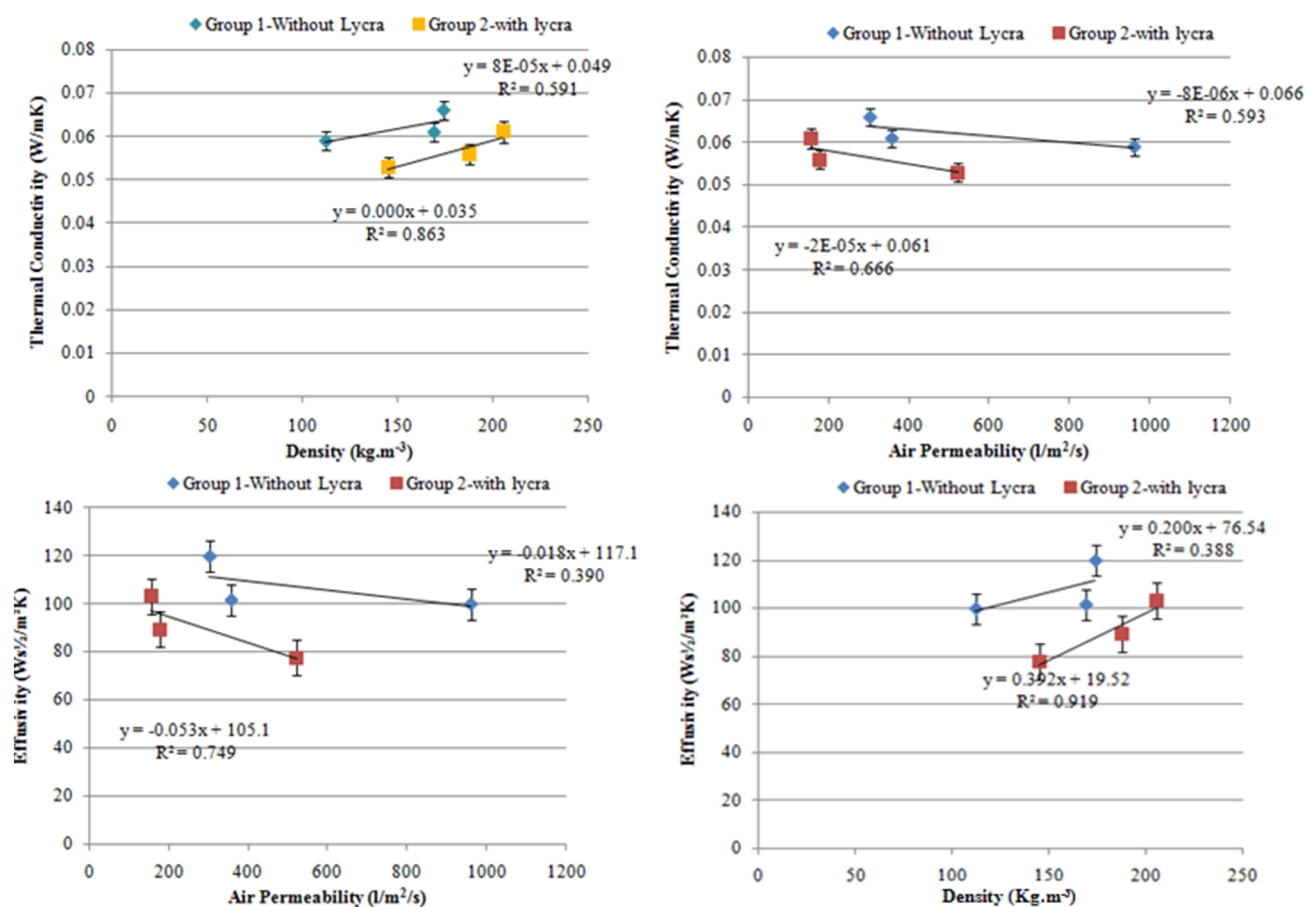


**Figure 3** Influence of density and air permeability on thermal conductivity and thermal effusivity

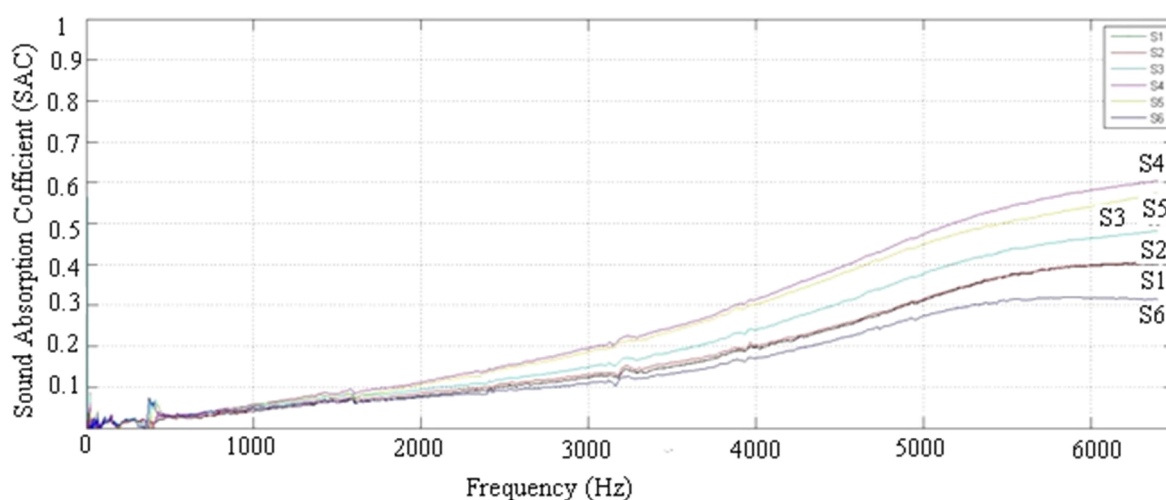


**Figure 4** Sound absorption coefficient of spacer knitted fabrics



#### 4 CONCLUSIONS

In knitted spacer fabrics, it is found that shear deformations depend very much on the type of spacer yarn and the fabric stitch density. The shear angles of samples using different methods are almost identical to each other before shear locking (buckling) effect takes place. The non-linearity of shear deformation increases after limiting locking angle which initiates the buckling of the sample. The 3D spacer fabrics have more tortuous path but still lower sound absorption because incident sound energy may get reflected away from the top layer and does not penetrate in to the fabric. The thickness of the porous material layer has also a great influence on the position of the peak value in the frequency spectrum. But the effect of density is more predominant in terms of sound absorbency as compared to effect of thickness.

#### 5 REFERENCES

1. Liu Y., Hu H.: Compression Property and Air Permeability of Weft-Knitted Spacer Fabrics, *Journal of the Textile Institute* 102(4), 366-372, 2011
2. Postle R.: A geometrical assessment of the thickness and bulk density of weft knitted fabrics, *Journal of the Textile Institute* 65(4), 155-163, 1974
3. Xu-Hong M., Ming-Qiao G.: The compression behaviour of warp knitted spacer fabric, *Fibers and Textiles in Eastern Europe* 16(1), 90-92, 2009
4. Mecit Armakan D., Roye A.: A study on the compression behaviour of spacer fabrics designed for concrete applications, *Fibers and Polymers* 10(1), 116-123, 2009
5. Yip J., Ng S.: Study of three-dimensional spacer fabrics: Physical and mechanical properties, *Journal of Material Processing Technology* 206(1-3), 359-64, 2008
6. Liu Y. et al.: Dynamic Response of 3D Biaxial Spacer Weft-Knitted Composite Under Transverse Impact, *Journal of Reinforced Plastics and Composites* 25(15), 1629-1641, 2006
7. Liu Y. et al.: Compression Behavior of Warp-Knitted Spacer Fabrics for Cushioning Applications, *Textile Research Journal* 82(1), 11-20, 2008
8. Walker K. et al.: Active Protection System, *Advanced Materials and Processes* 166(9), 36-37, 2008
9. Charmetant A. et al.: Hyper elastic Model for Large Deformation Analyses Of 3D Interlock Composite Preforms, *Composite Science and Technology* 72, 1352-1360, 2012
10. Arumugam V. et al.: Thermo - acoustic Behavior of 3D Knitted Spacer Fabrics, *Fibers and Polymers* 16(11), 2467-2476, 2015

# PERFORMANCE CHARACTERIZATION OF BASALT HYBRID WOVEN FABRIC REINFORCED CONCRETE

Hafsa Jamshaid<sup>1,2</sup>, Rajesh Mishra<sup>1</sup>, Jiri Militky<sup>1</sup>, Muhammad Tayyab Noman<sup>1</sup>, Mohanapriya Venkataraman<sup>1</sup>, Veerakumar Arumugam<sup>1</sup>, Tao Yang<sup>1</sup> and Xiaoman Xiong<sup>1</sup>

<sup>1</sup>Department of Material Engineering, Faculty of Textile Engineering, Technical University of Liberec, Czech Republic

<sup>2</sup>Department of Fabric Manufacturing, Faculty of Textile Engineering, National Textile University, Faisalabad, Pakistan

**Abstract:** In this work structural performance and durability of Textile reinforced concrete (TRC) is investigated. The aim of this work is to understand the bonding characteristics between different yarns and concrete that was studied by yarn pull out test. Impact of accelerated ageing under alkaline environment on basalt, polypropylene, polyester and jute are studied. The present study provides information about durability of different fiber-reinforced cement composites which can be forecast by fiber/cement bonds and accelerated aging conditions. It helps in better insight into the specific material behavior of the concrete with textile reinforcement

**Key words:** TRC, basalt yarn pull out, durability, textile reinforcement, woven structures

## 1 INTRODUCTION

The structural materials most often used in civil engineering are concrete and steel. It is noteworthy that concrete material is more brittle than other materials and has inherent disadvantages including low tensile strength and weakness in impact resistance. Besides this the concrete materials are easy to crack because of the shrinkage of the materials and the concentration of stress [1-5]. Thus, plain concrete is not applicable if significant tensile loading cannot be ruled out in advance, as it is the case in arch structures or short columns where predominantly compressive loading comes into picture. Usage with steel, it has also some limitations in terms of weight, thick concrete covers and more importantly resistance against corrosion of reinforcement. As a result the structures begin to suffer degradation after a period of using time. How to use structures safely has become a major concerned issue in the development of sustainable engineering structures.

In the 1950s, textile-reinforced concrete gained the interest due to evolution of the concept of composite materials. There are many researches about the properties of TRC. A number of previous studies have shown that the introduction of fibers increases the mechanical strength of the concrete [6-8]. A combination of non-corrosive fiber grid along with finely grained concrete formulates Textile reinforced concrete (TRC). It can be categorically defined as a combination of fiber/yarn structure, cementitious matrix and fiber/matrix interface. The presence of fibers also lowers the number and the width of cracks in the concrete due to the bridge action of them [6]. As soon as the health risks associated with asbestos were found.

An urge to find a replacement for building materials was raised and generated. By the 1960s, materials for reinforcement of concrete were glass, steel and synthetic fibers such as polypropylene. Extensive research work is carried out to find out new fiber-reinforced concretes [9, 10]. Variety of fibers was used to increase toughness and prevent cracking of cement. Sustainable, energy efficient and eco-friendly construction material is sought around the world. Sustainable, green construction material, natural fiber based reinforcement in a cement matrix is a feasible approach.

If fibers are exposed to aggressive environments, durability could become an issue. High concentration of alkali ions present in civil applications of concrete can be main reason of fiber damage. Reduction in mechanical properties and weight loss can be consequent outcomes of exposure to alkali ions. Different studies are quoted in the technical literature, yet the results reported show a contrast in them. As a matter of fact, TRC-based research reveals multi-promising attributes; recognition of them still needs to reach a conclusion due to absence of standard & long term behavior and lack of availability of design tools.

Basalt fibers are very promising materials due to their fire resistance, superior mechanical properties and relatively low cost. On the other hand, being a relatively new kind of fiber, its in depth study is yet to be done. There are very few indications in technical papers about their behavior after aging treatments. The current study investigates the possibility of using basalt with other types of yarns on load bearing capacity and durability. In the present work, the load-bearing behavior of Textile Reinforced Concrete (TRC), which is a composite of a fine-grained concrete matrix and

a reinforcement of high-performance fibers processed to textiles, when exposed to uniaxial tensile loading was investigated. When textile yarns are embedded in concrete, they are not entirely impregnated with cementitious matrix, which leads to associated heterogeneity of the concrete and the yarns to a complex load-bearing and failure behavior of the composite system. The main objective of the work is the investigation of hybridization effects in the load-bearing behavior of TRC. The scope and target of this work was to investigate durability and structural performance of TRC in order to evaluate its usage for civil applications

## 2 EXPERIMENTAL

### 2.1 Materials

The materials: polyester (PET), Polypropylene (PP) and jute (J) yarns used in this study were available commercially. The basalt (B) yarn was used as received (from company Kamenny Vek, Russia).

A commercial ordinary Portland cement (OPC) was used and green cement GEOPOLYMER BAUCIS L110 (produced by České lupkové závody, a.s., Pecínov, CZ) was taken. The alkalis used for accelerated aging treatment are analytical grade sodium hydroxide NaOH (Lach-ner, s.r.o., Brno, CZ) and calcium hydroxide  $\text{Ca}(\text{OH})_2$  (Lachema Brno, CZ)

### 2.2 Methods

#### 2.2.1 Preparation of Cement Matrix

The OPC pastes were prepared by mixing the cement with distilled water, with water/cement (w/c) ratio of 0.4. The samples were thoroughly mixed using glass rod for two minutes and then samples were subsequently cast in the molds with yarn in it. After 1 day, the samples were removed from the molds and after 2 days testing was done. Preparation of geopolymers (GPC) mixture is typically done with 5 parts by weight of cement and 4 parts by weight of alkali (NaOH).



TIRA Tester

#### 2.2.2 Yarn pull out test

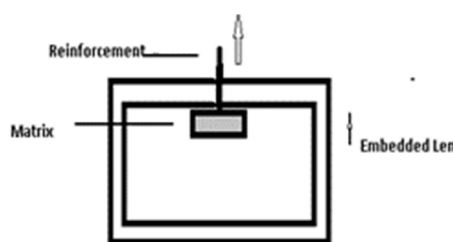
The pull-out test primarily gives information on the compatibility/interfacial behavior between the yarns selected for the reinforcement and the cement matrix. From this test, estimates can be derived for the failure behavior, and thus for the durability and load bearing capacity. The pull-out tests encompassed the evaluation of both pull-out and rupture of the textile material as failure modes.

So strand/yarn in cement test is used to quantitatively analyze this test. The yarn specimens were embedded into cement slab of 40x40x10 mm. The yarn is precisely placed in the center of the specimen. The yarn lengths have to be set so as to ensure protruding ends, for mounting in a tensile tester. It is important to protect the protruding yarn ends from the exposure to avoid strength losses. The specimens were demolded after 48 h and then dried again for 48 h at room temperature. Five specimens were produced for each yarn in order to obtain a representative trend of the pull-out behavior.

The yarn was pulled out from the cement by an TIRA 2300 (LaborTech s.r.o., Opava, Czech Republic) universal tensile testing machine at the rate of 2.0 mm/min. The experimental setup developed to conduct the pull-out tests is illustrated in Figure 1. In the standard pull-out test, load applied to the yarn end is recorded as a function of the displacement of this end with respect to a "stationary" point in the specimen.

#### 2.2.3 Accelerated aging in alkaline solution

The action of aqueous sodium hydroxide and calcium hydroxide solutions 10 g/L (w/V) on basalt, PET, PP and jute yarns were investigated under a variety of conditions of pH. For this purpose, loss in weight (W), breaking load, % elongation to break and scanning electron micrographs of the yarn surfaces were studied. Tensile tests were conducted on specimens before and after ageing treatment, given that the materials could be tested based on their level of degradation. Furthermore, the interpretation of the experimental results involved the documentation of visual observations before and after testing.



Experimental set up

Figure 1 Pull out test method

### 2.2.4 *Scanning Electron Microscope (SEM) for characterizing surface degradation*

SEM was used for morphological analysis and for investigating the surface degradation of alkali treated samples. SEM images were prepared with different magnifications ranging from 2.5 to 50 KX. The microstructures of yarns were prepared on a Vegas-Tescan Scanning Electron Microscope (SEM) with accelerating voltage of 20 kV.

### 2.2.5 *Tensile measurement to evaluate loss of mechanical properties*

Textile materials are exposed to an alkaline environment in the cement matrix, which makes them susceptible to damage. A comparison of the measured breaking strength to the breaking strength of undamaged yarns allows an assessment of the selected reinforcement. Tensile properties of all alkali treated and control samples were measured on a TIRA 2300 (LaborTech s.r.o., Opava, Czech Republic) universal testing machine according to standard ASTM E 2098-00.

## 3 RESULTS AND DISCUSSION

### 3.1 Yarn pull out

The interaction between the concrete matrix and reinforcement is characterized by the bond behavior. It is very important that there is good adhesion between the reinforcing fibers and the concrete or cement matrix, otherwise debonding may take place. If bond strength at the interface between the fiber and the matrix is too high, the reinforcement ruptures after the first crack initiates. On the other hand, the reinforcement is easily pulled out if the bond strength is too low. Bond strength may dominate the mechanical properties of fiber-reinforced concrete. Pull out test is most general test for this purpose. This test is useful to get information about the load transfer behavior between matrix and reinforcement. The pull-out tests characterize both pull-out and rupture of the textile yarn as failure modes. The breaking point does not designate the definitive breaking point of the yarn in itself, but rather the location of crack initiation.

The yarn pull out was carried by testing machine. From the experiment, the average maximum force and the respective average crack-opening displacement, i.e. total slip, were calculated.

In case of basalt, very small slippage (displacement) is observed, as they have good adhesion with cement matrix. Maximum stress recorded as tensile

stress of yarn is highest in case of basalt yarn. Similar situation is observed in case of jute yarn, but in this case force recorded is much lower as jute yarn has overall lower strength value.

In case of PP and PET, adhesion is not good and it can be viewed by high slippage / displacement / deformation. Such large displacement prior to material failure is crucial with regard to structural safety as well as energy dissipation, in particular in the case of dynamic loading. However, the fact that high strength levels can be only reached at high deformations means that for the service state, where only small deformations are acceptable and the design load-bearing capacity of TRC must be considerably lower than its tensile strength. Moreover, relatively wide cracks observed at high deformations are undesirable.

It can be seen that performance of highly twisted yarn e.g. PP is higher than less twisted PET yarn. This can be explained on the basis of mechanical anchoring which is the result of waviness. Also if density of crimped yarn increased effect is more prominent. The experimental findings are given in Table 1.

Photographic investigation shows that overall the force is transmitted by adhesion and friction between the reinforcement and the concrete. The load transfer between the filaments enclosed in the yarn/roving will however occur either based on adhesion or friction depending on the quality of the bond. The bond quality differs across the depth of yarn/roving which causes a complex failure mechanism involving the partial rupture and pull-out of singular filaments. The failure mechanism denoted as pull-out was often observed to be a telescopic failure (i.e. partial rupture and pull-out) a common failure phenomenon.

### 3.2 Accelerated aging in alkaline solution

The degradation of fiber due to the alkaline pore solution in the cement matrix seriously decreases the durability and may cause premature failure of the concrete composite. Calcium hydroxide is the primary cause of alkaline environment in cement. In this case the high concentration of alkali ions is the main cause of fiber damage. Particularly, weight loss and reduction in mechanical properties could appear. In the technical literature different studies are present, but the reported results appear somewhat contrasting.

**Table 1** Experimental findings of the pull out study

Reinforcement type	Max force [N]		Crack opening displacement at max force [mm]		Failure mechanism
	OPC	GPC	OPC	GPC	
B	82.90	33.24	2.56	1.46	Telescopic
PP	53.54	17.87	21.19	9.30	Pull out
PET	52.61	10.14	10.84	7.28	Pull out
J	5.68	3.21	2.30	4.24	Rupture

After a careful scientific research, accelerated aging tests were made to evaluate the weight loss and the loss of mechanical properties of basalt, PP, PET and jute fibers in order to quantify their performance limits. The 5 samples for each category were tested and their averages are reported.

### 3.2.1 Visual observations

The external appearance of the yarns specimens was examined pre- and post-alkali treatment, for comparison of color, surface degradation and change in shape. In basalt yarn, no significant visible change of color or surface texture were observed after 7 days of immersion in pH10, pH11 and pH12 of two types of alkali namely NaOH and  $\text{Ca(OH)}_2$ . The jute samples degradation was marked by color change. These samples lost a great deal of stiffness to the point that they broke prior to removal from the solution. For those exposed to pH12, the observed degradation was similar to the pH11 samples, yet these could be further tested in tension. The PP and PET specimens also lost a significant amount of physical stiffness. Effect of sodium hydroxide is stronger in all samples as compared to calcium hydroxide.

### 3.2.2 % weight loss

The specimen's weight was measured both before and after the aging in order to evaluate weight loss.

**Table 2** % weight loss

Reinforcement type	Weight loss [%] (1 week)					
	NaOH			$\text{Ca(OH)}_2$		
	pH10	pH11	pH12	pH10	pH11	pH12
<b>B</b>	0.4	0.8	1.0	0.3	0.5	0.7
<b>PP</b>	1.4	1.6	1.7	0.9	1.0	1.1
<b>PET</b>	2.8	3.2	3.5	2.0	2.5	3.0
<b>J</b>	4.7	6.2	7.2	4.1	5.0	5.2

These results reflect the conditions for a range of pH of alkali treatment in aqueous sodium hydroxide and calcium hydroxide solution. The weight loss increases with increasing pH and use of stronger

alkali (NaOH). The weight loss of basalt fiber is minimum as it is least affected by alkali followed by PP fiber.

### 3.2.3 Tensile test of alkali treated yarns

After the aging in alkali solution, tensile tests were made in order to evaluate the maximum load  $F_{max}$  and the ultimate tensile elongation % of all the yarns before and after the aging, comparing the values obtained from controlled sample. ASTM E 2098-00 standard test method was used for this test.

These results reflect the conditions for a range of pH and duration of alkali treatment in aqueous sodium hydroxide and calcium hydroxide solution. The weight loss increases with increasing treatment pH and use of stronger alkali (NaOH). The weight loss of basalt fiber is minimum as it is least affected by alkali followed by PP fiber. The graphical representation of strength loss is given in Figure 2.

The tensile test results for the controlled samples are compared to the alkali treated samples in terms of applied maximum load versus elongation %. It can be noticed that ultimate tensile strain decreases in all the fiber types along with decrease in  $F_{max}$ . Reduction in mechanical properties in basalt yarn is minimum. Basalt yarn mechanical properties are decreased probably due to the crystallographic structure of basalt, which is made by olivine (single tetrahedron), pyroxenes (linear chain) and plagioclase (tetrahedral space structure). In fact, alkaline aggressive environment can break some bonds of the linear tetrahedral chain of pyroxenes, so that a strength reduction can be seen.

Jute is a ligno-cellulosic fiber with hemicellulose (22-24%),  $\alpha$ -cellulose (58-60%) and lignin (12-14%) as the main constituents with other minor constituents as well. Among the three main organic components, hemicellulose and lignin are amorphous with relatively low polymerization degree, so they have a higher hydrolysis rate and solubility in alkaline medium than cellulose, which is the main reason for the degradation.

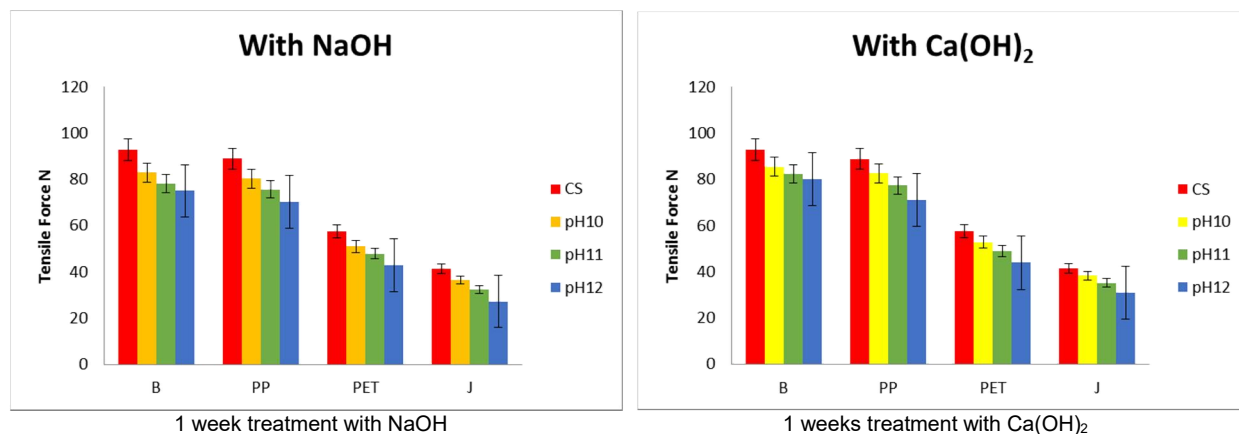


**Figure 2** Effect of pH on degradation of yarn after alkali treatment

The alkaline pore water dissolves the lignin and hemicellulose of fiber, which are sensitive to  $\text{Ca}(\text{OH})_2$  and high alkalinity causes hydrolysis of cellulose molecules which leads to degradation of molecular chains and then a reduction in degree of polymerization and lower tensile strength. The crystallization of lime in the lumen of the fibers and middle lamellae leads to a decrease in the technical fiber flexibility and strength and relatively lower durability of jute fiber in cement matrix.

The alkali treatment produced a drop in both tensile strength and Young's modulus of the fibers. This was attributed to the damage induced in the cell walls and the excessive extraction of lignin and hemicellulose, which play a cementing role in the structure of the fibers. SEM images showed that some of the fibers were split, had ramifications and presented a tape form rather than cylindrical.

Although PET can offer good mechanical properties and is suitable for some applications; however it is susceptible to hydrolysis under strong alkaline conditions, when hydroxyl anion attacks the electron deficient carbonyl carbon atom of the ester group (the polar  $\text{C}=\text{O}$  bond provides an active site for chemical reaction) and, in turn, results with a scission of the bond in the polymer chain. PET can also be susceptible to heightened degradation where there is concrete or cement present. The PET material loses its weight when the polymer chains break down and dissolve in the alkaline bath. The attack of highly ionized aqueous sodium hydroxide is limited essentially to the surface of the PET material as the nonpolar PET disfavors diffusion of ionic bodies inside the polymer phase. Thus the diameter of PET filaments decreases with the loss of polymer on the surface. However, the molecular weight and tenacity of the slimmed filaments remain essentially unchanged.

Polypropylene can be considered as inert to acid and alkali attack. Polypropylene fibers have a high resistance to acids and alkalis in all concentrations and up to comparatively high temperatures. Although PP has not very good bond with the cement matrix, this fiber is considered as attractive for the reinforcement of cement matrices, because of their high resistance to the alkaline environment of cement matrix and of low cost.

### 3.3 SEM morphology analysis

The time-dependent degradation of fiber surface is additionally investigated using an electron-microscope. Surface morphology of fiber samples was analyzed by using a scanning electron microscope. The microstructure of yarn surfaces indicated that the jute fiber encountered the most severe alkali attack and precipitation of hydration products in the cement matrix. Fibrillation and

diameter reduction is evident in the jute fiber. Figure 3 also shows the damage in the cell walls and a rougher fiber surface. Also, the collapse of fiber lumen can be seen. This is responsible for the decrease in capillary pressure and therefore decreases in permeability.

On the contrary, the controlled jute fiber (Figure 3) shows open lumens. Besides, SEM images showed the presence of diffused micro-cracks on fiber surface and evidenced a variation in surface morphology before and after aging.

## 4 CONCLUSIONS

Textile-reinforced composites are gaining popularity within the construction sector. This study investigated the effect of using different yarns on load bearing capacity and durability in cement composite. It has been discussed that the interfacial bond between textile reinforcement and the concrete matrix is greatly heterogeneous. The bond behavior of textile reinforcement embedded in a concrete matrix was experimentally investigated in this work. All tests results reveal that addition of fibers to the cement can significantly enhance the interfacial bonding. The increase in the bond strength can be attributed to this fact that, on one hand, the use of fiber in the cement reduces shrinkage cracking in the interfacial transition zone and bleeding at the interface.

The results obtained from tensile tests demonstrated clearly the positive influence of basalt yarn on the mechanical performance of TRC. In general, the use of high strength fibers like basalt increases the strength and toughness of the cement composites providing strain-hardening behavior. Low modulus fiber such as PP and PET enhance mainly the ductility of the cement composites, but not its strength in a strain softening behavior. The PP/PET structure did not bond strongly with the cement matrix resulting in relatively low composite performance. The B/PP, B/J or B/PET yarn combination in a hybrid fabric should be considered as reinforcement for cement composites. The hybridization of PP/PET yarn with basalt during weaving can solve this problem.

According to the results it can be concluded that the accelerated ageing test was too aggressive for textiles made of jute and PET, leading to extensive degradation; however, basalt and PP textiles were found to be promising alternative as they have superior durability properties in an alkaline environment without undergoing much strength loss. Despite the hydrophobic characteristics of PP fibers and their poor bond with the cement matrix, these fibers are considered as attractive for the reinforcement of cement matrices because of their high resistance to the alkaline environment of the cement matrix and their low cost.



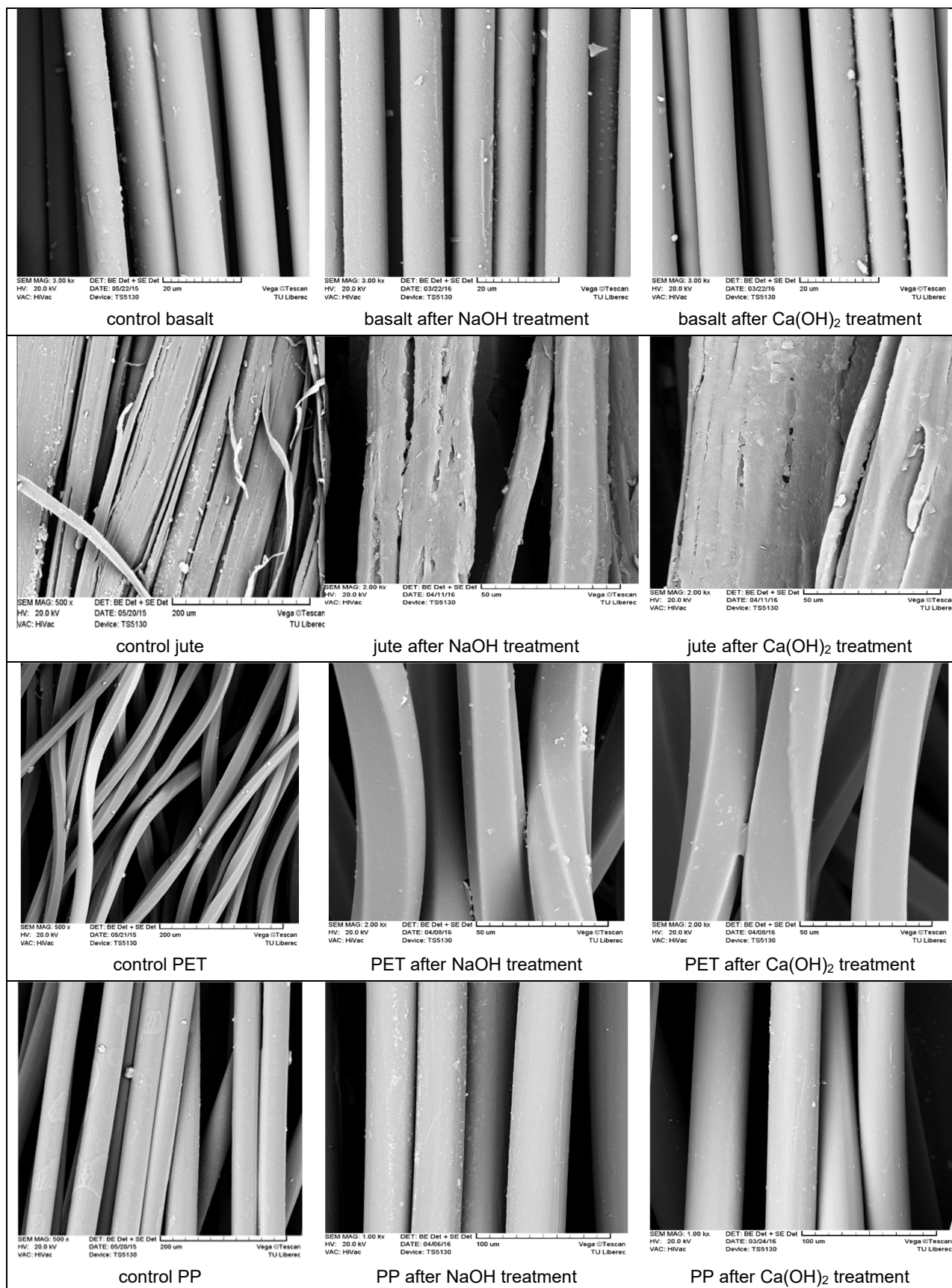


**Figure 3** SEM images of fibers after alkali treatment

## 5 REFERENCES

1. Banthia N., Zanotti C., Sappakittipakorn M.: Sustainable fiber reinforced concrete for repair applications, *Construction and Building Materials* 67, 405-412, 2014
2. Karahan O., Atis C.D.: The durability properties of polypropylene fiber reinforced fly ash concrete, *Materials & Design* 32(2), 1044-1049, 2011
3. Kim S.B., Yi N.H., Kim H.Y., Kim J.-H.J., Song Y.-C.: Material and structural performance evaluation of recycled PET fiber reinforced concrete, *Cement and Concrete Composites* 32(3), 232-240, 2010
4. Dawood E.T., Ramli M.: The effect of using high strength flowable system as repair material, *Composites Part B: Engineering* 57, 91-95, 2014
5. Hsie M., Tu C., Song P.S.: Mechanical properties of polypropylene hybrid fiber-reinforced concrete, *Materials Science and Engineering A*. 494(1-2), 153-157, 2008
6. Song P.S., Hwang S.: Mechanical properties of high strength steel fiber-reinforced concrete, *Construction and Building Materials* 18(9), 669-673, 2004
7. Izaguirre A., Lanas J., Alvarez J.I.: Effect of a polypropylene fibre on the behaviour of aerial lime-based mortars, *Construction and Building Materials* 25(2), 992-1000, 2011
8. Wang Y., Wu H.C., Li V.: Concrete Reinforcement With Recycled Fibers, *Journal Of Materials In Civil Engineering* 12:4(314), 314-319, 2000
9. Jump Up, Ochia T., Okubob S., Fukuib K.: Development Of Recycled PET Fiber And Its Application As Concrete-Reinforcing Fiber, *Cement And Concrete Composites* 29(6), 448-455, 2007
10. Liu Q., Giffard H.S., Shaw M.T., McDonnell A.M., Parnas R.S.: Preliminary investigation of basalt fiber composite properties for applications in transportation, *The Official Newsletter of the International Institute for FRP in Construction* 2, 6-8, 2005

# ELECTROSPUN POLYESTERS: COMPARISON OF POLYMERIC FIBROUS STRUCTURE AND ITS INFLUENCE ON FIBROBLAST PROLIFERATION

Aleš Šaman, Lucie Vejsadová, Jana Horáková, Věra Jenčová and Petr Mikeš

Technical university of Liberec, Department of Nonwovens and Nanofibrous Materials  
Studentska 2, 461 17 Liberec, Czech Republic  
[ales.saman@tul.cz](mailto:ales.saman@tul.cz), +420 485 353 230

**Abstract:** Polyesters have been recognized as promising polymers for use in tissue engineering applications due to their biocompatibility and biodegradability. The main advantage of synthetic polymers is its reproducibility of fabrication process due to a controllable narrow molecular weight distribution in comparison with natural polymers. Fibrous materials were prepared by needleless electrospinning. Planar layers from polycaprolactone and polylactic acid with various molecular weights were fabricated. Resulting fibrous mats were seeded with fibroblasts and cell viability was compared using metabolic MTT test.

**Key words:** Polylactide, polycaprolactone, electrospinning, *in vitro* testing

## 1 INTRODUCTION

Electrostatic spinning (electrospinning) is a method for production of sub-micron fibers with highly potential applications in tissue engineering and regenerative medicine. Nanofibrous structures are characterized by large specific surface area, high porosity with a small pore size that makes these materials tremendous interest for various applications. Electrospinning uses high electric field intensity which is affecting surface of polymeric solution. Electric forces create instabilities on the polymeric solution surface and when it reaches its critical values, the polymeric jet appears. During the process, the most of the solvent is being evaporated and dry nanofibers are collected on the counter electrode [4].

Electrospun fibers mimic extracellular matrix of native tissue therefore they are extensively investigated for various types of scaffolds [3]. An idea of tissue engineering and regenerative medicine is based on designing of an optimal scaffold that degrades during the time of cell infiltration and proliferation that could be enhanced by releasing of supporting factors [2]. This demands a list of requirements on material properties. An appropriate scaffold possesses slightly hydrophilic surface, adequate mechanical properties and degradation rate. Usage of natural polymers is limited due to their broad distribution of molecular weights that is one of the main parameters affecting electrospinnability. To the contrary, synthetic polymers benefit of relatively narrow molecular weight distribution. Aliphatic polyesters such as polyglycolic acid (PGA), polylactic acid (PLA) and polycaprolactone (PCL) belong among the most investigated synthetic polymers in the field of tissue

engineering nowadays [6]. These materials have already been approved in a variety of biomedical applications such as bioresorbable sutures used in a surgery [5].

In this work, polycaprolactone and polylactic acid with different molecular weights were electrospun and the influence of molecular weight and resulting fibers were discussed. Further *in vitro* testing investigated the influence of fibrous scaffold composition on fibroblast proliferation rate.

## 2 EXPERIMENT

The work was focused on the preparation of nano/microfibrous layers made from aliphatic polyesters using electrospinning. Polycaprolactone and polylactic acid electrospinning conditions were firstly optimized using needle electrospinning. Then, the method was transferred to high production needleless electrospinning where planar samples for further *in vitro* testing were obtained.

### 2.1 Materials

Biodegradable polyesters, namely polycaprolactone (PCL, Sigma Aldrich) and poly(L-lactic) acid (PLA, Polysciences) were selected for preparation of fibrous samples. Two different molecular weights were used for further fabrication of fibrous mats. Lower molecular weight was approximately 45,000 g/mol (samples marked as PCL45 and PLA45), higher molecular weight was around 80,000 g/mol (samples marked as PCL80 and PLA80). Polycaprolactone **PCL45** had the average number molecular weight ( $M_n$ ) of 45,000 g/mol ( $M_n$  40,000-50,000 g/mol) and polydispersity index (PDI) between 1.2 and 1.8 with the mass average molecular weight ( $M_w$ ) of 48,000-90,000 g/mol.

**Table 1** Spinning parameters of PCL45, PCL80, PLA45, PLA 80 using needleless electrospinning

Sample name	Mass concentration [wt %]	Distance [mm]	Voltage		Speed of EWM (Endless Motion Wire) [mm/sec]	Fiber diameter [nm]
			Positive source [+kV]	Negative source [-kV]		
PCL45	16	180	35	25	220	319.8 ± 575.7
PCL80	10	170	40	25	140	487.6 ± 407.3
PLA45	10	175	40	25	190	921.2 ± 617.3
PLA80	6	185	45	25	140	1161.0 ± 666.3

Polycaprolactone with average  $M_n$  80,000 g/mol (**PCL80**) had polydispersity index lower than 2. Poly(L-lactic) acid **PLA45** molecular weight was in range of 45,000 and 55,000 g/mol with polydispersity index of 1.94 and **PLA80** had molecular weight of 80,000 -100,000 g/mol.

## 2.2 Electrospinning

At first, needle electrospinning was performed in order to optimize polymeric concentration for further experiments. The electrospinning apparatus consisted of a syringe filled with electrospinning solution, a needle, a syringe pump, a high-voltage power supply and a flat collector covered with an aluminum foil. Electrospinning solutions were prepared 24 hours before the spinning. Aliphatic polyesters were dissolved in solvent system composed of chloroform, ethanol and acetic acid in ratio 8/1/1 (v/v/v).

Optimized electrospinning solutions were transferred for the spinning using strings within the device Nanospider™ NS 1W500U (Elmarco). Electrospinning conditions of each tested polymer are depicted in Table 1. The positive voltage (35-45 kV) was applied to the wire that served as a spinning electrode and the negative voltage of 25 kV was applied to the collector. The distance between the spinner and the collector was kept between 160 and 185 mm. The temperature during the experiments was kept at  $21 \pm 1^\circ\text{C}$  and the relative humidity  $40 \pm 5\%$ .

Resulting fibrous mats were analyzed using scanning electron microscopy (SEM) Tescan Vega 3SB. Fiber diameters were measured using NIS Elements software ( $n=100$ ). The data were expressed as median  $\pm$  standard deviation.

## 2.3 Cell Sources and Seeding

Prior to cell seeding, scaffolds were cut into round patches of 6 mm in diameter and sterilized by immersion in 70% ethanol for 30 minutes followed by double washing in phosphated buffer saline (PBS, Lonza).

Mouse 3T3 fibroblasts (ATCC) were cultivated in Dulbecco's Modified Eagle Medium (DMEM, Lonza) supplemented by 10% fetal bovine serum (FBS, Lonza), 1% glutamine (Biosera) and 1%

penicillin/streptomycin/amfotericin B (Lonza). The cells were placed in humidified incubator at an atmosphere of 5%  $\text{CO}_2$  at  $37^\circ\text{C}$ . When cells became confluent, they were suspended using trypsin-EDTA (Lonza). Fibroblasts (passage 10) were seeded on the scaffolds placed in 96 well plate at density of  $5 \times 10^3$  per well plate. Medium was changed twice a week during the experiment (11 days). Materials incubated in the complete medium without cells served as negative controls for MTT test ( $n=2$  per each testing day).

## 2.4 Metabolic MTT assay

Viability of the cells seeded on the scaffolds was analyzed by MTT test after 3, 7 and 11 days of culture period. MTT [3-(4,5-dimethylthiazol-2-yl)-2,5-diphenyl-2H-tetrazolium bromide] has been reduced to purple formazan by mitochondrial dehydrogenase in cells indicating normal metabolism. 50  $\mu\text{l}$  of MTT solution was added to 150  $\mu\text{l}$  of complete medium and samples were incubated at  $37^\circ\text{C}$  for 4 hours. Formed violet crystals of formazan were dissolved with acidic isopropanol. Optical density of suspension was measured ( $\lambda_{\text{sample}}$  570 nm,  $\lambda_{\text{reference}}$  690 nm). Each testing day, 8 samples of each material were incubated with MTT solution and final absorbance was calculated as the difference between absorbance measured by 570 nm and by reference wavelength 690 nm. The absorbance of negative controls was subtracted from measured values of absorbance of tested samples and placed into the graph comparing viability of cells cultured on tested materials. The data were expressed as mean of measured absorbance  $\pm$  standard error of the mean.

# 3 RESULTS AND DISCUSSION

## 3.1 Electrospinnability of aliphatic polyesters

Polycaprolactone and polylactic acid in both tested molecular weight were spinnable using needle electrospinning as well as in needleless setup. The electrospinning parameters using needle were optimized as follows: voltage 15-20 kV, distance 180 mm, needle diameter 0.9 mm, feed rate of 1-1.5 ml/h, temperature  $20-23^\circ\text{C}$  and relative humidity 35-40%. Conditions of needleless electrospinning are summarized in Table 1.



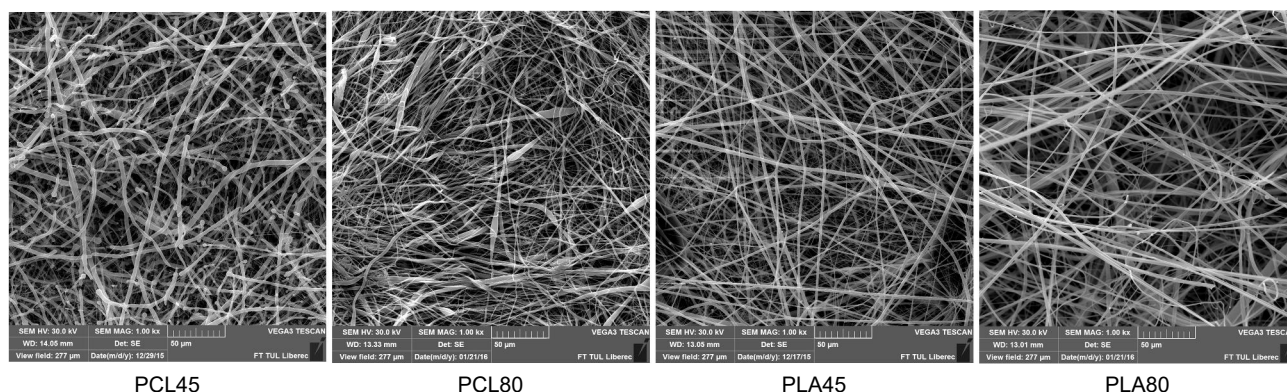


**Figure 1** Scanning electron microscopy pictures of electrospun PCL45, PCL80, PLA45 and PLA80

Resulting fibrous structures are depicted by scanning electron microscopy in Figure 1. Spinnability of higher molecular weight polymers (PCL80 and PLA80) was strongly dependent on process parameters such as distance between the string and collector and speed of EWM (Endless Motion Wire). If the processing conditions were not kept precisely, resulting fibers were pulled out during the deposition on the collector. Lower molecular polymers (PCL45 and PLA45) were spinnable in more robust conditions.

Optimal concentration of polymer mass was found as: 16 wt% for PCL45, 10 wt% for PCL80 and PLA45 and 6 wt% for PLA80. Polylactic acid was electrospun from more concentrated solutions than polycaprolactone of corresponding molecular weights. Other properties such as viscosity or polymer crystallinity can influence the optimal amount of polymer in the electrospinning solution.

### 3.2 Fiber diameter characterization

Fiber diameter of resulting planar fibrous mats was compared using image analysis software. Electrospun polycaprolactone mat formed uniform fibers with fiber diameter median  $\pm$  standard deviation of  $319.8 \pm 575.7$  nm in case of PCL45 and  $487.6 \pm 407.3$  nm in case of PCL80. Similarly polylactic acid with lower molecular weight (PLA45) resulted in fiber diameter of  $921.2 \pm 617.3$  nm and with higher molecular weight (PLA80) of  $1161.0 \pm 666.3$  nm. The fiber diameter distribution was wider in PLA samples as seen from fiber diameter characterization that is depicted in Figure 2. Fiber distribution could be influenced by polydispersity index of polymer. Polycaprolactone PCL45 with lower PDI than PLA45 possessed narrow fiber distribution compared to PLA45. PCL80 with PDI less than 2 showed also wider fiber diameter distribution compared to PCL45 with PDI between 1.2 and 1.8. No data of PLA80 polydispersity index were available from the supplier. However, based on the fiber diameter characterization it could be

assumed that polydispersity index will be around 2 or even higher.

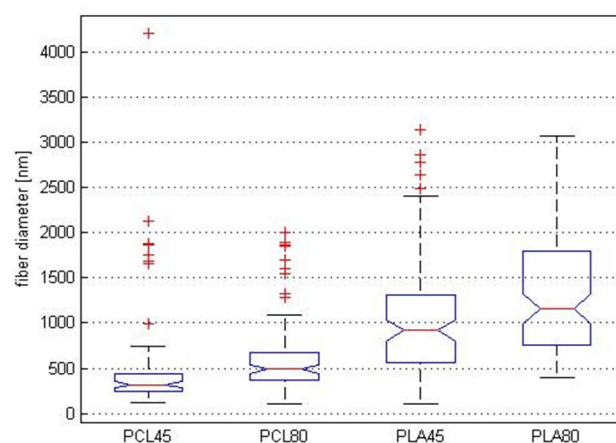


**Figure 2** Box plot of fiber diameter distribution of electrospun PCL45, PCL80, PLA45 and PLA80 with standard settings including 50% percentile for the box with median, maximum and minimum values and the extremes

### 3.3 Metabolic activity of fibroblasts

Fibroblasts were seeded on prepared electrospun layers made from PCL45, PCL80, PLA45 and PLA80. During the cell culturing, fibroblast metabolic activity was measured using MTT test after 3, 7 and 11 days. The results showed that electrospun polylactide in both molecular weights supported fibroblast proliferation since their metabolic activity was continuously increasing during the culture period as depicted in graph in Figure 3. Electrospun polycaprolactone supported cell adhesion (cell viability in day 3 was comparable to electrospun PLA) but the proliferation was delayed compared to electrospun PLA. It is assumed that PCL did not possess ideal surface properties because of its hydrophobicity [1].

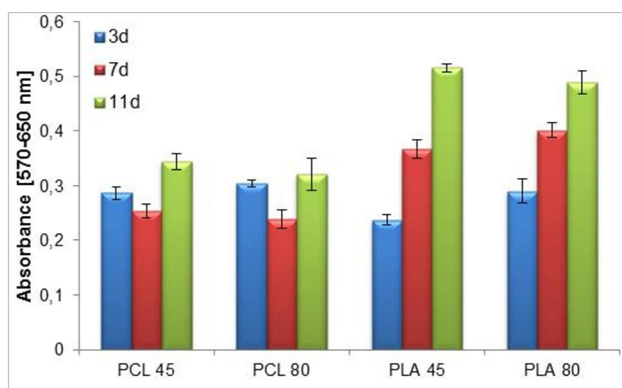


**Figure 3** Metabolic MTT test of fibroblasts seeded on electrospun PCL45, PCL80, PLA45 and PLA80 after 3, 7 and 11 days of culturing

#### 4 CONCLUSIONS

Aliphatic polyesters in different molecular weights were successfully electrospun. Polycaprolactone formed fiber diameters in range of hundreds of nm (300-500 nm) whereas polylactide created mostly microfibers with wide range distribution. Lower molecular weight of 45,000 led to thinner fiber diameter compared to higher molecular weight of 80,000 in both tested polymers. *In vitro* tests showed that electrospun layers support fibroblast adhesion. However, cell proliferation was accelerated on electrospun PLA compared to PCL.

**ACKNOWLEDGEMENTS:** The authors are thankful to the grant of the Ministry of Health of the Czech Republic: NV15-29241A (Nanofibrous Biodegradable Small-Diameter Vascular Bypass Graft) and to the Department of Nonwovens and Nanofibrous materials, Faculty of Textile Engineering, Technical University of Liberec. Aleš Šaman, Lucie Vejsadová and Jana Horáková thank the Student's Grant Competition of Technical University of Liberec: 21150 (Development and modification of nanofibrous drainage implant for use in the treatment of glaucoma).

#### 5 REFERENCES

1. Bacakova L., Filova E., Parizek M., Ruml T., Svorcik V.: Modulation of cell adhesion, proliferation and differentiation on materials designed for body implants, *Biotechnology* 58, 739-767, 2011
2. Hu X., Lui S., Zhou G., Huang Y., Xie Z., Jing X.: Electrospinning of polymeric nanofibers for drug delivery applications, *Journal of Controlled Release* 165, 12-21, 2014
3. Lanza R., Langer R., Vacanti J.P.: Principles of Tissue Engineering (2<sup>nd</sup> edition), Academic Press, Cambridge, 2000
4. Lukáš D., Sarkar A., Martinová L., Vodsed'áková K., Lubasová D., Chaloupek J., Pokorný P., Mikeš P., Chvojka J., Komárek M.: Physical principles of electrospinning (Electrospinning as a nano-scale technology of the twenty-first century), *Textile Progress* 41(2), 59-140, 2009
5. Middleton J.C., Tipton A.J.: Synthetic biodegradable polymers as orthopedic device, *Biomaterials* 21, 2335-2346, 2000
6. Zhan J., Singh A., Zhang Z., Huang L., Elisseeff J.H.: Multifunctional aliphatic polyester nanofibers for tissue engineering, *Biomaterials* 2(2), 202-212, 2012



# COMPARISON OF THE WELL KNOWN SPINNING AND ELECTROSPINNING METHODS FOR POLYVINYL ALCOHOL

Lenka Blažková, Jana Hlavatá, Jana Horáková, Tomáš Kalous, Patrik Novák, Martin Pelcl, Kateřina Strnadová, Aleš Šaman and Jiří Chvojka

Technical University of Liberec, Department of Nonwovens and Nanofibrous Materials  
Studentská 2, 461 17 Liberec, Czech Republic  
[jiri.chvojka@tul.cz](mailto:jiri.chvojka@tul.cz)

**Abstract:** The electrospinning is known for more than 100 years. Since then, many spinning and electrospinning techniques have been developed. This article aims to introduce and compare spinning methods which are used to create nanofibers and nanofibrous mats. Polyvinyl alcohol (PVA) has been chosen as a polymeric model. Different concentrations of PVA were spun using various techniques. Depending on the spinning method, different fibrous morphologies have been created. Spinnability of PVA as well as fiber diameter measurement was evaluated showing that spinning techniques provide large tool for various applications.

**Key words:** Electrospinning, polyvinyl alcohol, spinning techniques, spinnability

## 1 INTRODUCTION

A method of using electrostatic forces for creating very fine fibers has been known for more than 100 years. Electrospinning has proved relatively simple method for forming submicron fibers, typically from 100 nm to 1 µm. The exception is not the fibers reaching of few micrometers. Nanofiber structures are characterized by large specific surface area, high porosity, but with a small pore size. These materials are built foreground interest for various applications. This method can prepare fibers of different polymers, natural, synthetic polymers and containing various additives depending on the use and desired properties [1]. Depending on the final application, various requirements on nanofibrous layers are demanded. Therefore, the novel techniques are being discovered leading to new properties of fibrous mats, higher fibrous production or improved spinnability of some polymers.

This article aims to describe and compare various spinning techniques which are investigated at the Technical university of Liberec, Department of nonwovens and nanofibrous materials. The description of used spinning methods is introduced in experimental part and results with chosen model polymer polyvinyl alcohol (PVA) are shown. Polyvinyl alcohols are water soluble polymers manufactured by alcoholysis of polyvinyl acetate. The properties of the various grades are mainly governed by the molecular weight and the remaining content of acetyl groups.

Nowadays it is possible to develop novel spinning techniques based on the older ones that are known for many years. The electrospinning process could

be transformed to new ways of spinning techniques such as bubble spinning, drawing technique and centrifugal spinning. Some of them use the high voltage for production of fibers, the others use capillary forces or their combination. Here, we present the results of spinning of various concentration of PVA ranging from 8% to 28% using centrifugal spinning, drawing, electrospinning from the rod, from the needle, bubble spinning, needle-less spinning and alternative current spinning. Spinnability of these solutions is evaluated and the fibrous morphology is characterized by fiber diameter measurement.

## 2 EXPERIMENTAL

### 2.1 Materials

The experiments were carried out with a chosen polymer polyvinyl alcohol (PVA), Mowiol grade 18-88 (Kuraray) supplied in granule form.

The polymeric solutions were prepared from the PVA granules that were dissolved in the distilled water. The experimentally tested concentrations of polymeric solutions were set as 8%, 12%, 16%, 20%, 24% and 28% (w/w). The volume of polymer solution (each concentration) was 100 ml that was further divided into smaller amount of volume and distributed to individual spinning technologies. All these solutions were spun by spinning technologies, namely centrifugal spinning, drawing, electrospinning from the rod, from the needle, bubble spinning, needle-less spinning and alternative current spinning that are described in the following subchapter.

Polymeric solution was characterized by dynamic surface tension and viscosity measurement since

these parameters are useful for prediction of spinnability of polymeric solutions. Dynamic surface tension of PVA solutions was measured by the maximum pressure in a bubble using the bubble pressure tensiometer PocketDyne (Krüss). Surface tension values are presented as the average of five measurements ( $n=5$ ). Viscosity measurement was carried out on the rotational viscometer Haake Rotovisco 1 (Thermo Scientific) with a rotary nozzle C35/1°TIL. Each sample was measured 5 times at a constant speed of  $300 \text{ s}^{-1}$  and 5X at increasing speeds from 10 to  $300 \text{ s}^{-1}$  (8%, 12%, 16%, 20%), respectively, from 10 to  $1000 \text{ s}^{-1}$  (8%, 12%) according to the density of the polymer. The viscosities were averaged and plotted ( $n=5$ ).

## 2.2 Methods

**2.2.1 The centrifugal spinning technology** is based on a relatively simple idea. Spinning fluid is placed into spinneret unit [2]. When the rotating speed reaches critical value, the centrifugal force overcomes the surface tension of spinning fluid, and liquid jets are ejected from the nozzles of the spinneret unit (Figure 1). The centrifugal force, together with the air frictional force, elongates the jets and leads to the formation of nanofibers. In addition to the centrifugal force and air friction force, other forces such as rheological force, surface tension, and gravitational force, might also influence the nanofiber formation [3].

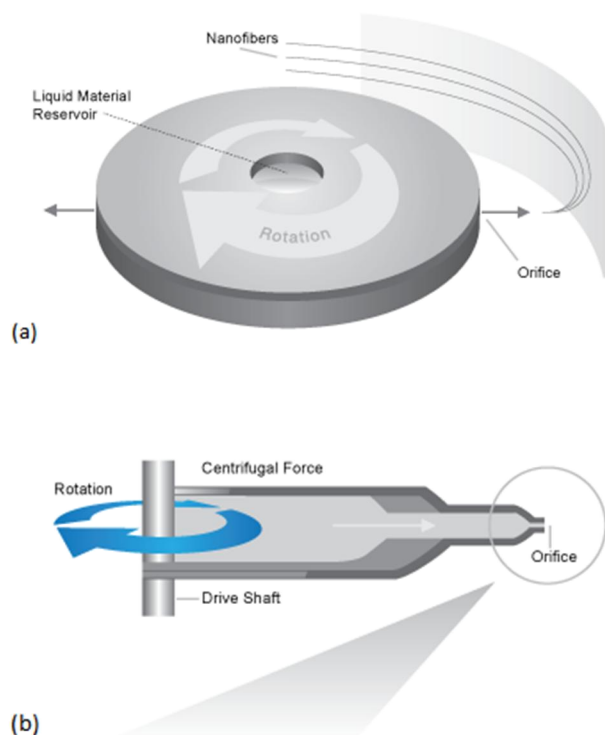


**Figure 1** Detail of the spinneret for needle force spinning and fiber formation developed by FibeRio: a) diagonal view, b) side view [4]

**2.2.2 The drawing technique** has been known for centuries. Nevertheless, our team is focused on its innovation and application. Polymer solution in a form of a droplet is placed on a workbench. The droplet is eroded with drawing element which retracts from it, pulling a bridge of material as depicted in Figure 2. The bridge stretches, solidifies, and finally forms a single fiber which is accurately positioned. If the parameters are optimized, the fiber diameter reaches hundreds of nanometers [5]. Periodical repetition of this process will give rise to a defined structure. The technique enables drawing of fibers made from polyvinyl alcohol, polyvinyl butyral (PVB), polycaprolactone (PCL) and polystyrene (PS) where single nanofibers are precisely arranged on a holder. To accomplish such goals, a micro manipulating machine has been developed and used for parameter tuning, due to its repeatable accuracy.

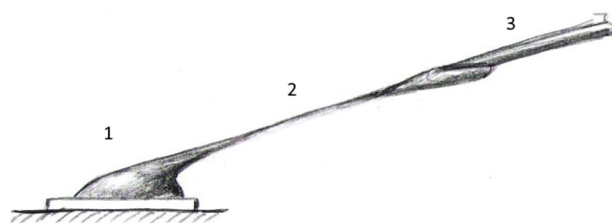


**Figure 2** Detail of the drawing setup: 1) polymer droplet on the workbench, 2) polymeric fiber, 3) drawing element

**2.2.3 Electrospinning from the rod, respectively from a conductive cylinder**, is technology particularly suitable for verification of polymeric solution spinnability in a laboratory conditions rather than for large scale fibrous production. The basic setup of electrospinning from the rod is described in Figure 3. Small amount of polymer solution (about 3 g) can be used for testing the spinnability of polymer solution that makes the technology useful in laboratory conditions since the polymers could be very expensive. The rod is made from integrated conductive roller having a diameter of approximately 5-15 mm which is placed in vertical position on the non-conductive frame. High voltage is supplied on the body of the rod. Polymer solution is manually applied on said the top of the where the action of the electrostatic field produces nanofibers. Nanofibers dropped on the collector that can be in a various forms such as coated backing fabric with black paper or aluminum foil. It is possible to influence the morphology of the resultant fibers changing a few parameters. At first, there are technological parameter settings such as the diameter of the rod or distance between the peak of the rod and the collector, value of the used electric voltage. Secondly, parameters of the polymer solution, especially concentration that

is directly proportional to the viscosity of the solution, composition of used solvent system, the molecular weight of the entering polymer, play an important role in the characteristics of resulting fibrous mats [6, 7].

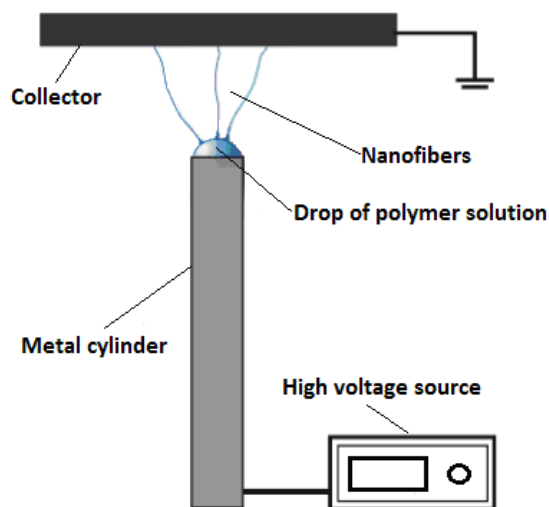


**Figure 3** Schematic representation of electrostatic spinning from rod

2.2.4 Another electrospinning technique is spinning from the needle where polymeric solution is ejected from the needle as depicted in Figure 4. The needle is connected to a syringe which serves as a reservoir for the polymer solution and simultaneously applying a pressure in induced dosage. Linear pump acts on the syringe set speed and thus leads to a controlled flow polymer solution from needle. Formation of the fibers depends on the high voltage which is supplied across the wire to the body of the needle and thereby into the solution. At the end of the needle is formed Taylor cone by applying a high voltage where the fibers are drawn from. Electrospinning from the needle, as well as from the rod mentioned in the previous paragraph, is from the perspective of production very inefficient. The methods are more suitable for laboratory use where large scale production is not required. These techniques are mainly used for

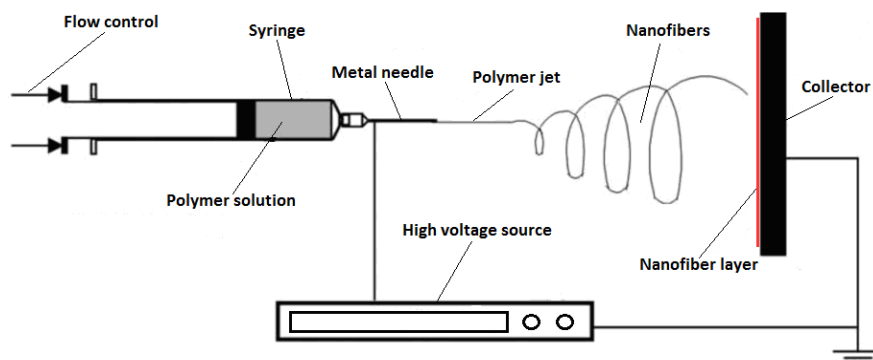


**Figure 4** Schematic representation of electrospinning from the needle

the testing of new polymers, solvents or additives, optimizing of solution parameters and spinning conditions. Their main advantage is simple construction and rapid response to change of various parameters settings. The resulting morphology can unlike rods also affect needle diameter, shape and type of the collector etc. [2].

2.2.5 Bubble electrospinning was firstly mentioned in the year of 2007. Recently, the technology belongs to novel technology of electrospinning (see Figure 5) capable of large scale fiber production [4].

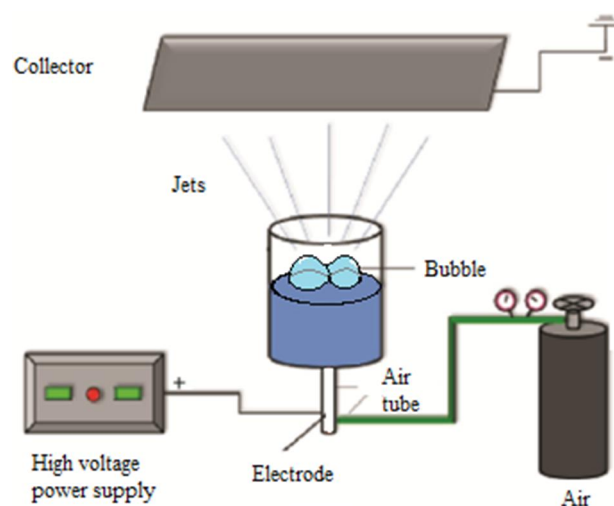


**Figure 5** Bubble spinning technology

This method utilizes the electrostatic force to overcome the surface tension of the bubbles, instead of classical electrospinning, where a Taylor's cones occurs. The main part of this device is electro conductively round container which serves as a reservoir of polymer solution. On the bottom part of this round container, a hole is drilled for air supply which provides the bubble effect. The container is fixed to the electrically conductive tube through the air flows and is connected to a high voltage. Electrospinning process takes place in an optional distance on a flat collector.

**2.2.6 Nanospider technology** is needle-less technology using high voltage where fibers are created directly from free liquid surface. The principle of the Nanospider is based on the possibility of producing nanofibers from a thin layer of polymer solution. In this case, Taylor cones are created on the surface of a rotating roller or wire immersed in a polymer solution. Because the Taylor streams are formed next to each other throughout the entire length of spinning electrode, this revolutionary idea produced many advantages such as high production rate. This commercial method for production of polymeric nanofibers is used in industry [8]. This is a simple and versatile method for production of nanofibers from a variety of polymeric materials. In the experiment, the laboratory scale machine Nanospider Production Line NS 1WS500U (Elmarco) was used (see Figure 6).

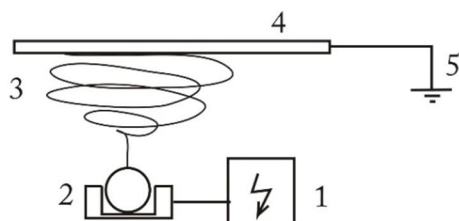


**Figure 6** Scheme of Nanospider: 1) High voltage supplies, 2) roller in polymer solution, 3) nanofibers, 4) collector, 5) grounding

**2.2.7 The technology alternating current spinning** is currently being developed at Technical university of Liberec as a novel method that uses alternating current (AC) power sources for the creation of nanofibrous materials through the phenomenon of electrospinning. This technology requires a high voltage transformer for step up conversion of standard voltages to high voltages [9]. There is no need for frequency control therefore it is possible to use the standard 50 Hz source. This technology is much more productive than standard direct current (DC) setups employed in previously introduced technologies but does not produce materials with the same degree of homogeneity. The use of collector, powered or grounded, is merely a matter of convenience for AC electrospinning because it typically creates a rising smoke-like column of electrically neutral nanofibers as shown in Figure 7. This is of great interest for numerous potential applications because it simplifies the required engineering solutions for operations with nanofibrous material. Materials produced by this technology have potential to be used for filtration and absorption of harmful substances (bacteria, gasses) or in medical products.

All above mentioned techniques were used for spinning of PVA in different concentrations from 8%

to 28%. Spinnability and fiber diameter was evaluated for each technology.

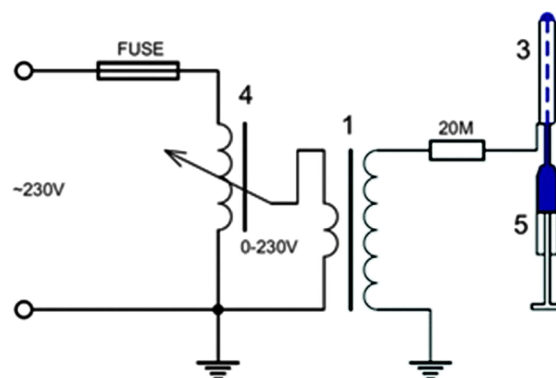


**Figure 7** Schematic AC – spinning setup and the spinning electrode, 1) high voltage supply, connected on 4) variable transformer, 3) spinning electrode, 5) controlled infusion pump

Morphology of fibrous samples was assessed by scanning electron microscopy (SEM) and image analysis software to characterize fiber diameter. Samples for SEM analyses were sputter coated with gold and analyzed using TESCAN Vega 3SB Easy probe (Czech Republic). All specimens were recorded in appropriate magnification to enable image analysis of fibrous morphology. Image analysis of fibers was evaluated from SEM pictures using software NIS Elements (LIM s.r.o., Czech Republic). Fiber diameter characteristics were assessed from 100 measurements ( $n=100$ ) and showed in a box plot.

Centrifugal spinning technology O = force spinning diameter of spinneret 50 mm, speed of spinneret 3000 rpm, distance between spinneret and collector 100 mm,  $t=23^{\circ}\text{C}$ ,  $\text{RH}=35\%$ . OT = force spinning jets diameter of spinneret 100 mm, speed of spinneret 2500 rpm, diameter of jets 1.2 mm, distance between spinneret and collector 100 mm,  $t=22^{\circ}\text{C}$ ,  $\text{RH}=40\%$ . EO = force electrospinning diameter of spinneret 50 mm, speed of spinneret 2500 rpm, distance between spinneret and collector 100 mm,  $t=21^{\circ}\text{C}$ ,  $\text{RH}=41\%$ . Drawing technique the fibers were pulled onto micromanipulator second generation (MMP II) at 1000 m/s with an acceleration of 500 m/s and 0.3 radius. The fibers were pulled in the length of 18 cm at an air temperature of  $19.6^{\circ}\text{C}$  and humidity 30%. On the campaign was used 20 G peak (OKI International, Taper Tip 20G x 1-1/4 "). The concentration of 8%, 12% and 15% percent were not suitable to form fibers. At a concentration of 20% PVA has been possible fiber winding. Dosing pump was used with a pressure piston of 0.25 bar for 0.8 seconds. The polymer was dosed approximately every two stretch fiber. SEM analysis of the samples was prepared of fibers fixed in the fixation rings having about 400 fibers per sample. Samples were prepared a total of five levels



from this one. For further experiments with drawing fibers were prepared two higher concentrations of PVA. Drawing of the 28% PVA was at a temperature of 19.8°C and humidity 35% (1 February 2016). For drawing was used pressure of 0.25 bar for 1.5 seconds. Again we gave 5 samples for SEM. Electrospinning ROD the voltage +40-55 kV, distance 150 mm and needle the voltage +25-36 kV, distance 150 mm, feeding 6-7 ml/h, temperature 21°C humidity 31%, bubble spinning the voltage +23 kV, set distance 150 mm,  $t=22^{\circ}\text{C}$ ,  $\text{RH}=40\%$ , Nanospider voltage +50 kV and -10kV, distance 150 mm,  $t=22^{\circ}\text{C}$ ,  $\text{RH}=35\%$ , AC spinning 37-38 kV, spinning without collector,  $t=23^{\circ}\text{C}$ ,  $\text{RH}=42\%$ .

### 3 RESULTS AND DISCUSSION

Polyvinyl alcohol granules were dissolved in water in concentrations ranging between 8% and 28%. The various concentrations and technologies lead to different diameters of resulting nanofibers that was assessed after the spinning. The value of fibers diameters is connected with boundary condition surface tension summarized in Table 1 that also records the average temperature of the solutions during measurement.

The Table 1 showed that with increasing concentrations of PVA solutions, surface tension was growing. However, this increase was not linear and the values were influenced by varying solution viscosity. The surface tension of PVA solutions with a concentration of 24 wt% and higher was very difficult to measure because of the formation of bubbles spans approximately one thousand ms. In contrast, in the case of solutions having lower concentrations, respectively. Viscosities, the emergence of bubbles ranged from tens to hundreds of milliseconds.

The polymer concentration of 20 wt% was not possible to measure at higher speed than  $300 \text{ s}^{-1}$ . The measurement of viscosity of each sample is shown in the Figures 8 and 9. The concentration of 24 wt% and 28 wt% are not mentioned in Figures 8 and 9 due to their higher viscosity. The electrospinning with this higher concentration was not able; these high viscosity solutions were suitable only for drawing technique as described later.

**Table 1** Surface tension, incl. standard deviations, and the temperature of the PVA solutions in different concentrations

	concentration [w/w %]	Surface tension [mN/m]	Temperature of polymer solution [ $^{\circ}\text{C}$ ]
PVA	8	$59.38 \pm 0.30$	25.1
	12	$61.96 \pm 0.49$	25.0
	16	$81.46 \pm 0.31$	25.1
	20	$115.46 \pm 1.06$	25.3
	24	$182.70 \pm 1.85$	23.7
	28	$209.42 \pm 3.62$	24.1

Spinnability of the polymers is summarized in the Table 2, where resulting fiber diameter characteristics are displayed. It is seen that fiber diameter is increasing with polymeric content within the spinning solution. Different technologies require various parameters of solution properties. For example drawing is able to create fibers from highly viscose solution of 20 wt% and higher. On the other hand, needle less electrospinning was possible to carry out from low viscose solution ranging from 8 to 16 wt%. Electro centrifugal spinning was the most versatile technique since all tested concentrations were electro spun.

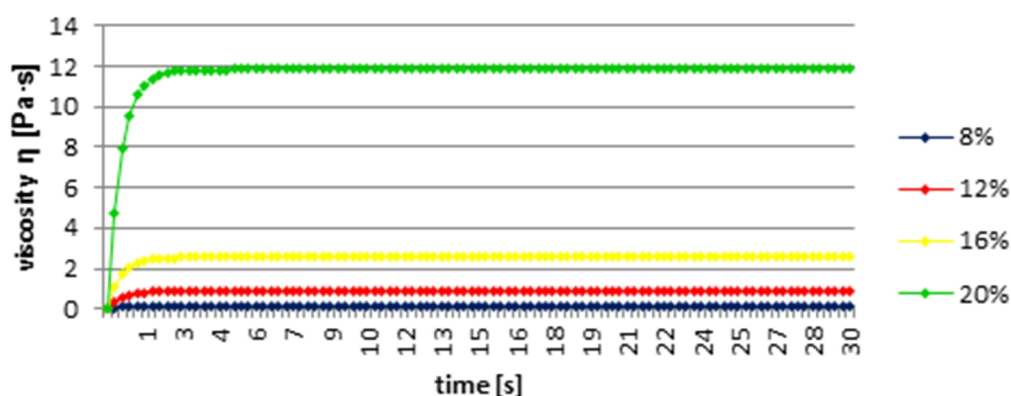


**Figure 8** Viscosity of PVA at constant shear rate  $300 \text{ s}^{-1}$

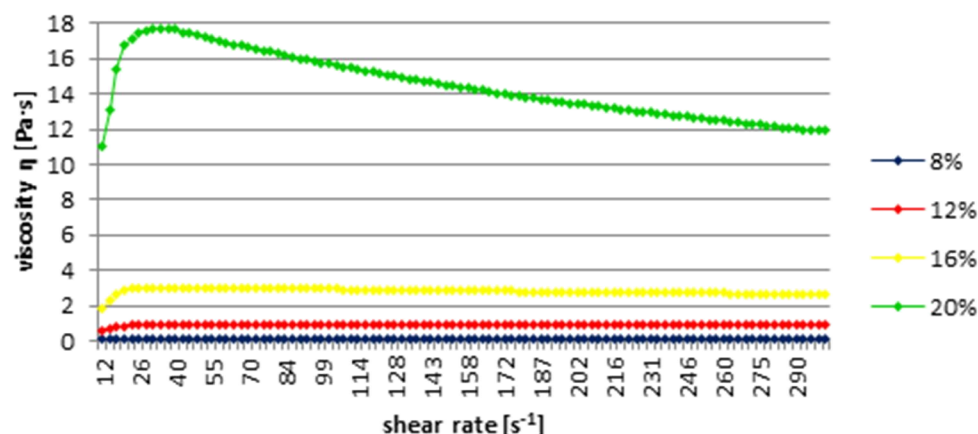


**Figure 9** Viscosity of PVA at linearly increasing shear rate 10-300 s<sup>-1</sup>

**Table 2** Spinnability of PVA solutions using spinning technologies and their corresponding fiber diameter median ± standard deviation

	8 wt%	12 wt%	16 wt%	20 wt%	24 wt%	28 wt%
Centrifugal spinning	x	409±168 nm	338±139 nm	474±411 nm	4670±4265 nm	X
Electro-centrifugal spinning	391±194 nm	361±177 nm	519±221 nm	1002±697 nm	2275±2482 nm	2804±2483 nm
Centrifugal spinning - Rod	393±150 nm	572±211 nm	915±258 nm	2212±1069 nm	X	X
Drawing	X	x	X	1093±236 nm	1777±648 nm	1895±763 nm
Electrospinning from the rod	145±57 nm	279±63 nm	321±102 nm	725±256 nm	X	X
Electrospinning from the needle	155±45 nm	318±68 nm	442±71 nm	795±151 nm	X	X
Bubble spinning	177±42 nm	302±74 nm	413±75 nm	692±107 nm	962±254 nm	X
Needle-less electrospinning	239±79 nm	423±75 nm	450±155 nm	X	X	X
AC spinning	174±73 nm	310±168 nm	502±126 nm	878±470 nm	2734±1109 nm	X

The resulting fibers were analyzed by SEM followed by fiber diameter measurement. Box plot of fiber diameter distribution of 16 wt% is depicted in Figure 11 showing that centrifugal spinning led to the fibers

with high range distribution of fiber diameters whereas electrospinning from the rod, needle or bubble spinning possess homogeneous fibrous mats as seen also from SEM pictures in Figure 10.

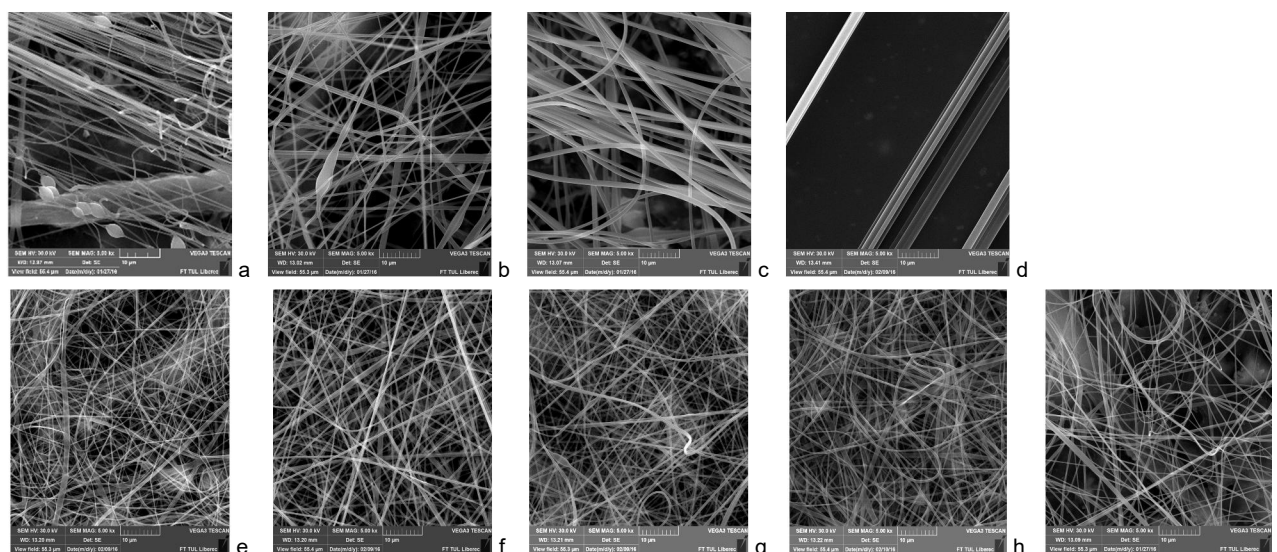


**Figure 10** Morphology of the PVA fibers spun from 16 wt% solution (except of drawing technology where 24 wt% solution was used) using centrifugal spinning (a), electro-centrifugal spinning (b), centrifugal spinning with rod collector (c), drawing (d), electrospinning from the rod (e), electrospinning from the needle (f), bubble spinning (g), needle-less electrospinning (h) an AC spinning (i), scale bars 10 µm



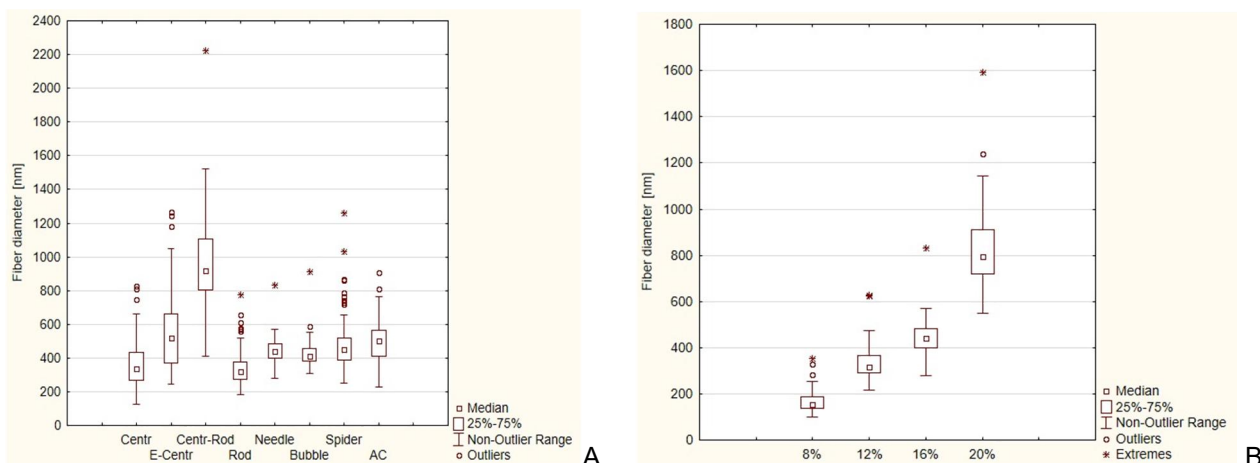


**Figure 11** Box plot of fiber diameters obtained by spinning of 16 wt% PVA (A) using centrifugal spinning (Centr), electro-centrifugal spinning (E-Centr), centrifugal spinning with rod collector (Centr-Rod), electrospinning from the rod (Rod), electrospinning from the needle (Needle), bubble spinning (Bubble), needle-less electrospinning (Spider) and AC spinning (AC); box plot of fiber diameter distribution of increasing PVA concentrations and their respective fiber diameter obtained by needle electrospinning (B)

The voltage used during electrospinning process play a crucial role for fibers formation and their diameter. The most important factor that has to be considered is the electric intensity which is connected with geometry of spinnerets. This article compares various spinning processes therefore it is not possible to set common spinneret and stable voltage or distance. Considering these facts, spinning parameters were described for each spinning technology separately.

#### 4 CONCLUSIONS

The polymer concentration and spinning conditions play important role in formation of fibrous mats and their morphology. The article was focused on introduction of variety of accessible spinning technologies that allow production of micro- and nanofibers. The concentrations of 12 wt%, 16 wt% and 20 wt% are the most common for electrospinning and spinning in general. The highest concentration of PVA (28 wt%) was capable of spinning using only electro centrifugal spinning and drawing. These methods are using mechanical capillary forces for elongation the polymer solution therefore highly viscose polymer solutions were able to spin. On the other hand, low concentration of 8 wt% was not spin able by centrifugal and drawing techniques. The low viscosity polymer solutions don not allow creation of fibrous structures using these methods. The concentrations of 12 wt%, 16 wt%, and 20 wt% were spinned by majority of technologies except drawing and needleless electrospinning.

**ACKNOWLEDGEMENTS:** This research was supported by the project "Nanofiber materials for tissue engineering", reg. No. CZ.1.05/3.1.00/14.0308, which is co-financed by the European Social Fund and the state budget of the Czech Republic.

#### 5 REFERENCES

1. Lukáš D., Sarkar A., Martinova L., Vodseďáková K., Lubasová D., et.al.: Physical principles of electrospinning (Electrospinning as a nano-scale technology of the twenty-first century), Textile Progress 41(2), 59-140, 2009
2. Bhardwaj N., Kundu S.C.: Electrospinning: A fascinating fiber fabrication technique, Biotechnology Advances 28(3), 325-347, 2010
3. Zhang X., Yao L.: Centrifugal Spinning: An Alternative Approach to Fabricate Nanofibers at High Speed and Low Cost. Polymer Reviews 54(4), 677-701, 2014, online, cited 2015-09-18, <http://dx.doi.org/10.1080/15583724.2014.935858>
4. Chen Rou-Xi; Li Ya, He J.: Mini-review on Bubble spinning process for mass-production of nanofibers, Matéria (Rio J.) 19(4), 325-343, 2014, online, cited 2016-06-14, <http://dx.doi.org/10.1590/S1517-70762014000400002>
5. Amrinder S. Nain, Joanna C. Wong, etc.: Drawing suspended polymer Micro/nanofibers using glass micropipettes, Applied Physics Letters 89(18), 183105-7, 2006
6. Sill T., Recum H. A.: Electrospinning: Applications in Drug Delivery and Tissue Engineering, Biomaterials 29(13), 1989-2006, 2008
7. Hu X., Lui S., Zhou G., Huang Y., Xie Z., Jing X.: Electrospinning of polymeric nanofibers for drug delivery applications, Journal of Controlled Release 165, 12-21, 2014
8. Mohamed H. El-Newehy, Salem S. Al-Deyab, El-Refaie Kenawy, Ahmed Abdel-Megeed: Fabrication of Electrospun Antimicrobial Nanofibers Containing Metronidazole Using Nanospider Technology, Fibers and Polymers 13(6), 709-717, 2012
9. Pokorny P.; Kostakova E.; Sanetnik F., et al.: Effective AC needleless and collectorless electrospinning for yarn production, Physical Chemistry Chemical Physics 16(48), 26816-26822, 2014

# A HYDROGEL PHANTOM FOR TESTING BIOSIGNALS FROM A TEXTRONICS T-SHIRT

Emilia Frydrysiak<sup>1</sup>, Michał Frydrysiak<sup>2</sup> and Łukasz Tęśiorowski<sup>2</sup>

<sup>1</sup>Lodz University of Technology, Institute of General Chemistry, Stefanowskiego 4/10, 90-924, Lodz, Poland

<sup>2</sup>Lodz University of Technology, Faculty of Material Technologies and Textile Design

St. Zeromskiego 116, 90-924 Lodz, Poland

[em.frydrysiak@gmail.com](mailto:em.frydrysiak@gmail.com), tel. +48 42 631-34-10, fax +48 42 631-28-42

**Abstract:** A textronics system in the form of T-shirt was designed for elders for controlling their life parameters. For testing in a phantom with proper filling is required. That filling should be hydrogel: made of agar mixed with an electrolyte or polyacrylamide which maintain their 'jelly-like' properties at temperatures between 36-40°C (human body temperature). The resistance of agar gel with sodium chloride in concentrations of 0, 1, 2, 3, 4 and 10% was obtained and also there were obtained gels made of polyacrylamide in concentrations of 5, 10 and 15%. The best results were for 3, 4 and 10% sodium chloride-agar gel and for 10% PAM gel. As a phantom filling the 10% PAM gel and 3% agar hydrogel were chosen because of their electrical conductive properties and durability under certain temperature over a long period of time.

**Key words:** Hydrogels, phantom, biosignals, textronics, T-shirt, elders

## 1 INTRODUCTION

A textronics system in the form of T-shirt was designed for elders for controlling their life parameters. The system allows to measure pulse, frequency of breathing, temperature of a body and also can show a patient's electrocardiogram. However such systems cannot be tested in humans in the first place, because a medical bioethics commission agreement is required. That is why phantoms are designed – for testing such systems on them. The best phantom fulfillment are hydrogels.

Hydrogels are crosslinked polymeric structures, absorbing significant quantities of water. According to the type of hydrogels, they can be divided into two groups: chemical or physical cross-linking hydrogels. Chemical ones are crosslinkable permanently, and physical ones - temporary (e.g. Agar, gelatin), which is a result of the entanglements of their chains or physical interactions, e.g. ionic or hydrogen bonds. Hydrogels can also be divided based on their origin: natural or synthetic. Natural polymers include collagen or gelatin which are proteins and polysaccharides: agarose and alginate. Synthetic hydrogel-forming polymers are prepared with the use of polymerization reactions [1, 2].

## 2 EXPERIMENTAL

Presented research concerns execution of the phantom chest which allows for testing of physiological parameters of a man. Substance which is a filling of the phantom must have similar properties to physiological properties of human tissue. The perfect fulfillment of this type of application are hydrogels which have 'jelly-like' consistency at temperatures between 36-40°C, which is the temperature range of the human body.

### 2.1 Materials

Agar and polyacrylamide were chosen as testing substances which could be good as a phantom fulfillment. Agar (Figure 1.a) is a polysaccharide which consists of two linear heterogeneous fractions: agarose and agarpectin combined with glycoside binds. Agarose has gelling properties and agarpectin hinders the formation of gels. However if gel is formed, agarpectin increases its flexibility. Polyacrylamide (PAM) (Figure 1.b), is a polymer which is obtained by the acrylamide polymerization. It is important that in contrast to mentioned acrylamide, polymer is not toxic.

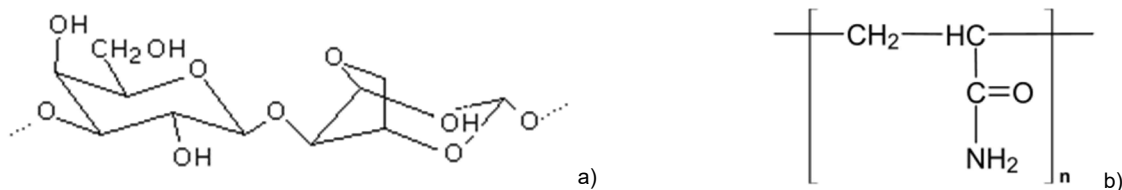


**Figure 1** Chemical structures of: a) agar; b) polyacrylamide

Agar was mixed with cold water and heated up. After heating agar solution it was mixed with an electrolyte in forms in order to reduce the resistance of the gel. The electrolyte used in samples was sodium chloride in concentrations: 1, 2, 3, 4 and 10%.

There were prepared three probes of the acrylamide/bisacrylamide gels in their concentrations of 5, 10 and 15%. An acrylamide/bisacrylamide solution (30% of acrylamide and 0.8% of bisacrylamide), buffer, tetramethylen diamine (TEMED) and distilled water were mixed. Then a prepared 10% solution of ammonium persulphate (APS) in distilled water was added to the solution in an amount of 0.1 ml to 15 ml sample. APS was added slowly with stirring. The polymerization last for approximately 30 minutes.

## 2.2 Methods

In both kinds of gels there was resistance measured. In agar gel the measurement was done with the use of indirectly method, and in polyacrylamide gel – with directly method (Figure 2).

The aim of those measurements was to obtain the resistance gels similar to resistance of human skin which was approximately 200  $\Omega$ . The construction of phantom for testing the textronics system for elders requires the choice of the proper fulfillment.



**Figure 2** Measuring bridge for testing the resistance of the agar gel and the polyacrylamide gel

## 3 RESULTS AND DISCUSSION

A concentration of 3, 4, 10% of electrolyte in agar gel allowed to obtain the gel characteristics of the electrical conductive properties which is the closest to human skin (approx. 200  $\Omega$ /1 cm) (Table 1).

**Table 1** The averaged results of the resistance of the agar gels depending on the electrolyte concentration

The electrolyte concentration [%]	0	1	2	3	4	10
Resistance [ $\Omega$ ] series I	4214	307	300	253	214	264
Resistance [ $\Omega$ ] series II	5040	837	320	793	660	685

Agar gel maintained its consistency after staying in the oven at 40°C, but had cracked due to drying. The best properties of electrical conductivity in the interesting range was gel concentration of 10% (Table 2). The obtained gel well maintain its consistency in the temperature range of 36-40°C. The measurements scheme of resistance distribution in gels' samples is presented in Figure 3.

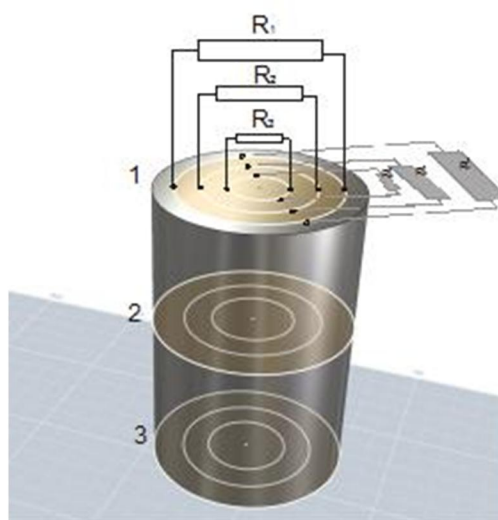


**Figure 3** The measurements scheme of resistance distribution in gels' samples

**Table 2** The averaged results of the resistance of the PAM gels

Diameter, $\phi$ [cm]	Resistance [ $\Omega$ ]					
	Distance [cm]					
	0	1	2	1	2	0
PAM 5%						
3	307.10	115.70	94.90	132.80	89.46	305.40
2	202.30	114.31	63.29	110.75	83.64	174.50
1	189.20	97.73	52.99	80.14	47.19	224.00
PAM 10%						
3	367.00	178.10	93.23	164.50	117.25	428.90
2	361.60	131.51	81.75	139.11	92.78	349.50
1	345.40	109.42	72.90	108.34	66.18	315.10
PAM 15%						
4.5	590.30	312.60	-	333.10	-	603.50
3	683.20	230.20	-	216.14	-	666.40
2	376.50	181.70	-	168.30	-	584.70
1	440.00	138.70	-	149.37	-	423.00

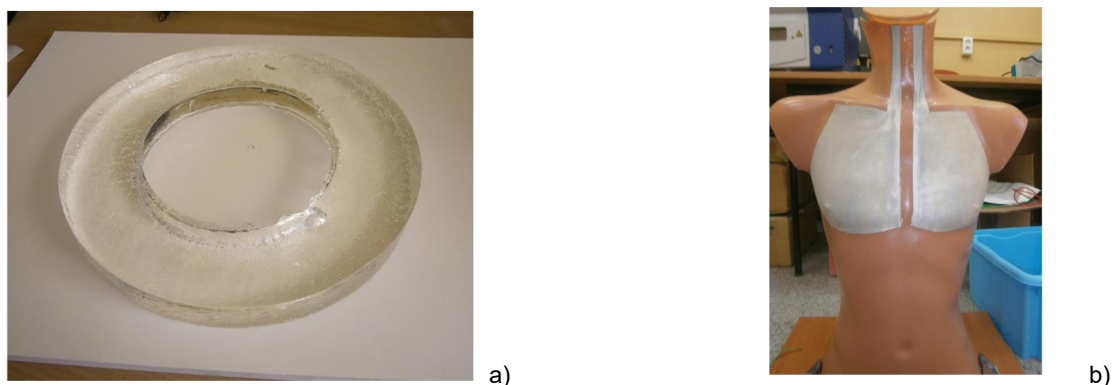


**Figure 4** a) The phantom filling PAM gel in the form of a cylinder; b) Phantom filled with agar hydrogel

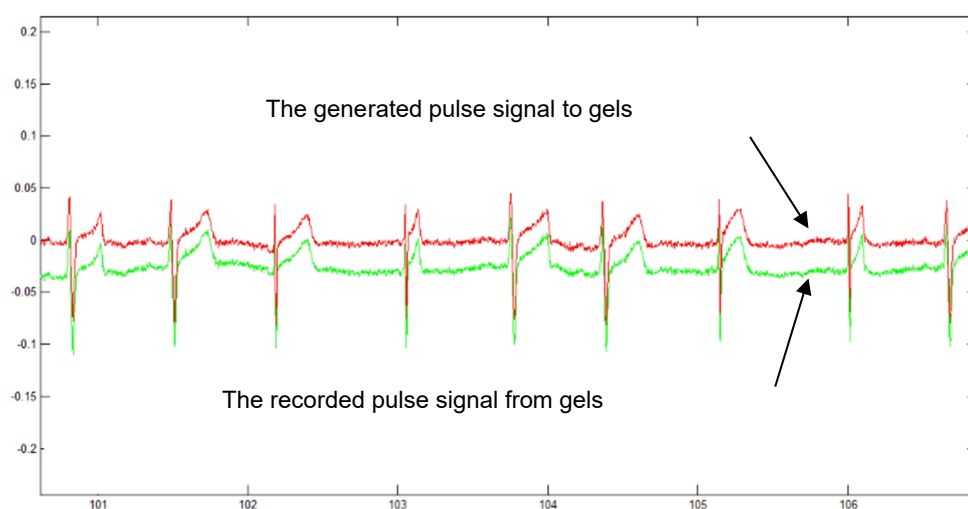


**Figure 5** Measurement results of recorded pulse signal

The chosen PAM fulfillment of phantom was presented in Figure 4.a, and the phantom fulfilled with agar hydrogel is presented in the Figure 4.b. Silver-colored stripes painted on the phantom are made with electroconductive paint in both sides: outside and inside. Thanks to that the textronics system in the form of the T-shirt can be tested – because the agar hydrogel and the paint conducts current and so that biosignals can be measured.

For phantom verification, an arbitral generator was connected to it. The generator contained a reference pulse signal. A textronics measurement system was put on the phantom and it recorded pulse signal from the phantom. Measurement results are presented in the Figure 5.

#### 4 CONCLUSIONS

Presented solution of the gel phantom is useful for non-conventional measurement systems. Textronics biomeasurement systems are the types of applications which should be tested on phantoms. For the construction these kinds of phantoms

different kinds of electroconductive gels can be used, such as polysaccharides or polyacrylamide. Very important of gels features are their electroconductive and mechanical stability parameters at higher temperatures equal to the body temperature. That makes tests possible to carry out under conditions similar to real measurement conditions.

Based on the study of the different concentrations of agar gel with the addition of electrolyte and PAM gels there were chosen the best fillings of the phantom which are the polyacrylamide hydrogel in the concentration of 10% and agar hydrogel in the concentration of 0.5% and the electrolyte concentration of 3%. These gels were selected because of their electrical conductive properties and durability under certain temperature over a long period of time.

**ACKNOWLEDGEMENTS:** Presented research is financed by The National Centre for Research and Development in Lider IV program, based on decision number 035/657/L-4/12/NCBR/2013.

## 5 REFERENCES

1. <http://thesis.library.caltech.edu/1774/1/Chapter1.pdf>, 1-2, access: June 2016
2. Tyliszczak B., Pielichowski K.: Charakterystyka matryc hydrożelowych - zastosowania biomedyczne superabsorbentów polimerowych. Czasopismo techniczne 1, 1-9, 2007
3. Frydrysiak M., Tęśiorowski Ł., Adamowicz E.: Fantom do testowania systemów pomiarowych przetwarzających sygnały bioelektryczne (Phantom for testing measurement systems processing bioelectric signals) Patent Application (P. 409096). August 4, 2014
4. Frydrysiak M., Tęśiorowski Ł., Adamowicz E., Zięba J.: Pulse-human phantom to testing textronic measurement system, IEEE - Institute of Electrical and Electronics Engineers, 2014



# PARAMETERS AFFECTING SPORTS SOCKS PRESSURE AND PRESSURE PREDICTION FROM TENSILE CHARACTERISTICS

Sertaç Güney, Betül Akgünoğlu and Sibel Kaplan

Süleyman Demirel University, Engineering Faculty, Textile Engineering Department, Isparta, Turkey  
[sertacguney@sdu.edu.tr](mailto:sertacguney@sdu.edu.tr)

**Abstract:** The interaction between lower leg and the lower leg part of socks is an important factor affecting sports performance and wearing comfort. Garment fit, garment slip and fabric stretch are three essential components effecting comfort of the wearer's dynamic movement: 'Garment slip' is mostly determined by the coefficient of friction between skin and fabric and between different layers of garments. 'Fabric stretch', an important factor in pressure comfort, depends largely on elastic characteristics of fabrics. Sports socks were designed to give necessary pressure on leg muscles and enable comfort for not to decrease the performance of the sports people. If a fabric has high friction and stretching resistance, high clothing pressure is likely to be exerted on the body, which could result in discomfort feeling. This study aims to investigate the effects of structural mechanics of knitted fabrics on the amount of pressure generated on the underlying body. Five sports socks made of polyamide, polyester and cotton including different amounts of elastane fibers and having different knits on different parts of leg regions according to the necessities of sports were selected from the market. We carried out friction and tensile tests on different parts of sports socks. We also measured the pressure generated by socks' fabrics by pressure sensors and then discuss a method of validating the reliability of Laplace law for calculating pressure applied to a cylindrical body of known radius and compare the predicted and objectively measured pressure values. Results show that the fabrics having high tensions exerted high pressure values on body and the factor of tension given in Laplace law is very important in pressure evaluation. But the fabric weight and friction coefficient are also important for the pressure applied on body. We can see these influences when comparing the predictive and objective pressure results. The Laplace Law was not clear and acceptable for all the results.

**Key words:** Pressure comfort, sports socks, material, fabric structure.

## 1 INTRODUCTION

Socks play an important role in maintaining foot comfort. Therefore, designers can not ignore pressure comfort parameters while producing functional socks, especially the top part of socks [1]. Nowadays, various functional socks are available in the market; necessary compression support is provided in sports socks to help increasing movement performance and in compression stockings and pantyhose for patients suffering some diseases such as varicose vein. The pressure value of the top part of sock is an important factor to consider when designing and developing socks. Degree of pressure produced by a garment is determined by complex interrelations between the following principle factors: the construction and fit of the garment, structure and physical properties of its materials, the size and shape of the body parts to which it is applied and the nature of the sports activity undertaken [2]. Dan et al. (2013) investigated the relationships between pressure and material properties of the top part of socks and established four indices which closely relate to pressure level; these are elastic coefficient of top part of socks, Poisson's ratio, elastic elongation and width of top part of socks [3]. Matsumoto et al. (2004) measured

leg size, tensile properties and pressure values of the top of socks and found comfortable pressure values as  $2.02 \pm 0.29$  kPa and investigated the feeling of pressure changes depending on wearing period. They pointed out that for accurate estimations of pressure feelings, it is necessary to measure the pressure approximately 2 hours after putting on the socks [5]. Kirk and Ibrahim (1966) explained that the garment slip which is mostly related to the friction coefficient of fabric is an important factor effective on the garment pressure [4].

Existing research in the area of compression garments indicates that, application of the Laplace law formula is a suitable method to predict the magnitude of the pressure that can be applied to a cylindrical body of known radius by applying specific amounts of tension to an external fabric covering [6].

## 2 EXPERIMENTAL






### 2.1 Materials

Five men's sports socks having different compositions and knit structures (Figure 1) were selected from the market. Their physical and structural parameters were given in Table 1.



Code	A	B	C																
Knit Structure	<table><tr><td>X</td><td>X</td></tr><tr><td>X</td><td>X</td></tr></table>	X	X	X	X	<table><tr><td>X</td><td>X</td><td>X</td><td>X</td></tr><tr><td>X</td><td></td><td></td><td></td></tr></table>	X	X	X	X	X				<table><tr><td>X</td><td>X</td></tr><tr><td>X</td><td></td></tr></table>	X	X	X	
X	X																		
X	X																		
X	X	X	X																
X																			
X	X																		
X																			

**Figure 1** Sock knit structures**Table 1** Physical parameters of fabric samples

Fabric	Fiber Composition [%]	Course/Wale density stitch/cm	Mass per unit area [g/m <sup>2</sup> ]	Knit structures
1	87/12/1% PA/PES/Elastane	9/7	A: 264 B: 338 C: 160	
2	99/1% PA/Elastane	9/7	A: 325 B: 398 C: 279	
3	96/3/1% PES/ Elastane/PA	10/7	A: 240 B: 280	
4	82/15/2/1 % Cotton/PES/Elastane/PA	12/8	A: 425 B: 479 C: 472	
5	81/17/1/1% Cotton/PES/PA/Elastane	12/9	A: 422 B: 500 C: 552	

## 2.2 Methods

Each section having different structures on the lower leg part of socks were separated and the tensile characteristics under different extension rates (30-40-50%) were tested according to ASTM D 4964-96. Friction coefficients (static and dynamic) were tested and calculated from the force-displacement graphics for each section for course direction according to ASTM D-1894 by using a Lloyd Tensile Tester (LR5K plus). Dimensions of the cradle was 4.5 x 4.0 cm and test was carried out on the sample placed on a horizontal platform by movement of the cradle with a speed of 50 mm/min. Extra weights were used to obtain a normal force of 1.2 g/cm<sup>2</sup> by the cradle. The objective pressure was measured by flexible pressure sensor system (Tekscan, USA). A plastic cylinder of 23.5 cm circumference was adopted in this test. The cylinder surface was covered by extended knitted fabrics. The interfacial pressure between fabric and cylinder was recorded at the center marked location of the circumferential line [7].

Laplace law formula can explain the relation between the pressure ( $P$ ) and the tension on a curved surface and is expressed by the following equation:

$$P = \frac{T}{r} \quad (1)$$

where  $T$  is the tension of the shell [N/m],  $r$  is the radius of curvature [m] and  $P$  is the pressure [Pa]. The ratio of the tensile force  $T$  to radius  $R$  represents a quantitative measure of the relevant structural properties of that particular fabric. A high  $T/r$  ratio represents a tight fitting fabric, and a low ratio represents a looser fitting fabric. This single quantitative measure may provide approximation of many fabric properties that are relevant in the design of compression and general sport garments and may provide insight for the development of a predictive model for the behavior of garments under tension. It is important to note however, that due to the nonlinear

dynamics of stretching and deformation in fabrics and garments, the ratio  $T/r$  may not be constant over a whole garment over time [2]. In the pressure prediction part, the following assumptions were made; the relationship between the pressure  $P$  generated by the sock, circumferential tension force in the fabric  $T$  and the cylinder radius  $r$  [m] is described by the Laplace formula (1); the longitudinal stretch of the fabrics in the garment is not considered and value of predictive pressure only applies at the time of application.

### 3 RESULTS AND DISCUSSION

Tension characteristics of knit structures of the socks parts at different extension levels were tested. Figure 2 shows that knit structures exhibited different tension characteristics for each fabric because of their different material compositions and constructions (stitch density, weight).

Fabrics in knit structure C showed higher tension values. Knit structures in all fabrics showed different friction and elastic characteristics (Table 2). The values for Fabric 4A could not be measured because of inadequate fabric dimensions for the test.

According to the results, kinetic friction coefficients can be ranked as  $B > C > A$  for all fabric types. Float stitches have negative effects on friction characteristics. So the knit structures B and C have higher kinetic friction coefficients (except for fabric code 1). The knit structure C has more repeated

pattern and it gives an irregular fabric surface. As can be seen in Table 2, all sock parts and types have significantly different friction coefficient values. Statistically identical parts were coded with the same labels in Table 2. Objective pressure measurements taken on the cylinder surface are also given in Table 2. The fabrics having high tensions exert high pressure values. Results show that tension calculated by Laplace law is valuable in pressure evaluation. But the fabric weight and friction coefficients are also important. We can see this effect when the predictive and objective pressure results are compared (Table 3). The Laplace law is not clear and acceptable for all the results. As it was mentioned in some studies [8-9], fabric is assumed to be a shell, but the fabrics have dynamic behaviours under tension. So in pressure comfort evaluation, tension is not the only factor, the parameters friction coefficient, fabric weight, knit structures, materials etc. should also be taken into consideration. In this study, also fabrics having the same structures gave different pressure values under same tension values because of their physical differences (surface, weight, etc.). Tension values of fabric 1C are higher than the value of fabric 1B. But the objective pressure values are not in harmony with tension values. It can be explained by higher friction coefficients and higher weights. In Laplace law, the tension is very important factor so according to the predictive pressures, it seems that fabric 1C exerts higher pressure than fabric 1B.

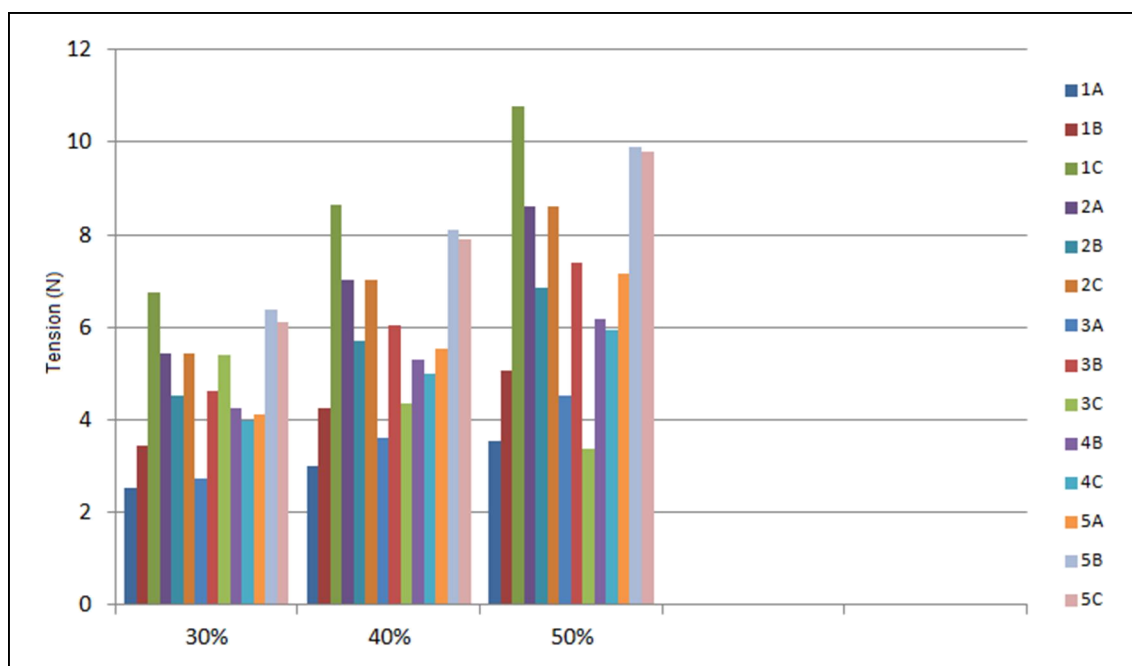


**Figure 2** Tension characteristics of fabrics at different extension level (30-40-50%)

**Table 2** Friction and elastic characteristics of different socks parts

Fabric Code/Knit Structure	Static Friction Coefficient (S.D.)	Kinetic Friction Coefficient (S.D.)	Tension [N]			Objective Pressure [gr/cm <sup>2</sup> ]		
			30% Extension	40% Extension	50% Extension	30% Extension	40% Extension	50% Extension
1.A	0.493 <sup>b</sup> (0.074)	0.482 <sup>b</sup> (0.062)	2.54 (0.635)	3.01 (0.752)	3.53 (0.882)	6.50 (1.33)	9.76 (1.33)	29.30 (2.31)
1.B	0.569 <sup>bc</sup> (0.104)	0.472 <sup>bc</sup> (0.088)	3.44 (0.86)	4.25 (1.062)	5.08 (1.27)	32.56 (1.33)	39.07 (2.31)	42.33 (2.66)
1.C	0.241 (0.048)	0.208 <sup>a</sup> (0.042)	6.74 (1.685)	8.66 (2.165)	10.77 (2.692)	3.25 (0)	6.50 (1.33)	22.78 (2.31)
2.A	0.225 <sup>a</sup> (0.129)	0.312 <sup>a</sup> (0.136)	5.44 (1.152)	7.04 (1.465)	8.61 (1.79)	6.50 (0)	9.76 (1.33)	13.01 (2.31)
2.B	0.648 <sup>c</sup> (0.073)	0.557 <sup>c</sup> (0.108)	4.54 (1.135)	5.7 (1.425)	6.87 (1.717)	9.76 (1.33)	19.53 (0)	29.30 (2.31)
2.C	0.372 (0.151)	0.368 <sup>b</sup> (0.108)	5.44 (1.36)	7.04 (1.76)	8.61 (2.152)	6.50 (1.33)	16.25 (1.33)	26.04 (2.31)
3.A	0.302 <sup>a</sup> (0.072)	0.293 <sup>a</sup> (0.700)	2.73 (0.682)	3.62 (0.905)	4.54 (1.135)	-	3.25 (0)	9.76 (1.33)
3.B	0.447 <sup>ab</sup> (0.090)	0.425 <sup>ab</sup> (1.105)	4.62 (1.155)	6.03 (1.507)	7.4 (1.85)	3.25 (0)	13.01 (1.33)	29.30 (2.31)
4.A	-	-	5.39 (0.847)	4.36 (1.09)	3.39 (1.347)	3.25 (0)	6.50 (1.33)	9.76 (1.33)
4.B	0.406 <sup>a</sup> (0.123)	0.311 <sup>a</sup> (0.118)	-	-	-	6.50 (1.33)	16.28 (0)	22.78 (1.33)
4.C	0.302 (0.063)	0.246 <sup>a</sup> (0.062)	4.27 (1.067)	5.29 (1.322)	6.18 (1.545)	6.50 (1.33)	9.76 (1.33)	13.01 (0)
5.A	0.297 <sup>a</sup> (0.038)	0.227 <sup>a</sup> (0.052)	3.97 (0.992)	5 (1.25)	5.94 (1.485)	6.50 (1.33)	13.01 (0)	19.53 (1.33)
5.B	0.463 <sup>ab</sup> (0.118)	0.368 <sup>ab</sup> (0.211)	4.12 (1.03)	5.55 (1.387)	7.15 (1.787)	16.28 (1.33)	29.30 (1.33)	45.59 (2.66)
5.C	0.354 (0.057)	0.264 <sup>ab</sup> (0.063)	6.38 (1.595)	8.11 (2.027)	9.89 (2.472)	16.28 (1.33)	32.56 (2.66)	42.33 (2.66)

**Table 3** Objectively measured, pressure values, predicted pressure values and deviations

Fabric Code/ Knit Structure	Objective Pressure [gr/cm <sup>2</sup> ]			Predictive Pressure [gr/cm <sup>2</sup> ]			Deviation [%]		
	30% Extension	40% Extension	50% Extension	30% Extension	40% Extension	50% Extension	30% Extension	40% Extension	50% Extension
1.A	6.50	9.76	29.30	6.84	8.10	9.50	4.88	-20.39	-208.28
1.B	32.56	39.07	42.33	9.26	11.44	13.68	-251.46	-241.32	-209.44
1.C	3.25	6.50	22.78	18.15	23.32	29	82.07	72.10	21.43
2.A	6.50	9.76	13.01	14.65	18.96	23.18	55.58	48.52	43.87
2.B	9.76	19.53	29.30	12.22	15.35	18.50	20.17	-27.24	-58.40
2.C	6.50	16.25	26.04	14.16	18.88	23.18	55.58	13.76	-12.30
3.A	-	3.25	9.76	-	9.74	12.22	-	66.63	20.17
3.B	3.25	13.01	29.30	12.44	16.24	19.93	73.85	19.86	-47.05
4.A	3.25	6.50	9.76	-	-	-	-	-	-
4.B	6.50	16.28	22.78	11.50	14.24	16.64	43.41	-14.27	-36.91
4.C	6.50	9.76	13.01	10.69	13.46	15.99	39.14	27.52	18.65
5.A	6.50	13.01	19.53	11.09	14.94	19.25	11.09	14.94	19.25
5.B	16.28	29.30	45.59	17.18	21.84	21.33	17.18	21.87	26.63
5.C	16.28	32.56	42.33	16.51	21.33	26.39	16.51	21.33	26.39

Objective pressures of the top part of socks at different extension levels were measured on cylinder surface and the pressure levels of socks at 50% extension level can be ranked as 5>3>2>1>4 respectively. Fabric code 5C has generally high friction coefficient, tension and weight so it generated higher pressure. Predictive pressures in

cuff parts were calculated according to the Laplace law formula at extension level of 50% and the values matched to the objective pressure measurement in 10-25% deviation (except for 3B and 4C). But the deviation is not generally uniform for all parts of socks. The fabrics at 50% extension level flattened and get a shell form. This may be

the reason of differences between predicted and objectively measured results (10-25% deviation for some parts of socks) (1C, 2C, 3A, 4C, 5A). In this study, it is not clear to see the influences of materials on pressure values but PA and Cotton materials are smoother than PES. It is expected that socks with PES may exert much more pressure on body.

#### 4 CONCLUSIONS

According the friction and pressure measurement results carried out on sports socks produced from different materials; tensile, friction characteristics and weight of fabrics have important effect on pressure generated on body. If a fabric has high friction and stretching resistance, high clothing pressure is likely to be exerted on the body, which could result in discomfort feeling. During designing and developing the pressure comfort of the socks, we should take account of these characteristics. This research also focused on the evaluation of the accuracy of Laplace law for sock fabrics. The results of this study show that Laplace law was not able to predict the measured pressure values in all parts of socks. The fabrics at extension level of 50% flattens and gets a shell form. Therefore the predicted pressure values matched objective pressure values with 10-25% deviation for some parts of socks.

#### 5 REFERENCES

1. Li J.: Study on the pressure comfort of the top part of socks, Shanghai, Donghua University, 2007
2. Troynikov O., Ashayeri E., Burton M., Subic A., Alam F., Marteau S.: Factors influencing the effectiveness of compression garments used in sports, *Procedia Engineering* 2, 2823-2829, 2010
3. Dan R., Fan X., Xu L., Zhang M.: Numerical simulation of the relationship between pressure and material properties of the top part of socks, *The Journal of The Textile Institute* 104(8), 844-851, 2013
4. Kirk W.J., ve İbrahim S.M.: Fundamental Relationship of Fabric Extensibility to Antropometric Requirements and Garment Performance, *Textile Research Journal* 57, 37-47, 1996
5. Matsumoto Y., Morooka H.: Comfort Pressure of the Top Part of Men's Socks, *Textile Research Journal* 74(7), 598-602, 2004
6. Chatard J.C., Atlaoui D., Farjanel J., lousy F., Rastel D., Guezennec C.Y.: Elastic stockings, performance and leg pain recovery in the 63-year old sportsmen, *European Journal of Applied Physiology* 93(3), 347-352, 2004
7. Sang J.S, Lee M.S., Park M.J.: Structural effect of polyester SCY knitted fabric on fabric size, stretch properties and clothing pressure, *Fashion and Textiles* 2, 22, 2015
8. Aghajani M., Jeddi A. ve Tehran M.A.: Investigating the Accuracy of Prediction Pressure by Laplace Law in Pressure Garment Applications, *Journal of Applied Polymer Science* 121, 2699-2704, 2011
9. Aghajani M., Tehran M.A., Jeddi A.A.A.: Precise Measurement of Tension on Curvature Elastic Shells, *Journal of Engineered Fibers and Fabrics* 8(1), 82-87, 2013

# BENDING BEHAVIOUR OF SPORTS BRA FABRICS: EXPERIMENTAL AND FINITE ELEMENT SIMULATION OF ASTM D1388 CANTILEVER TEST

Michaela Hassmann<sup>1</sup>, Seraphina Stöger<sup>1</sup>, Natalie Mentel<sup>1</sup> and Wolfgang Krach<sup>2</sup>

<sup>1</sup>University of Vienna, Institute of Sport Science, Vienna, Austria, +43-1-4277-48883

<sup>2</sup>CAE Simulation & Solutions GmbH, Vienna, Austria, +43-1-9748991-11

[michaela.hassmann@univie.ac.at](mailto:michaela.hassmann@univie.ac.at)

**Abstract:** Finite Element (FE) simulation of sports bra fabrics requires knowledge of textile material properties. Bending behaviour of textiles is determined according to ASTM D1388. Standard procedure of ASTM D1388 Cantilever test has been criticized in literature due to the fixed bending angle  $\theta = 41.5^\circ$ . Following extensive pre-tests, overhang length was defined to  $L = 70$  mm for stiff textiles and  $L = 20$  mm for flexible textiles in this investigation. From the bending lines of eight specimens of an ODLO High Padded sports bra, flexural rigidity  $G$  and bending modulus  $E_f$  were calculated. Formulae given in literature other than ASTM D1388 had to be used due to an unexplained factor and a different unit introduced in the 2008 issue. Experimental results were compared to nonlinear FE analysis in MSC Nastran using CQUAD4 shells with calculated material parameters. Separate trends of mostly overestimating vertical tip displacement  $f$  for stiff and flexible textiles were found. This leads to the conclusion that the assumption of pure bending in the Cantilever test is not valid especially for flexible sports bra fabrics. For their FE simulation, shell elements with decoupled membrane and bending stiffness must be used and Young's modulus has to be determined from tensile testing.

**Key words:** knitted fabrics, preformed foam, flexural rigidity, decoupled shell elements, membrane stiffness

## 1 INTRODUCTION

Sports bras consist of one or more layers of knitted textiles, an elastic underbust band and straps. Padded sports bras additionally incorporate preformed foam to provide stability to cups and comfort to straps. Besides sewing pattern, Finite Element (FE) simulation requires material properties to model the sports bra's efficacy in reducing breast movement during sports activities [5]. If these properties are not known to the manufacturer, they have to be found out using standardized procedures.

Characterization of stiffness according to ASTM D1388 proposes the Cantilever test (Option A) as the preferred procedure, whereas very limp textiles with an overhang length of less than 4 cm at a bending angle of  $43^\circ$  [7] or those that show a marked tendency to curl or twist should rather be tested by Heart Loop test (Option B) [1]. Both these procedures go back to Peirce [7]. Peirce [7] himself as well as other authors [4; 10] propose further modifications of Cantilever test, indicating dissatisfaction with standardized procedures. Bending rigidity is not directly measured but calculated by approximated formulae [3; 2]. Peirce admitted that his formulae were only applicable for small deflections, while the ASTM D1388 standard specifies a bending angle of  $41.5^\circ$  which indicates large deflections [4].

This paper describes stiffness testing for all relevant fabrics of a sports bra using experimental Cantilever

test and comparing the results with FE simulation. The primary aim is to find the needed material properties, for which the Cantilever test is the easiest to perform for the wide range of fabrics used in sports bras. Moreover, the implications and limitations of this procedure will be pointed out.

## 2 EXPERIMENTAL

### 2.1 Specimens

One set of specimens was taken from one manufactured ODLO High Padded sports bra (size 95E), as fabric samples were not available. Specimens were cut according to ASTM D1388 guidelines [1], weight was measured using a precision scale, thickness and other dimensions were determined using sliding calliper.

Density  $\rho$  [t/mm<sup>3</sup>] was calculated as weight per unit area  $M$  divided by thickness  $T$  in modified SI units for FE. For the strap foam (1), underbust elastic band (2), piping (3) and elastic strap (4) no specimen in cross-machine direction could be cut due to limited size. For the cup foam (5), warp knit stretch mesh (6), single knit mesh (7) and single jersey (8) one specimen was cut along machine direction (A) and one along cross-machine direction (B). The base layer of the foam padded strap was excluded, as it was too limp to be considered relevant for mechanical analysis. Numbering and location of specimens can be seen in Figure 1, their specifications are given in Table 1.



**Figure 1** Numbering and locations of sports bra specimens

**Table 1** Specifications of sports bra specimens

specimen		length $l$ [mm]	width $b$ [mm]	weight per unit area $M$ [g/m <sup>2</sup> ]	thickness $T$ [mm]	density $\rho$ [t/mm <sup>3</sup> ]	description
1		150	25	298.7	3.50	$8.533 \cdot 10^{-11}$	strap foam
2		150	30	844.4	2.10	$4.021 \cdot 10^{-10}$	underbust elastic band
3		150	16	350.0	1.10	$3.182 \cdot 10^{-10}$	pipings
4		150	19	491.2	1.45	$3.388 \cdot 10^{-10}$	elastic strap
5	A	150	25	632.0	4.80	$1.317 \cdot 10^{-10}$	cup foam
	B	150	25	624.0	3.35	$1.863 \cdot 10^{-10}$	
6	A	150	25	160.0	0.45	$3.556 \cdot 10^{-10}$	warp knit stretch mesh
	B	105	25	160.0		$3.556 \cdot 10^{-10}$	
7	A	150	25	114.7	0.40	$2.867 \cdot 10^{-10}$	single knit mesh
	B	120	25	123.3		$3.083 \cdot 10^{-10}$	
8	A	150	25	208.0	0.50	$4.160 \cdot 10^{-10}$	single jersey
	B	150	25	178.7		$3.573 \cdot 10^{-10}$	

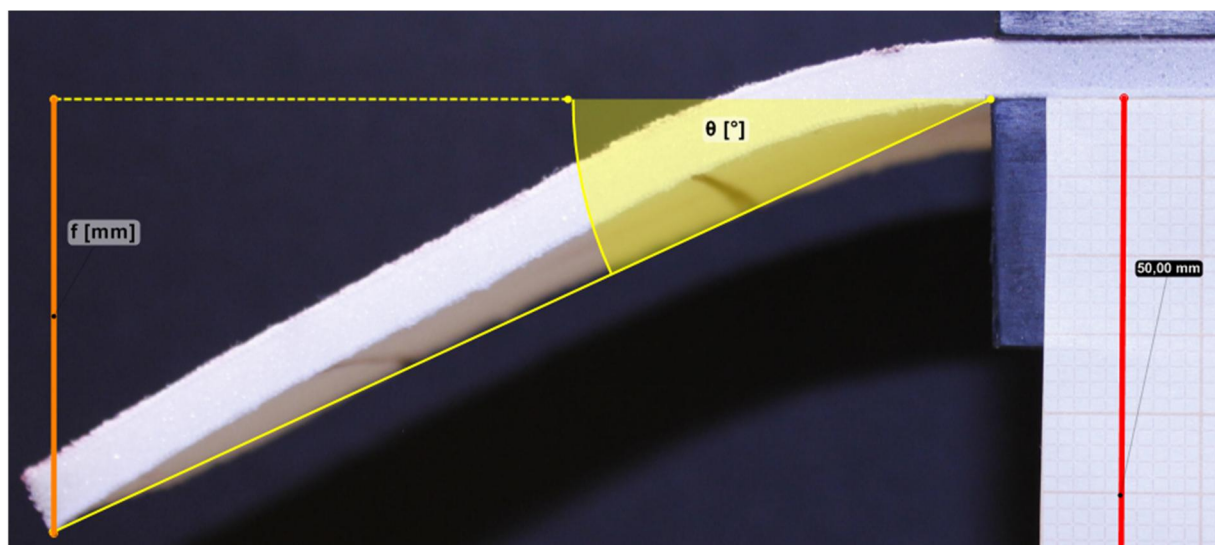


**Figure 2** Analysis of experimental Cantilever test in Kinovea



Difficulties in cutting specimens occurred due to the preformed cups, especially as thickness was not constant and had to be averaged. Specimen size was limited, for which 25 by 200 mm is recommended [1]. Yet bending length is not dependent on the width, and none of the specimens reaches an overhang length higher than 100 mm before bending to an angle of 90° which is the maximum amount of bending in Cantilever test.

## 2.2 Experimental Cantilever test

Extensive pre-tests concerning optimum overhang length  $L$  were carried out, for  $L = 10$  mm to 100 mm increasing by every 10 mm. They showed that the highest feasible overhang length was  $L = 70$  mm for stiff textiles (specimens 1 to 5) and  $L = 20$  mm for flexible textiles (specimens 6 to 8). Bending lines for all four directions (face and back of both ends) were photographed with a millimetre scale in the front plane. Bending angle  $\theta$  [°] and vertical displacement of tip  $f$  [mm] were measured using Kinovea 0.8.22 (Figure 2).

Calculation of flexural rigidity  $G$  relied on formulae and variables given in [9]. First, a so-called bending length  $C$  was calculated from overhang  $L$  [mm] and bending angle  $\theta$  (1), from which flexural rigidity  $G$  (2) was computed and averaged according to ASTM D1388 [1]. In a linear isotropic material, bending modulus  $E_f$  (3) and tensile Young's modulus  $E$  are identical [7]. For pure bending problems, this assumption can also be adopted for non-isotropic materials like textiles.

$$C = L \left( \frac{\cos \frac{1}{2} \theta}{8 \tan \theta} \right) \text{ [mm]} \quad \text{with } L \text{ [mm]} \quad (1)$$

$$G = M \cdot C^3 \cdot 9.807 \cdot 10^{-6} \text{ [}\mu\text{Nm]} \quad \text{with } M \text{ [g/m}^2\text{]} \quad (2)$$

$$E_f = \frac{12 \cdot G}{T^3 \cdot 10^3} \text{ [N/mm}^2\text{]} \quad \text{with } T \text{ [mm]} \quad (3)$$

ASTM D1388 introduced an unexplained factor of  $1.421 \cdot 10^{-5}$  for flexural rigidity  $G$  in the 2008 issue [4] that is still used in the 2014 issue [1] (4). Furthermore, the unit of flexural rigidity  $G$  has been changed from former [mg·cm] to [μjoule/m] in [1], which seems to be inconsistent in terms of units for the given formula and inconsistent with multiples of [Nm] in most other literature [8; 9] (5).

$$G = 1.421 \cdot 10^{-5} \cdot W \cdot c^3 \text{ [}\mu\text{joule/m]} \quad \begin{matrix} \text{factor [m/s}^2\text{],} \\ W \text{ [g/m}^2\text{]} \\ c \text{ [mm]} \end{matrix} \quad (4)$$

$$\begin{aligned} [G] &= \left[ 1.421 \cdot 10^{-5} \cdot \frac{\text{m}}{\text{s}^2} \right] \cdot \left[ \frac{\text{g}}{\text{m}^2} \right] \cdot [\text{mm}^3] = \\ &= 1.421 \cdot 10^{-5} \cdot 10^{-12} \left[ \frac{\text{kg} \cdot \text{m}^2}{\text{s}^2} \right] = \\ &= 1.421 \cdot 10^{-5} \cdot 10^{-12} [\text{Nm}] \end{aligned} \quad (5)$$

## 2.3 FE modelling

In [4] ABAQUS quadratic shell elements were used and material parameters of the specimen (density  $\rho$ , Young's modulus  $E$ , Poisson's ratio  $\nu$ ) were known. FE models in this paper were pre-processed in MSC Patran 2014.1. Standard PSHELL shell formulation with linear CQUAD4 elements and an average element size of 3 mm for  $L = 70$  mm and 1.5 mm for  $L = 20$  mm. Linear elastic material MAT1 with measured density, calculated bending modulus  $E_f$  and assuming  $\nu = 0.32$  [5] was defined. Inertial loading with the appropriate boundary conditions restraining displacements and rotations at the upper end simulated specimens hanging under their own weight.

## 3 RESULTS AND DISCUSSION

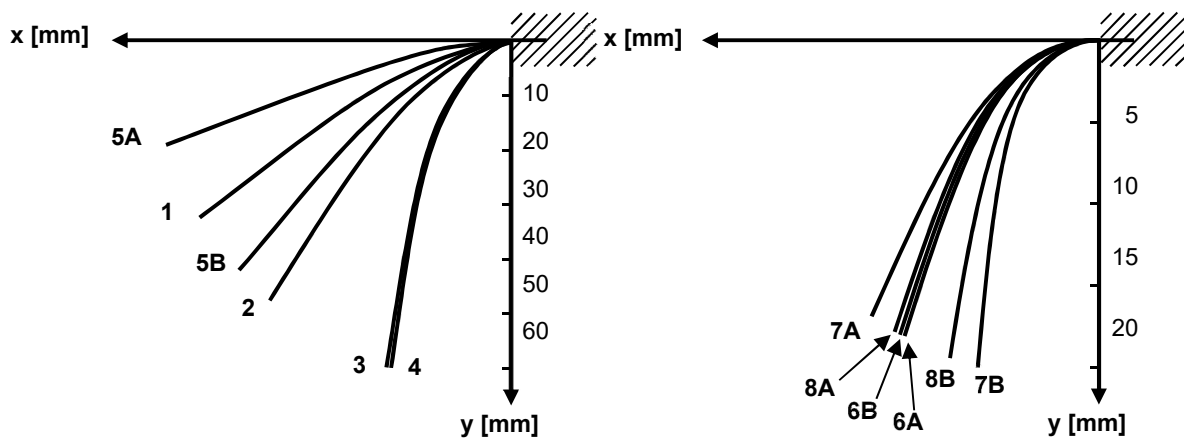
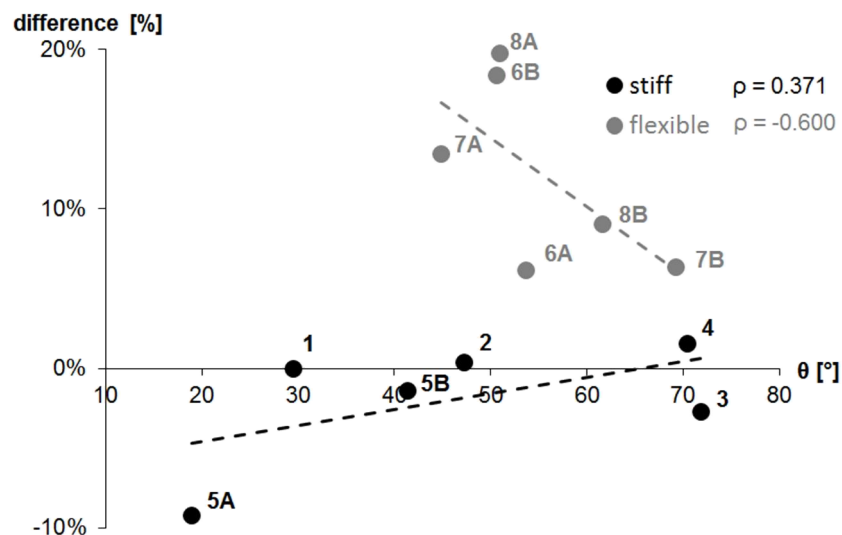
Table 2 summarizes the results of experimental and FE Cantilever test.

Resulting bending lines from MSC Nastran Implicit Nonlinear analysis (SOL 400) are shown in Figure 3 for stiff (left) and flexible (right) textiles separately.

Difference of vertical tip displacement  $f$  between FE result and experimental Cantilever test in percent of Cantilever result over bending angle  $\theta$  is shown in Figure 4. Comparison showed good accordance for stiff textiles with a maximum difference of -9.2% for specimen 5A. Spearman correlation calculated in IBM SPSS 23 revealed a slightly positive trend between difference and bending angle  $\theta$  ( $p = 0.234$ ,  $\rho = 0.371$ ). For the flexible specimens, overestimation of vertical tip displacement was collectively larger (up to 19.7% for specimen 8A) and strongly negatively correlated to bending angle  $\theta$  ( $p = 0.104$ ,  $\rho = -0.600$ ). Although strap foam (1) and cup foam (5A, 5B) had lower bending moduli than knitted textiles, they behaved like stiff textiles due to their thickness  $T = 3.50 / 4.80 / 3.35$  mm.

**Table 2** Results of Cantilever test of sports bra specimens

specimen	overhang $L$ [mm]	bending angle $\theta$ [°]	bending modulus $E_r$ [N/mm <sup>2</sup> ]	vertical tip displacement		
				experimental $f$ [mm]	FE $f$ [mm]	difference [%]
1	70	29.5	0.06151	32.688	32.682	0.0
2		47.3	0.40164	47.733	47.900	0.4
3		71.9	0.38309	62.314	60.621	-2.7
4		70.4	0.23703	59.639	60.576	1.6
5	A	19.0	0.09809	21.300	19.336	-9.2
	B	41.4	0.09435	44.063	43.446	-1.4
6	A	53.7	0.15338	14.650	15.554	6.2
	B	50.7	0.15543	13.099	15.510	18.4
7	A	44.8	0.19871	12.870	14.604	13.5
	B	69.3	0.07390	16.356	17.399	6.4
8	A	50.9	0.15140	12.913	15.462	19.7
	B	61.6	0.07892	15.405	16.797	9.0

**Figure 3** Bending lines of all stiff (left) and flexible (right) specimens with vertical tip displacement  $f$  [mm]**Figure 4** Difference of vertical tip displacement  $f$  [mm] between FE result and experimental Cantilever test, dashed lines indicate linear correlations for stiff and flexible specimens separately

#### 4 CONCLUSIONS

The main point of criticism for Cantilever test is the fixed bending angle  $\theta = 41.5^\circ$ , which is neither optimal for very flexible nor for very stiff textiles. Especially flexible sports bra fabrics yield a very low overhang making this test specification impracticable. We therefore suggest revising ASTM D1388 Cantilever test procedure by either allowing a variable bending angle  $\theta$  or by giving suitable ranges of overhang length  $L$  for different types of textiles. In accordance with [4], formulae given in the current issue could not be used due to an unexplained factor and inconsistent units.

Therefore, the intention was to invert fixed value and measured variable. Bending line photography can be assumed to achieve comparable accuracy in the order of (sub)millimetres to commercially available Cantilever test apparatus when manually setting a variable bending angle. The standard requires five specimens in each direction, which would not increase accuracy compared to measuring only one specimen in this investigation, where experimental and FE results were compared.

For stiff textiles, low differences between FE simulation and experimental Cantilever test occur, and a detailed stress tensor analysis exhibits only one nonzero value for  $\sigma_{xx}$  component. Values of bending modulus  $E_f$  calculated by approximated formulae can be regarded as accurate enough for bending problems, following Peirce's statement [7]. For larger bending angles and displacements occurring in flexible textiles, the Cantilever procedure is no longer a pure bending problem. Flexible specimens are also exposed to tensile stress when extension increases to about 3 to 5% as in this investigation or even higher in sports bra simulation. MSC Nastran's PSHELL property card offers decoupling of Young's modulus  $E$  for the membrane stiffness and bending modulus  $E_f$  for the bending stiffness. Decoupling in-plane and out-of-plane properties is supposed to yield more comparable results for flexible textiles, as proposed by [6] using a different modelling approach. Determination of Young's modulus  $E$  is done by tensile testing gaining the load-extension curve of the specimen [9]. Gaining a comparable plot for bending behaviour requires KES pure bending test [2].

Most textiles show different bending behaviour on face and back side which is taken into account by Note 8 in ASTM D1388 [1]. This differentiation might be necessary for FE simulation of sports bras where the orientation of bending is known. In contrast, curl and twist effects can be neglected in FE simulation of sports bras, as they are not expected to occur to a large extent compared to when fabrics are hanging under their own weight.

**ACKNOWLEDGEMENTS:** The project "Sports bra optimization by Finite Element simulation of interaction between breast tissue and textile" is funded by Vienna Business Agency (Call FemPower 2015).

#### 5 REFERENCES

1. ASTM D1388-14, Standard Test Method for Stiffness of Fabrics, 2014
2. Ghosh T.K., Zhou N.: Characterization of fabric bending behavior: A review of measurement principles, Indian Journal of Fibre & Textile Research 28, 471-476, 2003
3. Hummel F.H., Morton W.B.: XXXII. On the large bending of thin flexible strips and the measurement of their elasticity, The London, Edinburgh, and Dublin Philosophical Magazine and Journal of Science 4(21), 348-357, 1927
4. Lammens N., Kersemans M., Luyckx G., van Paepegem W., Degrieck J.: Improved accuracy in the determination of flexural rigidity of textile fabrics by the Peirce cantilever test (ASTM D1388), Textile Research Journal 84(12), 1307-1314, 2014
5. Li Y., Zhang X., Yeung K.: A 3D Biomechanical Model for Numerical Simulation of Dynamic Mechanical Interactions of Bra and Breast during Wear, Fiber 59(1), 12-21, 2003
6. Pabst S., Krzywinski S., Schenk A., Thomaszewski B.: Seams and Bending in Cloth Simulation. In F. Faure, M. Teschner (Eds.), VRIPHYS 08. 5<sup>th</sup> Workshop on Virtual Reality Interactions and Physical Simulations, 2008
7. Peirce F.T.: 26 – The "handle" of cloth as a measurable quantity, Journal of the Textile Institute Transactions 21(9), T377-T416, 1930
8. Plaut R.H.: Formulas to determine fabric bending rigidity from simple tests, Textile Research Journal 85(8), 884-894, 2015
9. Saville B.P.: Physical testing of textiles, Woodhead (Cambridge), 1999
10. Szablewski P., Kobza W.: Numerical Analysis of Peirce's Cantilever Test for the Bending Rigidity of Textiles, Fibres & Textiles in Eastern Europe 11(4), 54-57, 2003

# IMAGE ANALYSIS AND DESCRIPTION OF SINGLE JERSEY LOOP GEOMETRY

Monika Vysanska

Technical University of Liberec, Department of Textile Technologies, Liberec, Czech Republic  
[monika.vysanska@tul.cz](mailto:monika.vysanska@tul.cz) +420485353215

**Abstract:** Many geometrical models of single jersey loop and various approaches to its image analysis exist there. The contribution presents original approach to the image analysis of deformed loop and to the consequent substitution by polynomial functions. The loop is defined by the set of parameters; their changes are observed and evaluated during the NiTi knitted fabric deformation.

**Key words:** Single jersey loop, image analysis, polynomial function, MatLab, superelastic material

## 1 INTRODUCTION

Investigation into the dimensional properties of knitted structures began with experimental works. Doyle [1], Munden [2], Knapton et al. [3, 4] and Kurbak [5, 6] gave some empirical formulas by conducting experimental works. At the same time researches also tried to create some geometrical and physical models for knitted fabric structures. Previously created geometrical models for plain knitted fabric include those of Chamberlain [7], Peirce [8], Leaf and Glaskin [9], Leaf [10], Munden [11], Postle [12], Kurbak [13, 14] and Demiroz [15].

To overcome the problem for plain-knitted fabrics, a numerical model consisting of a system of rectangular cells is proposed, and a finite-element method (FEM) has been chosen as the basis for model evaluation [16, 17]. The FEM has been used successfully to solve a wide variety of problems. Originating from the study of structural mechanics in the 1950s the FEM is now well documented by thousands of publications [18], the majority being specialized papers. More general textbooks [19-23] have appeared during recent decades. The method was successfully employed in the area of the mechanics of textiles by Lloyd [24] and then developed in the mechanics of yarns [25-30].

The presented paper focuses on the problems of image analysis of chosen (marked) loop in NiTi knitted fabric. Further it pursues the change of defined parameters of the loop during the knitted fabric deformation. At the same time it deals with the possibility of substitution of loop shape by the mathematical functions differently from mentioned sources. The outputs are graphical illustrations of loop parameters changes in dependence on knitted fabric deformation. The observed knitted fabric was made from Nitinol with the superelastic properties. Thanks to these properties the behavior of this material is precisely

defined during the deformation. This fact should theoretically reflect also in changes in knitted fabric, loop respectively. The results of the measurement will show whether it really works.

## 2 NOTES TO NITI MATERIAL PROPERTIES

In this work the thin superelastic Nitinol (NiTi) filaments of diameter 100 microns as the material providing the functional properties to be projected onto the weft knitted textiles. The filaments were delivered in so called straight-annealed state i.e. they exhibited functional properties in as received state and no further heat treatment had to be applied. The selected NiTi alloy is called superelastic as the stable microstructure phase at room temperature is cubic austenite, which can be transformed into monoclinic martensite, stable at lower temperatures, by applying external loads.

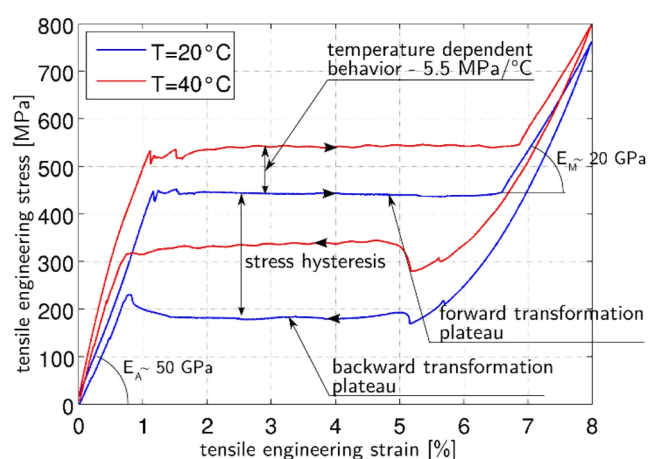


**Figure 1** Tensile behavior of the used superelastic NiTi filaments of diameter 0.1mm at two temperatures

Such so called stress induced martensitic transformation gives rise to nonlinear hysteretic tensile behavior shown in Figure 1 which depicts all

peculiar features of superelastic NiTi filaments such as large recoverable strain (8%), occurrence of plateaus, different Young module of austenite (~50 GPa) and martensite (~20 GPa), stress hysteresis and strong thermomechanical coupling shifting the transformation plateaus by 5.5 MPa per degree of temperature change [31].

### 3 NOTES TO THE ADJUSTMENT OF THE IMAGE OF THE KNITTED FABRIC LOOP

The procedure is determined for previously colored knitted fabric loop (the colored loop is contrast in relation to the rest of fabric and also to the background), see Figure 2. The image (the sequence of the images) is then adjusted in the system of the image analysis.

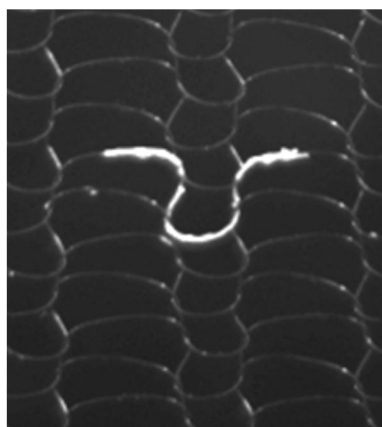


Figure 2 Colored loop in the knitted fabric

#### 3.1 Usage of the system of image analysis

The image sequence is adjusted in the system of image analysis NIS Elements semi-automatically by the macro with the possibility of user intervention. The presented procedure is not probably totally universal, because of image analysis high sensitivity on the reflections of non-colored knitted loops during the threshold, see Figure 2.

The following operations are executed through the macro on each image of the image sequence. The image sequence consists of the set of images of deformed knitted fabric captured once every second:

1. Open of the image, of the image sequence respectively.
2. The change of the contrast of the color image – recommended is exponential transformation.
3. Possible image rotation, if the knitted fabric is not oriented like on Figure 2.
4. Crop of all images in the sequence on the same size (the reducing of the image size – procedure speeding).

5. Interactive threshold of all images in the sequence at the same time.
6. Binary image cleaning by the optional structural element with one or more iterations to clear all binary objects except the loop.
7. Dilation of the binary image by octagon structural element, four time.
8. The function of the medial line is applied. It finds the object axis.
9. Object (loop axis).
10. Binary image is overlaid over the color one and single images are exported to the format \*.tif for further processing in MatLab.

#### 3.2 Usage of the programming language MatLab

Each image of previous sequence of image analysis NIS Elements are processed separately as follows:

1. Image segmentation first, when the threshold is determined according to the method of Otsu own MatLab [32].
2. Set the basic parameters of the loop, see Figure 3. Unfortunately not yet be utilized commonly used basic Dalidovic loop description [33] because of missing information on interlacing with other loops.

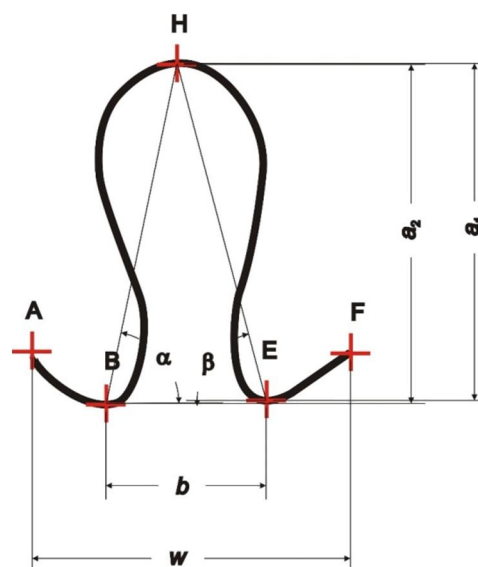


Figure 3 The shape of the loops with marked parameters measured

First are found points A, B, H, E, F according to the criteria:

A - the point with the smallest x-coordinate of the existing points of the loop

H - point with the biggest y-coordinate from existing points of the loop (if found more such points the middle is determined as the point H)

F - point with the biggest x-coordinate of the existing points of the loop



B - point with minimum y-coordinate of the left of the point x-coordinate of the point H

E - point with minimum y-coordinate of the right of point x-coordinate of the point H

Then follows the calculation of the loop actual parameter:

$$a_1 = y_H - y_E \quad (1a)$$

$$a_2 = y_H - y_B \quad (1b)$$

$$w = x_F - x_A$$

$$b = x_E - x_B$$

Because of the possibility of  $y_B \neq y_E$  the parameter  $a$  is counted both ways (see equations (1a), (1b) for the  $a_1$  and  $a_2$  above) and calculated the angle  $\gamma$ , which, if previous equality y-coordinate equal to 0:

$$\gamma = \arctan \frac{y_E - y_B}{x_E - x_B}, \quad (2)$$

then the following angles  $\alpha$  and  $\beta$  are expressed by:

$$\alpha = \arctan \frac{y_H - y_E}{x_H - x_B} \quad (3)$$

$$\beta = \arctan \frac{y_H - y_E}{x_H - x_E}$$

3. Furthermore, the loop is vertically bisected by the x-coordinate of the point H and rotated by 90°, see Figure 3. The resulting upper and lower

half of the loop is separately interspersed with a polynomial function of third degree together with 95% confidence intervals (Figure 4 - red curve - less accurate polynomial).

4. Next, the data are excluded from those that have the same x-coordinate and fit process of a polynomial function of the third degree with 95% confidence intervals is repeated (Figure 4 - black curve - more accurate polynomial).
5. The inflection points are calculated for all four of the polynomial functions.
6. Searched for x-coordinates 90° rotated halves of the loop  $\geq$  x-coordinate of the inflection points for every polynomial function separately of course.
7. The respective parts of the polynomial function are again rotated to its original position and according to the following relationship (4) (see Figure 5) approximate circle radius  $r$  is calculated [34]. This corresponds to the shape of the head of the loop (again for both options fit round points). Consequently, the curvature of the head of the loop as the inverse of radius  $r$  is calculated:

$$\begin{aligned} D &= x_2 - x_1 \\ L &= y_H - y_{1,2} \\ r &= \frac{\left(\frac{L}{2}\right)^2 + D^2}{2D} \end{aligned} \quad (4)$$

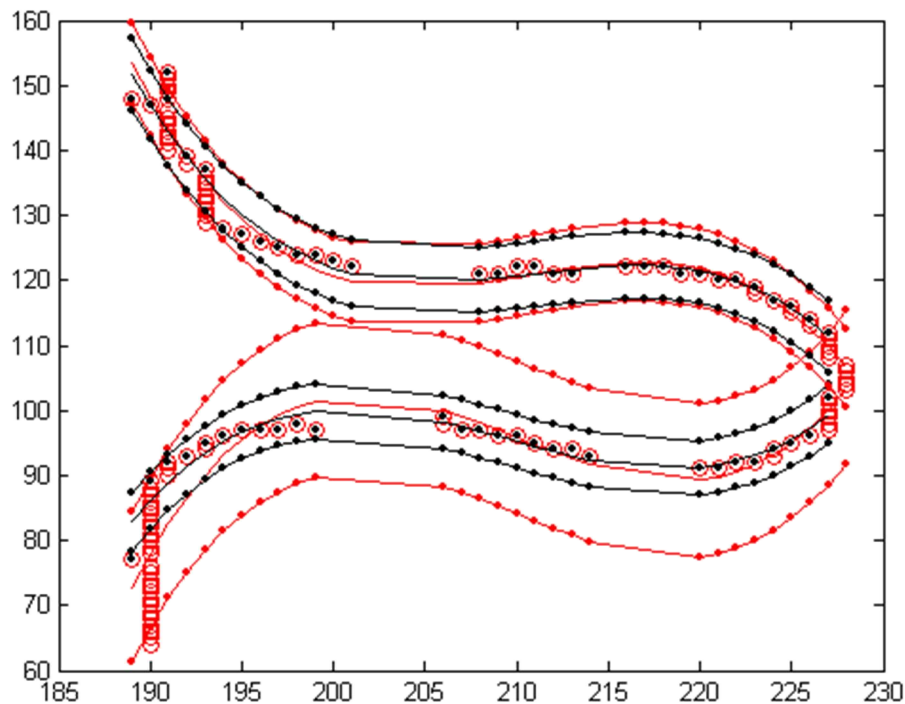


**Figure 4** The fit of loop points with two (resp. four) polynomial function of third degree + indicated 95% confidence intervals

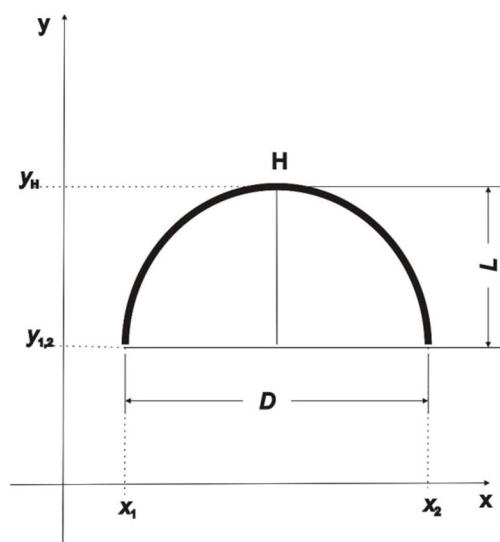


**Figure 5** Schematic representation of a distances  $L$ ,  $D$  to calculate the radius of the circle  $r^1$

#### 4 OUTPUTS AND DISCUSSION

NiTi jersey weft knitted fabric was cyclically loaded in the direction of columns; see Figure 1, chap. 2. One marked loop was observed, see Figure 2.

The following graphic reports show the change in the basic parameters of the loop during cyclic loading of the knitted NiTi in the direction of the columns.

Changes of parameters  $a_1$  and  $a_2$  (see Figure 3) practically correspond to deformation of knitting in the direction of columns, therefore, are shown depending on the other parameters just to them. Proof of this is Figure 8, on which, inter alia, to see the dependence of  $a_1$ , respectively  $a_2$  on the number of the image with observed loop. Relevant dependencies are linear with breakthrough curve, which indicates the second (return) half-cycle distortion.

Graphical representation of dependencies of parameters of the loop clearly illustrates the narrowing of the loop and at the same time enlarging the inclination angle of the walls of the loop, Figures 6 and 7. The effect of cyclic stress is unfortunately not legible on the graphs in Figures 6, 7. It is a superelastic material, where the values of the loop parameters return to the same position as at the beginning of the test.

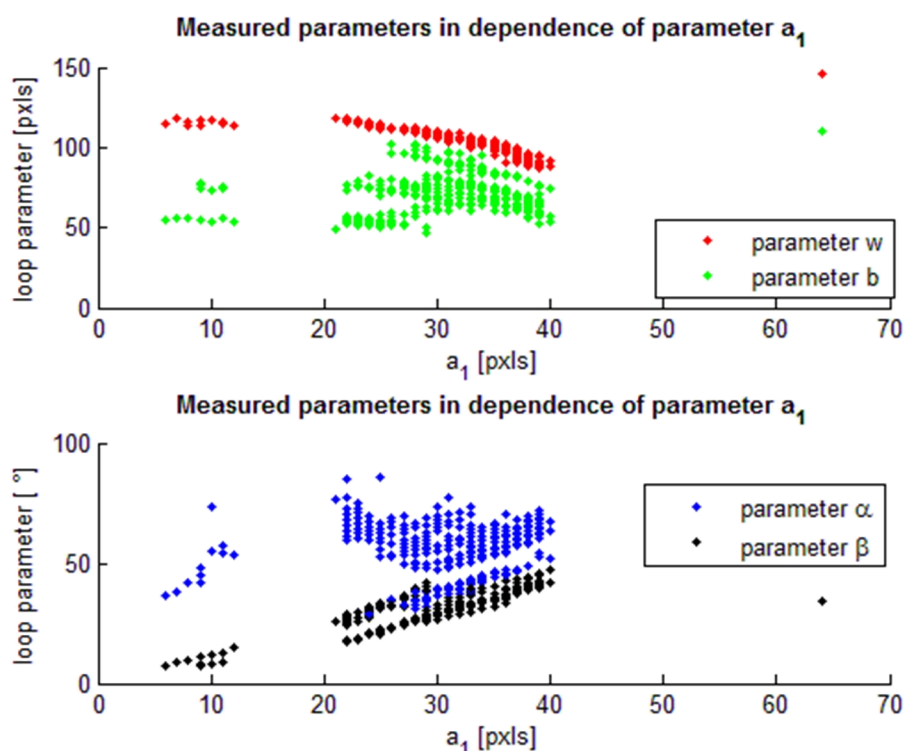


**Figure 6** Measured parameters in dependence of parameter  $a_1$

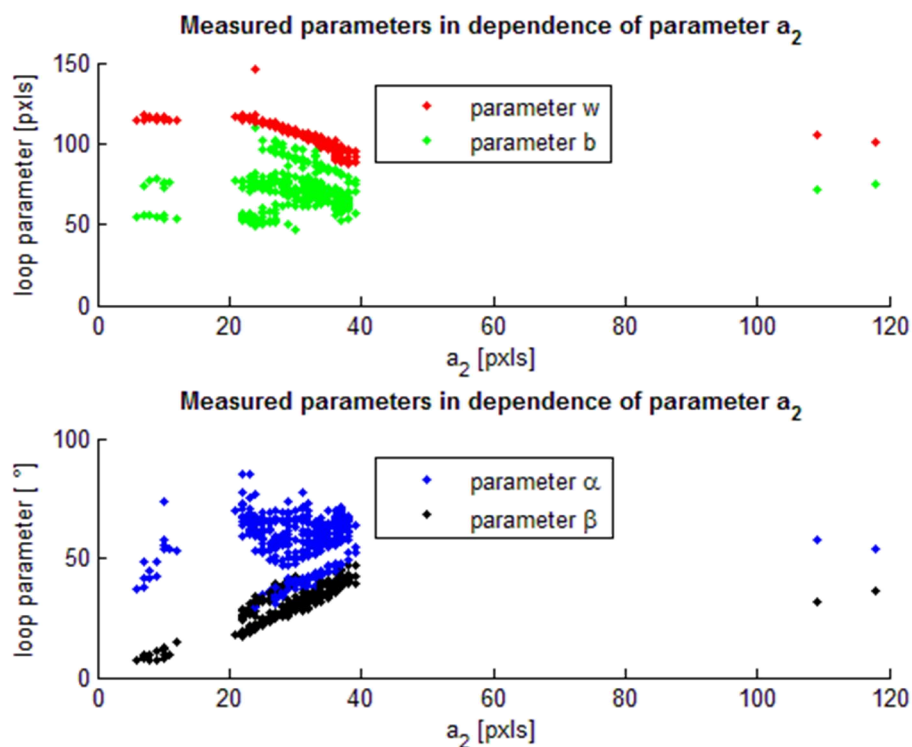


**Figure 7** Measured parameters in dependence of parameter  $a_2$

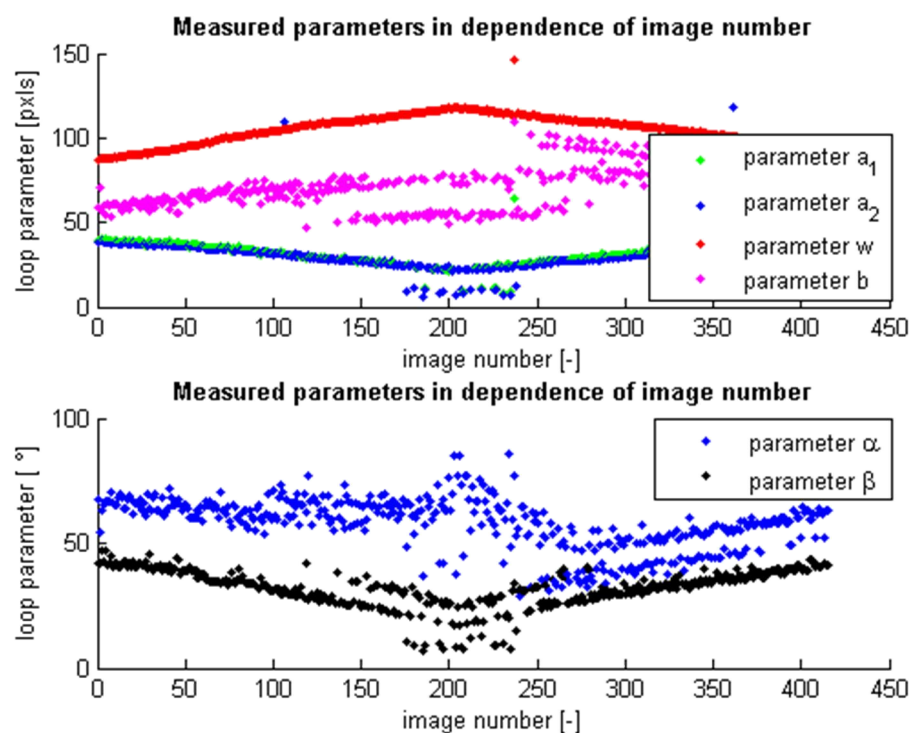


**Figure 8** Measured parameters in dependence of image number

Hysteresis during cyclic loading is clearly evident from Figure 8. It is the image numbers of about 200

to 250, where the values of the parameters are substantially constant.

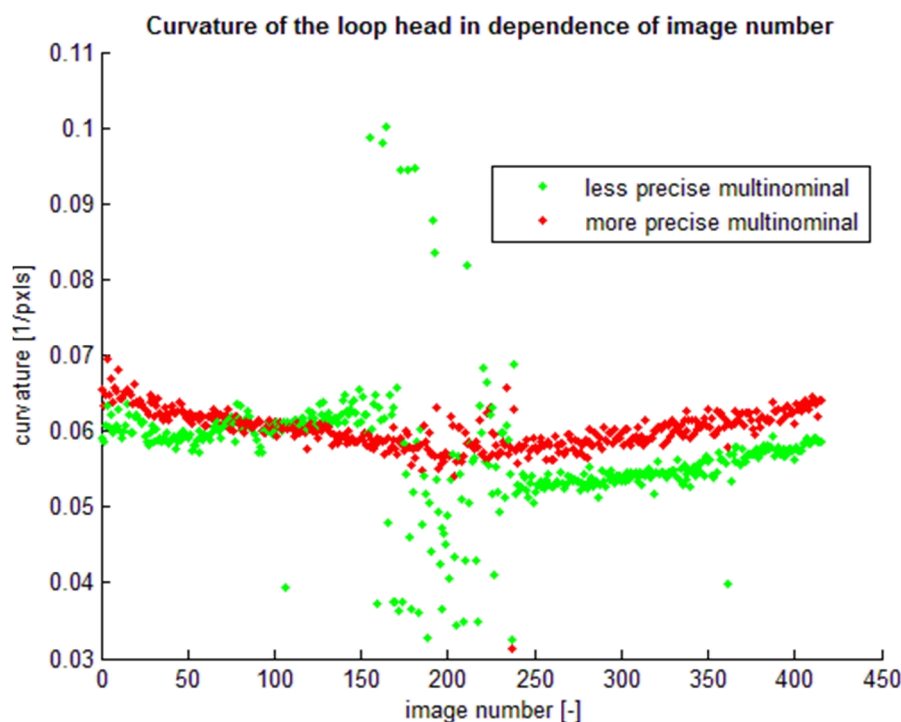


**Figure 9** Curvature of the loop head in dependence of image number

The final endpoint was the change of curvature of the head of the loop again depending on the applied deformation. Both methods of the fitting by polynomial functions show similar results, no significant difference in the change of radius of curvature due to deformation of the knitting in the direction of columns. This fact is most likely due to high stiffness of NiTi wire bending, which prevents deformation of the head of the loop. At the same time Figure 9 shows areas of the NiTi material hysteresis between the numbers of images 200-250, where values of curvature suddenly show higher values of dispersion identically to the previous parameters on the previous graphs, Figures. 6 to 8.

## 5 CONCLUSION

The presented article provides an overview of existing geometrical and physical models of the loop of jersey knitted fabric. Infinitely then followed by the actual parameters defining loop and original image processing of marked loop in the image analysis. It is presented the possibility of fitting of the loop shape by the polynomial functions and define the curvature of the head of the loop. The final outcome of this work there are dependences of the loop parameter changes on the knitting deformation in the direction of the columns. Specific knitted fabric monitored in the work is made of special NiTi material, which is characterized by the superelastic properties. Superelastic properties of NiTi wire are also reflected in the parameters of the loop of knitting, which proves the correctness of the approach to

image processing of the loop and a description of its parameters.

## 6 REFERENCES

1. Doyle P.J.: Fundamental Aspects of the Design of Knitted Fabrics, J. Textile Inst. 44, 561, 1953
2. Munden D.L.: Geometry and Dimensional Properties of Plain Knit Fabrics, J. Text. Inst. 50, T448, 1959
3. Knapton J.J.F., Ahrens F.J., Ingenthorn W.W., Fong W.: The Dimensional Properties of Knitted Wool Fabrics Part I: The Plain Knitted Structure, Textile Res. J. 38, 999, 1968
4. Knapton J.J.F., Ahrens F.J., Ingenthorn W.W., Fong W.: The Dimensional Properties of Knitted Wool Fabrics Part II: 1x1, 2x2 Rib and Half Cardigan Structures, Textile Res. J. 38, 1013, 1968
5. Kurbak A.: Relaxation Lines for Weft Knits, Tekstil ve Makine 2(9), 125-132, 1988
6. Kurbak A.: Plain Knitted Fabric Dimensions (Part I), Textile Asia, March 34-36, 41-44, 1998
7. Chamberlain J.: Hosiery Yarn and Fabrics, Vol. II, Leicester College of Technology and Commerce, Leicester, 1926
8. Peirce F.T.: Geometrical Principles Applicable to the Design of Functional Fabrics, Textile Res. J. 17, 123, 1947
9. Leaf G.A.V., Glaskin A.: Geometry of a Plain Knitted Loop, J. Textile Inst. 46, T587, 1955
10. Leaf G.A.V.: Models of the Plain Knitted Loop, J. Textile Inst. 51, T49, 1960
11. Munden D.L.: The Geometry of Knitted Fabric in its Relaxed Condition, Hosiery Times, April, 43, 1961

12. Postle R.: Structure Shape and Dimensions of Wool Knitted Fabrics, Applied Polymer Symposium, No. 18, John Wiley and Sons, New York, 149, 1971
13. Kurbak A.: Some Investigations on the Geometric Properties of Plain Knitted Fabrics, Tekstil ve Makine 2(11), 238, 1988
14. Kurbak A.: Plain Knitted Fabric Dimensions (Part II), Textile Asia, April, 34-36, 41-44, 1998
15. Demiroz A.: A Study of Graphical Representation of Knitted Structures, PhD Thesis, UMIST, Manchester, 1998
16. Loginov A.U., Grishanov S.A., Harwood R.J.: Modelling the Load-Extension Behavior of Plain-knitted Fabric, Part I: A Unit-cell Approach towards Knitted-fabric Mechanics, J. Text. Inst. 93, 218-238, 2002
17. Loginov A.U., Grishanov S.A., Harwood R.J.: Modelling the Load-Extension Behavior of Plain-knitted Fabric, Part II: Energy Relationships in the Unit Cell, J. Text. Inst. 93, 239-250, 2002
18. Norrie D.H., Vries G.: Finite Element Bibliography, Plenum Press, New York, USA, 1976
19. Postnov V.A., Harhurim I.: The Finite Element Method: Application to Naval Architecture Mechanics, Sudostroenie, Leningrad, USSR, 1974
20. Shabrov N.N.: The Finite Element Method: Application to Heat-engine Mechanics, Machinery Society, Leningrad, USSR, 1983
21. Obrasov L.F., Savelev L.M., Hazanov H.S.: The Finite Element Method: Application to Aircraft Mechanics, High School Press, Moscow, USSR, 1986
22. Matthews F.I.: Finite Element Modelling of Composite Materials and Structures, Woodhead, Cambridge, UK, 2000
23. Zienkiewicz O.C., Taylor R.I.: Finite Element Method, Butterworth-Heinemann, Oxford, UK, 2000
24. Lloyd D.W.: The Analysis of Complex Fabric Deformations, In Mechanics of Flexible Fibre Assemblies, Sijthoff and Noordhoff, Alphen aan den Rijn, The Netherlands, 311-342, 1980
25. Van Lwijk C.J.: Structural Analysis of Wool Yarns, PhD Thesis, University of Canterbury, New Zealand, 1981
26. Van Lwijk C.J., Carr A.J., Carnaby G.A.: Finite-element Analysis of Yarns, Parts I and II, J. Text. Inst. 75, 342-353, 354-362, 1984
27. Carr A.J., Moss P., Carnaby G.A.: The Tangent Compliance Matrix of Wool Fibre Assemblies, In The Application of Mathematics and Physics in the Wool Industry, Wool Research Organization of New Zealand and The Textile Institute New Zealand Section, Christchurch, New Zealand, 193-203, 1988
28. Djaja R.G., Moss P.P., Carr A., Carnaby G.A., Lee D.H.: Finite Element Modelling of an Oriented Assembly of Continuous Fibres, Text. Res. J. 62, 445-457, 1992
29. Munro W.A., Carnaby G.A., Carr A.J., Moss P.J.: Some Textile Applications of Finite-element Analysis, Part I: Finite Elements for Aligned Fibre Assemblies, J. Text. Inst. 88, 325-338, 1997
30. Munro W.A., Carnaby G.A., Carr A.J., Moss P.J.: Some Textile Applications of Finite-element Analysis, Part II: Finite Elements for Yarn Mechanics, J. Text. Inst. 88, 339-351, 1997
31. Heller L et al.: E-MRS2007, European Physical Journal: Special Topics 158(1)
32. Otsu N.: A Threshold Selection Method from Gray-Level Histograms, IEEE Transactions on Systems, Man, and Cybernetics 9(1), 62-66, 1979
33. Kovář R.: Struktura a vlastnosti plošných textilií, skriptum TUL, Liberec, 2006
34. <http://cs.wikipedia.org/wiki/Kru%C5%BEnice>





## CLINITEX CZ s.r.o.

CLINITEX CZ s.r.o., 1. máje 3236/103, CZ 703 00 Ostrava  
tel.: +421 597 578 688, fax: +421 597 579 005  
e-mail: [info@clinitex.cz](mailto:info@clinitex.cz)

[www.clinitex.cz](http://www.clinitex.cz)

## CONTACTS

CLINITEX CZ s.r.o. (Ltd. company) was established in 2005 and then it was focussed purely on medical textile manufacture. The company was certified with ISO 9001:2009 and ISO 14385:2012 and nowadays, it is a major supplier of CLINITEX brand products both to medical facilities of various types and especially to laundries oriented to provide services for them, i.e. renting linens and textiles in health care industry.

In the sector of medical aids' production the company is manufacturing and developing **surgical gowns, clothing and drapes for clean areas** under the CLINITEX brand; the parameters comply with EN 13795:2011+A1:2013 European standard. New products include production and supply of incontinence products in standard version as well as in special custom-made version.

If you choose CLINITEX medical wear, you will always get verified quality, appropriate materials and components as well as perfect design and ergonomic cut. We are anxious to listen carefully to our customers and combine their feedback with our extensive experience as well as hard work of the whole CLINITEX team. We feel this is the only way for our workshops to make professional and high quality wear.



Our manufacturing programme consists of these main product ranges:

- Outfits for doctors
- Outfits for nurses
- Outfits for patients
- Outfits for surgery personnel
- Surgery protection and drapes
- Bed linens and flat textile products
- Incontinence products



# ADFORS

## glass fibre fabrics producer



**2** production plants - in Litomyšl and Hodonice



**1 770** employees



**6,86 bn CZK** turnover



**110 k** tons of glass fibre per year



**6** brands of unique glass fibre products

### Vertex®

Glass fibre mesh fabrics designed for insulation systems and wall or façade reinforcement.

### Vertex® Grid

Glass fibre meshes for floor reinforcement, excellent alternative of heavy metal meshes.

### Fibatape®

Self-adhesive tapes for drywall joints and crack repair.

### Novelio®

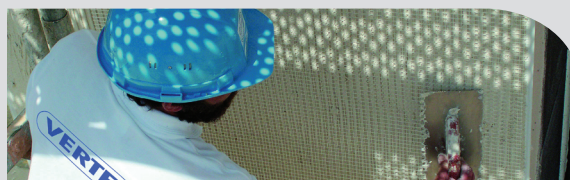
Glass fibre wall coverings used for decoration and wall protection in both public spaces and households.

### GlasGrid®

Glass fibre grids used as asphalt concrete overlays reinforcement and cracks prevention.

### TWINFAB® and glass fibre non-woven fabrics

Protective top layer for gypsum boards wall protection (as paintable wall coverings) and water resistant membrane and separating layers for roof reinforcement.



[www.adfors.cz](http://www.adfors.cz)

SAINT-GOBAIN ADFORS CZ s.r.o.

Sokolovská 106

570 21 Litomyšl

tel: 461 651 110

e-mail: [adfors-cz@saint-gobain.com](mailto:adfors-cz@saint-gobain.com)



Your Partner for Innovative Textiles

# Fehrer

## AUTOMOTIVE

**Fehrer Bohemia s.r.o. is a supplier of interior parts for the automotive industry.**

**Plant Liberec produces armrests, center and rear consoles for customers :**

- AUDI
- BMW
- Daimler
- Nissan
- Seat
- Škoda
- VW

### Interior Modules



**multifunctional armrests**



**center armrests**



**center consoles**



**side bolsters**



**console covers**



**seat-mounted armrests**



# BORGERS

## MAJOR SUPPLIER FOR GLOBAL CAR MANUFACTURERS

- tradition since 1866
- parts and moulded components from non-woven textiles for vehicle interiors and luggage compartments
- manufacture mostly from recycled raw materials
- 4 plants, more than 3000 employees in the Rokycany region

---

**Borgers CS spol. s r.o.**  
Stehlíkova 1111,  
337 01 Rokycany - Nové Město  
Tel.: 727 810 977  
[www.borgers-group.com](http://www.borgers-group.com)





made by



**Caledon** textile factory





**PITTI IMMAGINE FILATI**  
25-27 January 2017  
Florence

**ISPO**  
5-8 February 2017  
Munich

**TECHTEXTIL**  
9-12 May 2017  
Frankfurt am Main



SHIMA SEIKI ITALIA S.p.A.  
Via Redecesio, 11  
20090 Segrate -MI-  
Tel: +039 02/216621  
Fax: +039 02/2139410  
[www.shimaseiki.eu](http://www.shimaseiki.eu)  
[info@shimaseiki.eu](mailto:info@shimaseiki.eu)



Become a fan on Facebook  
Shima Seiki Italia Spa

Official agent for Czechia  
and Slovakia  
KNIT-TEX CS, s.r.o.  
Hlavní 227  
CZ-251 66 Mirosovice u Prahy  
Tel: +420 602 461 722  
[www.shimaseiki.cz](http://www.shimaseiki.cz)



Follow us on Instagram  
[@shimaseikiitalia](https://www.instagram.com/shimaseikiitalia)



# INSTRUCTIONS FOR AUTHORS

The journal „**Vlákná a textil**” (**Fibres and Textiles**) is the scientific and professional journal with a view to technology of fibres and textiles, with emphasis to chemical and natural fibres, processes of fibre spinning, finishing and dyeing, to fibrous and textile engineering and oriented polymer films. The original contributions and works of background researches, new physical-analytical methods and papers concerning the development of fibres, textiles and the marketing of these materials as well as review papers are published in the journal.

## Manuscript

The original research papers are required to be written in English language with summary. Main results and conclusion of contribution from Slovak and Czech Republic may be in Slovak or Czech language as well. The advertisements will be published in a language according to the mutual agreement.

The first page of the manuscript has to contain:

*The title of the article* (16 pt bold, capital letters, centred)

The full *first name* (s) and also *surnames* of all authors (11 pt, bold, centred).

*The complete address* of the working place of the authors, e-mail of authors (9 pt, italic, centred)

*Abstract* (9 pt, italic)

*Key words* (9 pt, italic)

**The manuscript** has to be written in A4 standard form, in **Arial, 10 pt**.

The text should be in **double-column format (width 8.1 cm) in single line spacing.**

*Page margins*: up and down 2.5 cm; left and right 2.0 cm.

**Do not number the pages and do not use footnotes. Do not use business letterhead.**

*Figures, tables, schemes and photos (centered)* should be numbered by Arabic numerals and titled over the table and under the figure or picture.

Photos and schemes have to be sufficiently contrastive and insert in text as pictures.

**Figures, tables, schemes and photos, please, send in separate file.**

*Mathematical formulae* should be centred on line and numbered consecutively on the right margin.

*Physical and technical properties* have to be quantified in SI units, names and abbreviations of the chemical materials have to be stated according to the IUPAC standards.

*References* in the text have to be in square brackets and literature cited at the end of the text.

References (9 pt), have to contain names of all authors.

- [1] Surname N., Surname N.: Name of paper or Chapter, In Name of Book, Publisher, Place of Publication, pp. xxx-yyy, YYYY
- [2] Surname N., Surname N.: Name of paper, Name of Journal Vol. (No.), pp. xxx-yyy, YYYY
- [3] Surname N., Surname, N.: Title of conference paper, Proceedings of xxx xxx, conference location, Month and Year, Publisher, City, Surname N. (Ed.), pp. xxx-yyy, YYYY
- [4] Surname N., Surname N.: Name of Paper, Available from <http://www.exact-address-of-site>, Accessed: YYYY-MM-DD

The final template of manuscript is available on **[http://www.ft.tul.cz/mini/Vlakna a textil](http://www.ft.tul.cz/mini/Vlakna_a_textil)**

Authors are kindly requested to deliver the paper (in Word form) to be published by e-mail: [marcela.hricova@stuba.sk](mailto:marcela.hricova@stuba.sk)

Address of the Editor Office:

**Marcela Hricová**

Faculty of Chemical and Food Technology,  
Slovak University of Technology in Bratislava

Radlinskeho 9

812 37 Bratislava,

Slovakia





9<sup>th</sup> Central European Conference 2017

Fibred - Grade Polymers, Chemical Fibres and Special Textiles  
**September 11<sup>th</sup> - 13<sup>th</sup> 2017, Liberec, Czech Republic**

We would like to invite you to the 9<sup>th</sup> Central European Conference (Fibre – Grade Polymers, Chemical Fibres and Special Textiles), which will be held at the Faculty of Textile Engineering, Technical University of Liberec from **11<sup>th</sup> to 13<sup>th</sup> September 2017**.

### Conference topics

- Advanced Fibres and Materials
- Innovations in Textile Technologies
- Textile Metrology and Quality Control
- Functional Clothing and Comfort
- Apparel Engineering
- Advances on Textile Chemical Processing
- Textile Structure Reinforced Composites
- Technical Textiles
- Nanotechnology and Nanotextiles

### Organized by



TECHNICAL UNIVERSITY OF LIBEREC  
Faculty of Textile Engineering ■

### Important dates

Abstract submission deadline	30th April 2017
Notification of abstract acceptance	15th May 2017
Earlybird registration and payment closes	30th June 2017
Late registration closes	31th August 2017
Full paper submission (optional) deadline	15th July 2017
Conference	11th - 13th September 2017

### Full paper submission (optional)

Full papers presented at the conference will be submitted to ***Vlákna a textil (Fibres and Textiles)*** journal. The journal is indexed in the database Scopus, it will be available in PDF file format after the conference and it will be sent to all authors of submitted papers.

If you are interested in publication of your paper, please submit the full paper via contact email address till **15<sup>th</sup> July 2017**.

All full papers will be reviewed and final acceptance for publication in the journal will be subjected to satisfactory revision according to the review comments.

<http://cec2017.ft.tul.cz>